

12-2021

## Catalytic Activity of Molybdenum-Dioxo Complexes

Randy Tran  
*University of Arkansas, Fayetteville*

Follow this and additional works at: <https://scholarworks.uark.edu/etd>

 Part of the [Organic Chemistry Commons](#)

---

### Citation

Tran, R. (2021). Catalytic Activity of Molybdenum-Dioxo Complexes. *Graduate Theses and Dissertations*  
Retrieved from <https://scholarworks.uark.edu/etd/4385>

This Dissertation is brought to you for free and open access by ScholarWorks@UARK. It has been accepted for inclusion in Graduate Theses and Dissertations by an authorized administrator of ScholarWorks@UARK. For more information, please contact [scholar@uark.edu](mailto:scholar@uark.edu), [uarepos@uark.edu](mailto:uarepos@uark.edu).

Catalytic Activity of Molybdenum-Dioxo Complexes

A dissertation submitted in partial fulfillment  
of the requirements for the degree of  
Doctor of Philosophy in Chemistry

by

Randy Tran  
University of Arkansas  
Bachelor of Science in Chemistry, 2011

December 2021  
University of Arkansas

This dissertation is approved for recommendation to the Graduate Council

---

Stefan Kilyanek, Ph.D.  
Dissertation Director

---

Robert Coridan, Ph.D.  
Committee Member

---

Colin Heyes, Ph.D.  
Committee Member

---

Ryan Tian, Ph.D.  
Committee Member

---

Nan Zheng, Ph.D.  
Committee Member

## Abstract

This dissertation details the development of rationally designed dioxomolybdenum catalyst active for deoxydehydration (DODH), the net reduction of diols and polyols into alkenes and dienes. Catalyst design involved variations on dioxomolybdenum(VI) supported by a dianionic meridional pincer ligand. Rational substrate scope was explored using aliphatic diols, aromatic diols, and biomass derived diols. Various reductants were tested for ability to catalyze the reaction. The substrate specific mechanism of DODH was explored utilizing NMR and in-situ infrared spectroscopy and important rate constants and rate determining steps were found to aid in the optimization of ideal reaction conditions. Catalytic activity was observed to be dependent on the ligand environment. The smaller electronically demanding ligand environment showed readily rapid reactivity for aromatic diols, but competitive side reactions and catalyst dimerization occurred. The more sterically demanding ligand environment was observed to slow the relative reaction times, decrease/block competitive side reactions, and increase the yields for specific diols. Electrochemical studies were performed on the more sterically demanding catalyst to gain a fundamental understanding of the proton transfer and electron transfer processes that are involved in transforming the molybdenum-dioxo catalyst into the active mono-oxo species. The processes may be coupled together in a proton coupled electron transfer (PCET) where the proton and electron are transferred stepwise. The catalyst was screened against a variety of Brønsted-Lowry acids within a pKa window of ~9-32 in THF. Electrochemical characterization of the molybdenum catalyst suggests a PTET mechanism. Future studies involve the further rational design of ligand environments to directly access the reduced catalytically DODH active species with minimum energy input as an efficient and alternative method to generate industrially relevant chemical precursors.

## Acknowledgements

The work in this thesis was supported by the National Science Foundation, award #CHE-1654553. Our laboratory is grateful for their support.

I want to thank my advisor, Dr. Stefan Kilyanek, for the guidance, support, and mentorship over the long years. His teachings will follow me for the rest of my life. I also want to thank the members of my committee -Dr. Robert Coridan, Dr. Colin Heyes, Dr. Tian, and Dr. Nan Zheng- for their continued support and feedback on this work.

I want to also thank my fellow colleagues within the Kilyanek Lab, past and present, -Joel Baker, Cody Canote, Kayla Denike, Dr. Rajesh Thapa- for stimulating and light-hearted conversations and consultation. I'll carry those moments with me long after this.

Lastly, I want to thank the chemistry graduate students and faculty at the University of Arkansas. There was never a dull moment.

## **Dedication**

To my parents, Can Tran and N. Quynh Nguyen, for allowing me to chase the American Dream.

## Table of Contents

<b>Chapter 1 Introduction</b> .....	<b>1</b>
References.....	8
<b>Chapter 2 Deoxydehydration Catalyzed By Dioxo(pyridine-2,6-dicarboxylato)(hexamethylphosphoramidate)molybdenum(VI)</b> .....	<b>10</b>
Introduction and Background.....	10
Results and Discussion .....	13
DODH of 1-phenyl-1,2-ethanediol, Reductant Scope .....	13
DODH of (R,R)-(+)-hydrobenzoin, Reductant Scope .....	17
Kinetic Studies of 1-phenyl-1,2-ethanediol and PPh <sub>3</sub> .....	17
Kinetic Studies of (R,R)-(+)-hydrobenzoin .....	19
Dehydration.....	21
Conclusions .....	21
Experimental Procedure .....	22
References.....	24
Supporting Information .....	26
<b>Chapter 3 Deoxydehydration of Polyols Catalyzed by a Molybdenum Dioxo-Complex Supported by a Dianionic ONO Pincer Ligand</b> .....	<b>51</b>
Introduction and Background.....	51
DODH Catalyzed by 1 and 2 .....	56

Preliminary Kinetics.....	58
Conclusions .....	58
Experimental Procedure.....	59
References.....	64
Supporting Information .....	67
<b>Chapter 4 Electrochemical Investigation of a Bisphenylatopyridyl Dioxomolybdenum Complex.....</b>	<b>87</b>
Introduction and Background.....	87
Results and Discussion .....	89
Cyclic Voltammetry.....	89
Tafel Analysis.....	93
Linear Sweep Voltammetry (LSV) .....	95
Conclusions .....	96
Experimental Procedure.....	98
References.....	100
Supporting Information .....	102
<b>Chapter 5 Conclusions and Future Directions.....</b>	<b>111</b>
Evaluation of Results and Completion of Aims .....	112
Future Directions.....	113
References.....	116

## List of Abbreviations

DODH	Deoxydehydration
NMR	Nuclear Magnetic Resonance
HMPA	Hexamethylphosphoramide
PCET	Proton Coupled Electron Transfer
THF	Tetrahydrofuran
$\text{MoO}_2(\text{acac})_2$	Bis(acetylacetonato)dioxomolybdenum(VI)
AHM	Ammonium heptamolybdate
$\text{Cp}^*\text{ReO}_3$	(Pentamethylcyclopentadienyl)trioxorhenium(VII)
$\text{CpReO}_3$	(Cyclopentadienyl)trioxorhenium(VII)
$\text{MeReO}_3$	Methyltrioxorhenium(VII)
$\text{PPh}_3$	Triphenylphosphine
$\text{OPPh}_3$	Triphenylphosphine oxide
DFT	Density Functional Theory
iPrOH	Isopropyl alcohol
$\text{CDCl}_3$	Deuterated Chloroform
$\text{CD}_2\text{Cl}_2$	Deuterated Dichloromethane
GC/MS	Gas Chromatography Mass Spectrometry
IR	Infrared Spectroscopy

## List of Figures

### Chapter 1

Figure 1. Generalized scheme for DODH.....	2
Figure 2. Square scheme of PCET and CPET .....	6

### Chapter 2

Figure 1. The competitive mechanisms of DODH.....	11
Figure 2. Molybdenum DODH catalyst and general reaction scheme.....	13
Figure 3. In-situ ReactIR traces.....	18
Figure 4. DODH mechanism of 1-phenyl-1,2-ethanediol .....	19
Figure 5. DODH mechanism of (R,R)-(+)-hydrobenzoin .....	20
Figure 6. Synthesis of <b>1</b> .....	22
Figure S1. <sup>1</sup> H NMR characterization of <b>1</b> .....	26
Figure S2. <sup>1</sup> H NMR of <b>1</b> , PPh <sub>3</sub> , and 1-phenyl-1,2-ethanediol. Toluene, 190°C, 1h .....	27
Figure S3. <sup>1</sup> H NMR showing polystyrene growth.....	28
Figure S4. <sup>1</sup> H NMR p-hydroquinone inhibiting polymerization .....	29
Figure S5. <sup>1</sup> H NMR p-hydroquinone as reductant.....	30
Figure S6. <sup>1</sup> H NMR (R,R)-(+)-hydrobenzoin C=C and C=O.....	31
Figure S7. <sup>1</sup> H NMR of <b>1</b> , PPh <sub>3</sub> , and 1,2-octanediol. Toluene, 190°C, 80h .....	32
Figure S8. Full ReactIR spectrum of <b>1</b> , PPh <sub>3</sub> , 1-phenyl-1,2-ethanediol (1:100:10) Toluene, 190°C, 20h .....	33

Figure S9. Full ReactIR spectrum of <b>1</b> , PPh <sub>3</sub> , 1-phenyl-1,2-ethanediol, OPPh <sub>3</sub> (1:100:10:10) Toluene, 190°C, 20h .....	34
Figure S10. Full ReactIR spectrum of <b>1</b> , PPh <sub>3</sub> , 1-phenyl-1,2-ethanediol, H <sub>2</sub> O (1:100:10:10) Toluene, 190°C, 10h .....	35
Figure S11. Full ReactIR spectrum of <b>1</b> , PPh <sub>3</sub> , 1-phenyl-1,2-ethanediol (1:10:100) Toluene, 190°C, 15h .....	36
Figure S12. Full ReactIR spectrum of <b>1</b> , PPh <sub>3</sub> , 1-phenyl-1,2-ethanediol (1:10:10) Toluene, 190°C, 20h .....	37
Figure S13. Full ReactIR spectrum of <b>1</b> , PPh <sub>3</sub> , (R,R)-(+)-hydrobenzoin (1:100:10) Toluene, 190°C, 20h .....	38

### **Chapter 3**

Figure 1. Generalized DODH reaction.....	51
Figure 2. Mechanisms of DODH .....	52
Figure 3. Synthesis of bisphenolatopyridyl dioxo-molybdenum(VI).....	54
Figure 4. X-Ray crystal structure of <b>1</b> .....	55
Figure 5. X-Ray crystal structure of <b>2</b> .....	55
Scheme 1. Ligand (P3) synthesis.....	60
Figure S1. <sup>1</sup> H NMR characterization of <b>1</b> .....	69
Figure S2. <sup>13</sup> C{ <sup>1</sup> H} NMR characterization of <b>1</b> .....	70
Figure S3. <sup>1</sup> H NMR characterization of <b>2</b> .....	71
Figure S4. <sup>13</sup> C{ <sup>1</sup> H} NMR characterization of <b>2</b> .....	72

Figure S5. $^1\text{H}$ NMR of <b>1</b> , $\text{PPh}_3$ , 1-phenyl-1,2-ethanediol, and Hexamethylcyclotrisiloxane. Toluene- $d_8$ , $150^\circ\text{C}$ , 48h.....	73
Figure S6. $^1\text{H}$ NMR of <b>2</b> , $\text{PPh}_3$ , 1-phenyl-1,2-ethanediol, and Hexamethylcyclotrisiloxane. Toluene- $d_8$ , $150^\circ\text{C}$ , 48h.....	74
Figure S7. $^1\text{H}$ NMR of <b>1</b> , $\text{PPh}_3$ , 1-phenyl-1,2-ethanediol, and 1,3,5-trimethoxybenzene. $\text{CD}_2\text{Cl}_2$ , $150^\circ\text{C}$ , 48h .....	75
Figure S8. Growth of styrene versus time .....	76
Figure S9. Consumption of 1-phenyl-1,2-ethanediol .....	76
Figure S10. ORTEP of <b>1</b> .....	79
Figure S11. ORTEP OF <b>2</b> .....	81
Figure S12. ORTEP of aquo-complex of <b>2</b> .....	83

#### **Chapter 4**

Figure 1. Competing mechanisms of proton and electron transfers.....	89
Figure 2. Voltammogram of P3 and <b>1</b> .....	90
Figure 3. Fitted current response to increasing concentrations of proton.....	92
Figure 4. Michaelis-Menten kinetic model .....	93
Figure 5. Tafel Plots derived from Chronoamperometry .....	94
Figure 6. Tafel Plots without Mass-Transport Limitations .....	96
Figure 7. PTET mechanism.....	97
Figure S1. Temporal Stability to Acids .....	106
Figure S2. Combined Tafel Plots .....	107

Figure S3. KL Analysis Plots in Various Conditions.....	108
Figure S4. Current Response to 2,6-dihydroxybenzoic acid.....	109
Figure S5. LSV Data and Subsequent KL analysis .....	110

## List of Tables

### **Chapter 2**

Table 1. Summary of Catalytic Activity of <b>1</b> at 190°C .....	16
Table T1. 1-phenyl-1,2-ethanediol yields.....	39
Table T2. 1,2-octanediol yields .....	43
Table T3. (R,R)-(+)-hydrobenzoin yields .....	45
Table T4. Trans-1,2-cyclohexanediol yields .....	46
Table T5. Meso-erythritol yields .....	47
Table T6. 1,4-anhydroerythritol yields .....	48

### **Chapter 3**

Table 1. Summary of catalytic activity of <b>1</b> and <b>2</b> .....	57
Table T1. DODH of aliphatic and biomass diols by <b>1</b> and <b>2</b> .....	77
Table T2. All reactions before averaging .....	78
Table T3. Crystal data and structure refinement of <b>1</b> .....	80
Table T4. Crystal data and structure refinement of <b>2</b> .....	82
Table T5. Crystal data and structure refinement of aquo-complex.....	84

### **Chapter 4**

Table 1. pKa values of acids in THF.....	91
Table 2. Exchange currents in different conditions .....	95
Table T1. Fitted data of current response to proton concentration.....	102

Table T2. Koutecky-Levich Data -2.5V ..... 105

Table T3. Koutecky-Levich Data -3.17V ..... 105

## List of Published Articles

### **Chapter 3: Deoxydehydration of Polyols Catalyzed by a Molybdenum Dioxo-Complex Supported by a Dianionic ONO Pincer Ligand.**

Tran, R.; Kilyanek, S. M. Deoxydehydration of Polyols Catalyzed by a Molybdenum Dioxo-Complex Supported by a Dianionic ONO Pincer Ligand. *Dalton Trans.* **2019**, *48*, 16304.  
[DOI:10.1039/C9DT03759D](https://doi.org/10.1039/C9DT03759D)

## Chapter 1

### Introduction

The global energy economy primarily relies on fossil fuels to meet its demands, making up nearly 80% of the total fuel mix.<sup>1,2</sup> Nuclear power contributes over 6% and the rest comes from various renewables like hydro and biomass. Current estimates place conventional oil reserves at 2.3 billion barrels with potential for more oil as better technologies are developed to increase recoverable oil. This means that the global energy needs can be met using fossil fuels through the mid-21<sup>st</sup> century. However, the unavoidable effects of burning fossil fuels are an immediate problem. Global trends in rising CO<sub>2</sub> and its link to global warming must be addressed. Global warming is approximately 1°C above pre-industrial levels (a likely range of 0.8°C – 1.2°C) and current projections with high confidence say it will likely reach 1.5°C between 2030 and 2052 at the current rate.<sup>3</sup> An increase of 1.5°C results in higher mean temperatures globally, risks of drought and heavy precipitation in some regions, and rising sea levels. These changes can lead to species loss and extinction on land and sea, disrupting the balance of the ecosystem and having severe impacts on human life. Therefore, it is pragmatic to increase the global energy contributions of non-fossil fuel sources to halt the climate changes.

Traditional and modern biomass contribute approximately 12% of energy needs.<sup>4,5</sup> Traditional biomass refers to basic combustion of wood, waste, and traditional charcoal. Modern biomass refers to liquid biofuels synthesized from agricultural byproducts such as leftover carbohydrates from the production of sugar cane, corn, and sorghum.<sup>6,7</sup> The advantage of converting the solid byproducts to liquid biofuels lies in the inherent energy density; the unit volume of solid biomass is considerably less than the unit volume of liquid biofuels when considering the same energy output.<sup>8</sup> Current industrial generation of these liquid biofuels heavily relies on precious metal catalysts and harsh conditions to deoxygenate the solid carbohydrates via steam reforming and cracking.<sup>9-11</sup> Deoxydehydration (DODH) is a potential

candidate to address this issue. DODH is a catalytic route that can deoxygenate the biomass at relatively lower temperatures using abundant earth poly-oxo transition metals; it converts diols and polyols into alkenes and dienes. The steps of DODH involve: 1) reduction of the poly-oxo catalyst into its active form 2) coordination of the alcohol substrate forming the diolate 3) extrusion of the reduced alkene product and regeneration of the poly-oxo catalyst. These pathways are summarized in **Figure 1**.

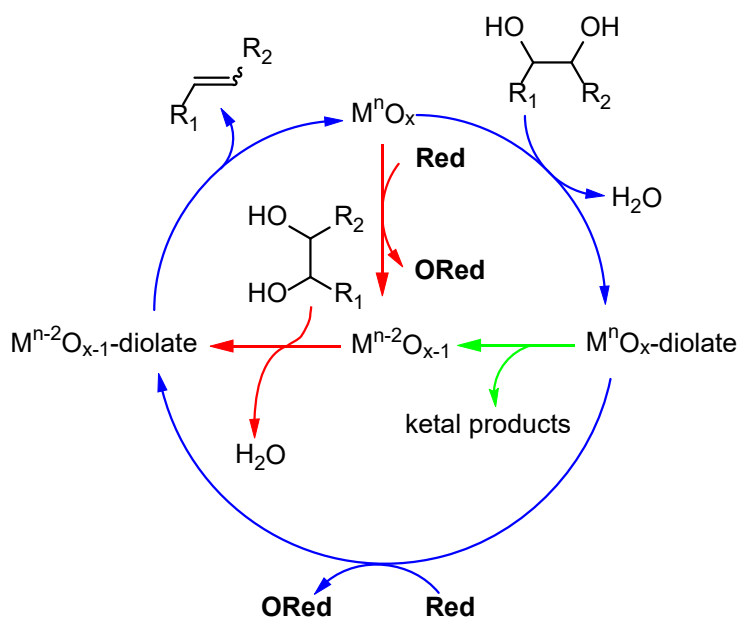


**Figure 1.** Generalized scheme for deoxydehydrogenation.

First reported in 1996 by Cook and Andrews,<sup>12</sup> they used pentamethylcyclopentadienyl trioxorhenium(VII) ( $Cp^*ReO_3$ ) and were able to demonstrate the quantitative conversion of 1-phenyl-1,2-ethanediol into styrene using triphenylphosphine ( $PPh_3$ ) as reductant and oxygen acceptor in chlorobenzene reporting 55 turnovers/Re atom. Further studies showed that the catalyst would also become over-reduced, denoted as Re(III), effectively killing catalyst activity. They demonstrate the competing kinetics of over-reduction ( $k_{5/3}$ ) and diolate formation ( $k_{ket}$ ). The ratio ( $k_{ket}/k_{5/3}$ ) between these rates varies with solvent; in benzene- $d_6$  the ratio is 60 while in tetrahydrofuran- $d_8$  it is 2. This is due to the inhibition of diolate formation by the hydrogen-

bonding ability of THF. Their attempts to minimize catalyst over-reduction by speeding up the diolate formation or slowing/inhibiting the over-reduction. The former was accomplished with the addition of p-toluenesulfonic acid as a cocatalyst; this yielded 91% conversion of substrate to styrene in 13 hours. The latter attempt was done by using alternative, less active, reductants such as tris(perfluorophenyl)phosphine. They achieved identical results to the speeding up the diolate formation. DODH using other diols and polyols yielded appreciable results but various challenges such as: 1) the relative prohibitive cost of rhenium compounds 2) the usage of phosphines and their role as sacrificial reductants 3) the over-reduction of the Re(VII) to Re(III) 4) the reliance on cocatalysts caused DODH to fall into relative obscurity until recently.

The Toste group in 2012 reported effective DODH catalysts for more challenging substrates such as large ( $C_5$  or greater) sugar alcohols using methyltrioxorhenium(VII) (MTO).<sup>13</sup> The focus of this work was on sugar alcohols as substrate and secondary alcohols as reductant. They demonstrated 90% conversion of glycerol to alkene at 2.5 mol % MTO as catalyst and using 3-octanol as reductant. Other sugar alcohols were tested and achieved similar results. They propose a catalytic cycle for MTO-catalyzed alcohol driven DODH. Abu-Omar and his group have extensively explored the MTO catalyzed DODH reaction mechanism using sacrificial alcohols as reductants and aromatic diols as substrates.<sup>14</sup> They have obtained reasonable yields (80%) while using relatively mild temperatures ( $140^\circ\text{C}$  -  $170^\circ\text{C}$ ). They observed that MTO-catalyzed DODH may occur via two possible pathways. Pathway A is the formation of the rhenium(VII) diolate followed by reduction to rhenium(V). Pathway B is the reduction of MTO to MDO (methylidioxorhenium(V)) followed by the diolate formation. Both pathways are ultimately followed by the olefin extrusion to regenerate the catalytic cycle.

Nicholas and coworkers have also studied the DODH reaction catalyzed by oxorhenium compounds. The Nicholas groups focused on expanding the reductant scope. In addition to secondary alcohols, Nicholas finds sulfite<sup>15</sup> ( $\text{Na}_2\text{SO}_3$ ), elemental reductants<sup>16</sup> (Zn, Fe, Mn, C),

and dihydroaromatic compounds<sup>17</sup> are competent oxo-acceptors in DODH. Using  $[\text{Bu}_4\text{N}][\text{ReO}_4]$ , sulfite afforded yields approaching ~89% and zinc powder yielded 46% for styrene as the major product. The mechanism of sulfite driven MTO DODH was also computationally studied by Nicholas<sup>18</sup> using ethylene glycol as substrate. They show that the lowest energy reaction pathway for this substrate was reduction by sulfite then formation of the diolate structure and the rate determining step to be the olefin extrusion. The coordination and association of auxiliary ligands on the Re(V) diolate was shown to increase the activation energies for olefin extrusion. In the absence of ligands, the activation energy was shown to be 15.6 kcal/mol while ligands such as water,  $\text{NaSO}_4^-$ , and  $\text{NaSO}_3^-$  were shown to increase the activation barrier to 27.1 kcal/mol (water) to 34.8 kcal/mol ( $\text{NaSO}_3^-$ ). The scope of rhenium based DODH has been extensively explored, but the prohibitive cost of rhenium has driven researchers to find alternative metals that are more abundant and can more cheaply catalyze DODH. Recently, Nicholas reported a variety of vanadium-based catalysts for DODH. Notably, ammonium dipicolinate dioxovanadium(V) catalyzed complete conversion of styrene glycol achieving yields of 95% and 87% when using  $\text{Na}_2\text{SO}_3$  and  $\text{PPh}_3$  (72h, 160°C), respectively. Some other vanadium catalysts reported were able to catalyze the transformation of carbohydrate derived diols.

The first molybdenum catalysts active for DODH was reported in 2014 by Fristrup et al.<sup>19</sup> The most notable among them was the commercially available ammonium heptamolybdate (AHM), capable of catalyzing the transformation of 1,2-hexanediol into 1-hexene albeit at lower yields and higher temperatures compared to rhenium. The low yields are due to the competing side reactions due to the ability of the molybdenum catalyst's ability to cleave C-C bonds. While these results are not impressive, the fact that molybdenum was capable of this catalytic transformation spurred other groups to find and develop molybdenum catalysts active for DODH. The same group later expands on the AHM work by showing that it can use the simplest

secondary alcohol as reductant yielding up to 49% olefin and up to 55% olefin with additional additives. Palkovits et al<sup>20</sup> reported that using TiO<sub>2</sub> as a support for AHM catalyzed DODH increased yields of olefin product. Various ligands have been employed to change/increase the activity of molybdenum catalyzed DODH. Ligands ranging from bisphenolate pincers, diketones, and acylpyrazolonates.<sup>21-24</sup> A common motif in the body of work done on DODH is the need for a chemical reductant that activates the catalyst. This generates stoichiometric amounts of chemical waste; secondary alcohols are advantageous due to the relative ease of hydrogenating the ketones or aldehydes and regenerating the secondary alcohols. However, this places more strain into the energetic needs of an industrially viable DODH. This dissertation proposes an alternative to the chemical reductants: electrochemical reduction. That is, directly reducing the catalyst at an electrode without the need of chemical reductants. Electrochemical reduction would require a close examination of both the proton transfer and electron transfer behavior of the catalyst. These can be defined as the fundamental hydrogen atom transfer (HAT) and electron transfer (ET) reactions. ET and HAT permeate vital life processes such as photosystem II of plant life and the redox steps of human metabolism. HATs and ETs are not mutually exclusive; they often follow one another or are coupled together. Depending on the situation, they are defined together as proton coupled electron transfer (PCET) or concerted proton electron transfer (CPET) shown in Figure 2.

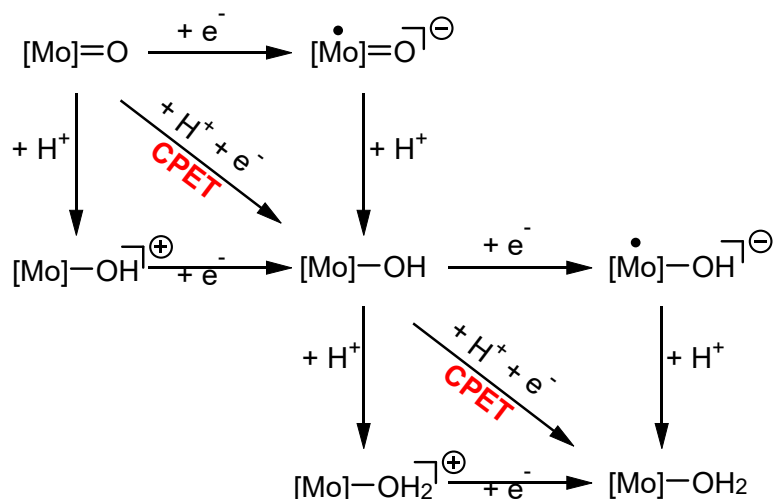


**Figure 2.** The possible mechanisms of PT and ET.

PCET refers to the stepwise addition of proton and electron while CPET refers to the proton and electron moving in a concerted fashion. There exists a massive body of work dedicated to studying PCET and CPET in various systems and contexts. Meyer et al and Mayer provide strong reviews of PCET processes in chemistry and biology.<sup>25,26</sup> When discussing the chemical reduction of the metal-oxo species by a secondary alcohol, it is a CPET event where both the proton and electron come from the same alcoholic source. PCET in the scope of this work is defined by the outer-sphere electron transfer coupled with the proton donation from Brønsted-Lowry acids. The square scheme shown for PCET shows the stepwise pathways of HAT or ET but the concerted path has been shown to be thermodynamically favored; the concerted path sidesteps the formation of high energy intermediates, radicals or cations.

The objective of the work reported in this dissertation is to catalog the discovery and development of novel dioxomolybdenum(VI) catalysts active for DODH. Chapter 2 discusses the catalytic activity and mechanism of DODH catalyzed by a dianionic ONO pincer ligand supported dioxomolybdenum(VI) catalyst. Chapter 3 builds on the work done in chapter 2 by altering the steric demands of the catalyst and examines the effects on catalytic activity.

Chapter 4 examines the fundamental redox behavior of the sterically demanding catalyst and demonstrates new strategies for approaching a more efficient DODH.

## References

- (1) United Nations Development Program (2015) World Energy Assessment: Energy and The Challenge of Sustainability (United Nations, New York).
- (2) Jackson, R. B.; Le Quéré, C.; Andrew, R. M.; Canadell, J. G.; Korsbakken, J. I.; Liu, Z.; Peters, G. P.; Zheng, B. Global Energy Growth Is Outpacing Decarbonization. *Environ. Res. Lett.* **2018**, *13* (12), 120401. <https://doi.org/10.1088/1748-9326/aaf303>.
- (3) IPCC. Global Warming of 1.5°C. 2019.
- (4) Popp, J.; Lakner, Z.; Harangi-Rákos, M.; Fári, M. The Effect of Bioenergy Expansion: Food, Energy, and Environment. *Renewable and Sustainable Energy Reviews* **2014**, *32*, 559–578. <https://doi.org/10.1016/j.rser.2014.01.056>.
- (5) Gallezot, P. Conversion of Biomass to Selected Chemical Products. *Chem. Soc. Rev.* **2012**, *41* (4), 1538–1558. <https://doi.org/10.1039/C1CS15147A>.
- (6) Zhang, H.; Li, X.; Su, X.; Ang, E. L.; Zhang, Y.; Zhao, H. Production of Adipic Acid from Sugar Beet Residue by Combined Biological and Chemical Catalysis. *ChemCatChem* **2016**, *8* (8), 1500–1506. <https://doi.org/10.1002/cctc.201600069>.
- (7) Ragauskas, A. J. The Path Forward for Biofuels and Biomaterials. *Science* **2006**, *311* (5760), 484–489. <https://doi.org/10.1126/science.1114736>.
- (8) Kunkes, E. L.; Simonetti, D. A.; West, R. M.; Serrano-Ruiz, J. C.; Gartner, C. A.; Dumesic, J. A. Catalytic Conversion of Biomass to Monofunctional Hydrocarbons and Targeted Liquid-Fuel Classes. *Science* **2008**, *322* (5900), 417–421. <https://doi.org/10.1126/science.1159210>.
- (9) DeNike KA, Kilyanek SM. 2019. Deoxydehydration of vicinal diols by homogeneous catalysts: a mechanistic overview. *R. Soc. open sci.* *6*: 191165. <http://dx.doi.org/10.1098/rsos.191165>
- (10) Akah, A.; Williams, J.; Ghrami, M. An Overview of Light Olefins Production via Steam Enhanced Catalytic Cracking. *Catal Surv Asia* **2019**. <https://doi.org/10.1007/s10563-019-09280-6>
- (11) Dutta, S. Deoxygenation of Biomass-Derived Feedstocks: Hurdles and Opportunities. *ChemSusChem* **2012**, *5* (11), 2125–2127. <https://doi.org/10.1002/cssc.201200596>.
- (12) Cook, Gerald K.; Andrews, Mark A. Towards Nonoxidative Routes to Oxygenated Organics: Stereospecific Deoxydehydration of diols and Polyols to Alkenes and Allylic Alcohols Catalyzed by the Metal Oxo Complex (C<sub>5</sub>Me<sub>5</sub>)ReO<sub>3</sub>. *J. Am. Chem. Soc.* **1996**, *118*, 9448-9449
- (13) Shiramize, Mika; Toste, Dean F. Deoxygenation of Biomass-Derived Feedstocks: Oxorhenium-Catalyzed Deoxydehydration of Sugars and Sugar Alcohols. *Angew. Chem. Int. Ed.* **2012**, *51*, 8082 –8086
- (14) Shuo Liu et al. Mechanism of MTO-Catalyzed Deoxydehydration of Diols to Alkenes Using Sacrificial Alcohols. *Organometallics* **2013**, *32*, 3210–3219

- (15) Vkuturi, Saidi; Chapman, Garry; Ahmad, Irshad; Nicholas, Kenneth M. Rhenium-Catalyzed Deoxydehydration of Glycols by Sulfite. *Inorg. Chem.* **2010**, *49*, 4744–4746 DOI: 10.1021/ic100467p
- (16) Michael McClain, J.; Nicholas, K. M. Elemental Reductants for the Deoxydehydration of Glycols. *ACS Catal.* **2014**, *4* (7), 2109–2112. <https://doi.org/10.1021/cs500461v>.
- (17) Boucher-Jacobs, C.; Nicholas, K. M. Oxo-Rhenium-Catalyzed Deoxydehydration of Polyols with Hydroaromatic Reductants. *Organometallics* **2015**, *34* (10), 1985–1990. <https://doi.org/10.1021/acs.organomet.5b00226>.
- (18) Liu, P.; Nicholas, K. M. Mechanism of Sulfite-Driven,  $\text{MeReO}_3$ -Catalyzed Deoxydehydration of Glycols. *Organometallics* **2013**, *32* (6), 1821–1831. <https://doi.org/10.1021/om301251z>.
- (19) Dethlefsen, J. R.; Lupp, D.; Oh, B. C.; Fristrup, P. Molybdenum-Catalyzed Deoxydehydration of Vicinal Diols. *ChemSusChem* **2014**, *7* (2), 425–428. <https://doi.org/10.1002/cssc.201300945>.
- (20) Sandbrink, L.; Beckerle, K.; Meiners, I.; Liffmann, R.; Rahimi, K.; Okuda, J.; Palkovits, R. Supported Molybdenum Catalysts for the Deoxydehydration of 1,4-Anhydroerythritol into 2,5-Dihydrofuran. *ChemSusChem* **2017**, *10* (7), 1375–1379. <https://doi.org/10.1002/cssc.201700010>.
- (21) Beckerle, K.; Sauer, A.; Spaniol, T. P.; Okuda, J. Bis(Phenolato)Molybdenum Complexes as Catalyst Precursors for the Deoxydehydration of Biomass-Derived Polyols. *Polyhedron* **2016**, *116*, 105–110. <https://doi.org/10.1016/j.poly.2016.03.053>.
- (22) Tran, R.; Kilyanek, S. M. Deoxydehydration of Polyols Catalyzed by a Molybdenum Dioxo-Complex Supported by a Dianionic ONO Pincer Ligand. *Dalton Trans.* **2019**, *48* (43), 16304–16311. <https://doi.org/10.1039/C9DT03759D>.
- (23) Stalpaert, M.; De Vos, D. Stabilizing Effect of Bulky  $\beta$ -Diketones on Homogeneous Mo Catalysts for Deoxydehydration. *ACS Sustainable Chemistry & Engineering* **2018**, *6* (9), 12197–12204. <https://doi.org/10.1021/acssuschemeng.8b02532>.
- (24) Hills, L.; Moyano, R.; Montilla, F.; Pastor, A.; Galindo, A.; Álvarez, E.; Marchetti, F.; Pettinari, C. Dioxomolybdenum(VI) Complexes with Acylpyrazolonate Ligands: Synthesis, Structures, and Catalytic Properties. *European Journal of Inorganic Chemistry* **2013**, *2013* (19), 3352–3361. <https://doi.org/10.1002/ejic.201300098>.
- (25) Huynh, M. H. V.; Meyer, T. J. Proton-Coupled Electron Transfer. *Chem. Rev.* **2007**, *107* (11), 5004–5064. <https://doi.org/10.1021/cr0500030>.
- (26) Mayer, J. M. Proton-Coupled Electron Transfer: A Reaction Chemist's View. *Annual Review of Physical Chemistry* **2004**, *55* (1), 363–390. <https://doi.org/10.1146/annurev.physchem.55.091602.094446>.

## Chapter 2

### Deoxydehydration Catalyzed by Dioxo(pyridine-2,6-dicarboxylato)(hexamethylphosphoramide)molybdenum(VI)

Fossil fuels supply 80% of the world's energy needs but the imminent threat of climate change from increasing CO<sub>2</sub> levels has spurred a race for a greener energy economy in the 21<sup>st</sup> century.<sup>1</sup> One facet of the greener energy economy is the conversion of modern biomass into liquid biofuels and industrial commodity chemicals. Modern biomass refers to the leftover carbohydrates from the production of sugar cane, corn, and sorghum. Conversion of these materials is advantageous from an energy density stance; a kilojoule worth of energy in solid biomass occupies more volume than liquid biomass of same energy. The leftover carbohydrates must be deoxygenated to convert them into liquid biofuels and current industry processes are reliant on steam reforming and cracking via harsh conditions or precious metal catalysts.<sup>2</sup>

Deoxydehydration (DODH) is an alternative method to reduce the carbohydrates at relatively lower temperatures and is not reliant on precious metal catalysts. DODH is the net reduction diols and polyols into alkenes and dienes using a poly-oxo metal catalyst. First reported in 1996 by Cook and Andrews,<sup>3</sup> they demonstrated the quantitative conversion of 1-phenyl-1,2-ethanediol into styrene using pentamethylcyclopentadienyl trioxorhenium(VII) (Cp\*ReO<sub>3</sub>) and triphenylphosphine (PPh<sub>3</sub>) as reductant/oxygen acceptor in chlorobenzene with 55 turnovers/Re atom. They proposed a catalytic cycle comprised of 1) Reduction of Cp\*Re<sup>VII</sup>O<sub>3</sub> to Cp\*Re<sup>VO</sup><sub>2</sub> 2) Ketalization of substrate to reduced catalyst forming the diolate structure 3) Extrusion of the olefin product and regeneration of Cp\*Re<sup>VII</sup>O<sub>3</sub>. Further studies showed that the catalyst could become over reduced, Re(III), effectively killing catalytic activity. Kinetic studies demonstrated the relation between the over reduction ( $k_{5/3}$ ) and diolate formation ( $k_{ket}$ ) to be dependent on the solvent's ability to hydrogen bond. They found that  $k_{ket}/k_{5/3}$  was higher in benzene (60) and lower in tetrahydrofuran (2); this is because the hydrogen bonding ability of

THF slows the ketalization. Efforts to minimize this were successful but required the use of a cocatalyst (p-toluenesulfonic acid) or less active reductants such as tris(perfluorophenyl)phosphine. The yields were comparable but due to the requirement of these additional or weaker components, DODH fell into relative obscurity until recently.

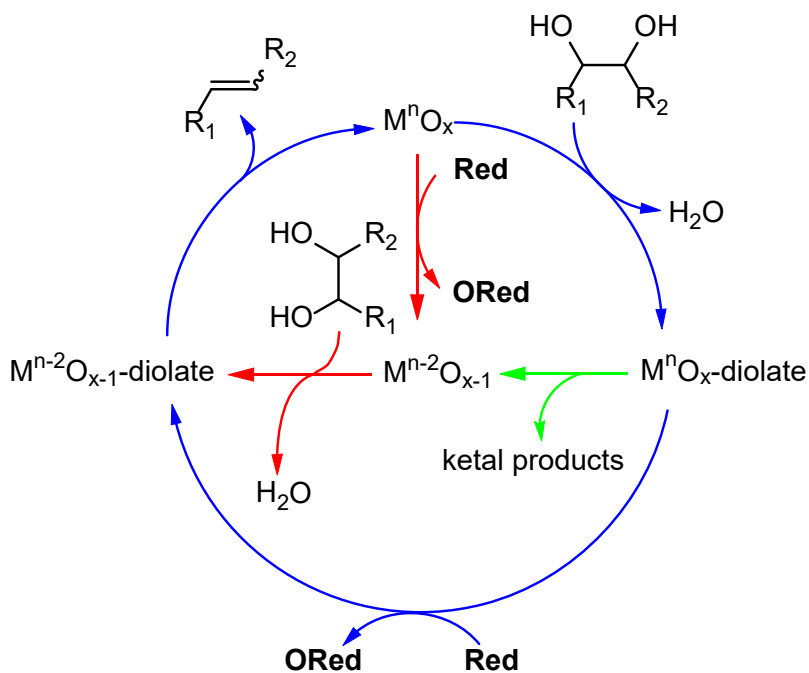


**Figure 1.** The competitive mechanisms of DODH

The Toste group in 2012 reported an effective DODH catalyst in methyltrioxorhenium(VII) (MTO).<sup>4</sup> They demonstrated 90% yield of glycerol to alkene using 3-octanol as reductant. They were able to achieve similar results with other sugar alcohols as well. This report helped to reignite the development of DODH. The Abu-Omar group also explored MTO-catalyzed DODH and studied its mechanism using sacrificial alcohol reductants and aromatic diols as substrates. They reported that the MTO-catalyzed DODH may proceed via two possible pathways: either the reduction of catalyst may occur first followed by ketalization/diolate formation or vice versa.<sup>5</sup> Both pathways are ultimately recycled by the extrusion of olefin product. The Nicholas group expanded the reductant scope of MTO showing

that sulfites<sup>6</sup>, dihydroaromatics<sup>7</sup>, elemental compounds (Zn, Fe, Mn, C)<sup>8</sup>, and reducing gases (H<sub>2</sub> and CO)<sup>9</sup> are able to reduce metal catalysts. They studied the mechanism of MTO-catalyzed DODH using sodium sulfite and confirmed computationally that the reduction by sulfite occurs before diolate formation. They applied these new features to novel vanadium-based catalysts active for DODH observing lower yields than rhenium but demonstrated that more abundant transition metals are capable of catalyzing DODH.<sup>10,11</sup>

This revelation spurred researchers to test other transition metals for potential catalytic activity. Fristrup et al demonstrated the first molybdenum-based catalysts active for DODH.<sup>12</sup> Notable among them was the commercially available ammonium heptamolybdate ((NH<sub>4</sub>)<sub>6</sub>Mo<sub>7</sub>O<sub>24</sub> • 4H<sub>2</sub>O, AHM), able to catalyze the transformation of 1,2-hexanediol into 1-hexene, albeit with lower yields and higher temperatures than rhenium systems. The low yields are explained by the competing side reactions, namely the C-C bond cleavage that can occur at the oxo-diolate structure. The novelty was that molybdenum can perform the catalytic transformation spurring further research into other molybdenum-based catalysts. AHM has been shown to use simple secondary alcohols as reductant<sup>13</sup> yielding up to 49% olefin product and it has been reported that the olefin yield can be increased with a variety of additives.<sup>14</sup> Other molybdenum-based catalysts have been reported to be active for DODH.<sup>15-18</sup>

Herein we report the DODH over a wide substrate and reductant scope catalyzed by a dioxomolybdenum(VI) supported by a dianionic ONO pincer ligand. Mechanistic and kinetic aspects of this system are considered.

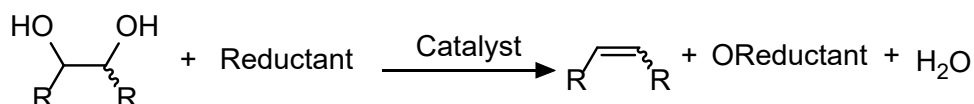
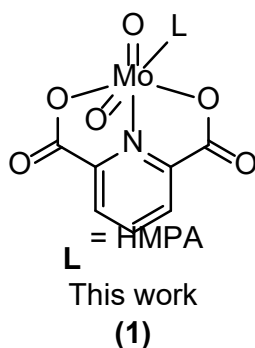


**Figure 2.** Molybdenum DODH catalyst and general reaction scheme.

## Results and Discussion

### DODH of 1-phenyl-1,2-ethanediol, Reductant Scope.

The transformation of 1-phenyl-1,2-ethanediol to styrene with  $\text{PPh}_3$  was catalyzed by **1**. We observed high selectivity for styrene, evidenced by the <4% formation of aldehyde side products. Heating the reaction for 30 minutes yielded 45% major product. Further heating led to decrease of yields, down to 13% after 22 hours. Close examination of  $^1\text{H}$  NMR spectra showed the characteristic peaks of the polystyrene and that the decrease in yield was due to the polymerization of styrene into polystyrene.<sup>19</sup> The chemical shifts for these two compounds are distinct from the other. This suggests that there is some in-situ radical process causing the polymerization to compete with DODH, likely the  $\text{Mo(VI)}$  and  $\text{Mo(IV)}$  dimerize and form a  $\text{Mo(V)-Mo(V)}$   $d^1$  species. Yields up to 65% were achieved before product decline occurred. The complete polymerization of styrene was never observed, indicative of some process terminating or inhibiting complete polymerization. Efforts to inhibit polymerization using a known polymerization inhibitor, p-hydroquinone, were tested.<sup>20</sup> Control reactions were performed to test if the polymerization inhibitor could also act as reductant. Small amounts of styrene were formed but it is readily outperformed by  $\text{PPh}_3$ . The resulting data showed that while the inhibition

was successful, higher yields were not achieved. Catalyst loading was lowered as another attempt to disfavor polymerization, but results showed significantly lower product yields. Conversion quantitation by GC/MS showed complete conversion of substrate.  $\text{PPh}_3$  was replaced with a bulky analogue, tris(o-tolyl)phosphine. Predictably, the yield of styrene is considerably less than when  $\text{PPh}_3$  is used as reductant. After 4 hours at  $190^\circ\text{C}$ , 31% C=C was generated. There was no polymerization detected by NMR however further heating did not increase the yield.

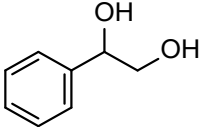
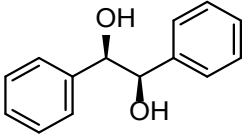
Secondary alcohols are an attractive reductant due to the low cost and the relatively benign ketones formed after reducing the catalyst. A hydrogen atom transfer from the alcohol onto the oxo group of the metal leads to coordination of the alkoxy moiety. Subsequent hydrogen transfer forms water and oxidizes the alkoxy group into the ketone and reduces the metal. Three secondary alcohols were tested: 2-propanol, 3-octanol, and 1-phenylethanol. 2-propanol proved to be the best among them, affording 23% C=C and 8% C=O after 24 hours of heating; further heating did not achieve higher yields. 3-octanol was not a strong reductant, only capable of 14%. Upon further heating the product yield was observed to decline and polymerization of styrene was observed. 1-phenylethanol was tested as a bulkier analogue of 2-propanol with the hypothesis that the additional steric bulk would increase the rate of olefin extrusion. Nicholas computationally derived the mechanism of sulfite-driven DODH catalyzed by MTO noting that there is some coordination of the sulfate occurring at the olefin extrusion step. The bulk of the acetophenone should then help make the extrusion more favorable by increasing the energy of the transition state. Unfortunately yields above 5% were never observed and an equal 5% yield of aldehyde side product informs us that under this regime, DODH occurs exclusively by the C-C bond cleavage path. Elemental reductants such as zinc and activated carbon were shown to perform better than the secondary alcohols. Zinc catalyzed yields up to 32% C=C and 11% C=O in 3 hours of heating. Activated carbon achieved similar

yields, 31% C=C and 10% C=O after 3 hours. Further heating did not increase major product yields for either reductant. Sodium sulfite was shown to perform nearly as well as the elemental reductants but slightly more selective, 29% C=C and 6% C=O.

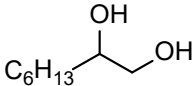
Tri(*o*-tolyl) phosphine was tested as the bulkier analogue of PPh<sub>3</sub>. As expected, the catalytic activity is much slower compared to PPh<sub>3</sub>. It does not achieve comparable yields to PPh<sub>3</sub>; yields up to 30% were observed after 6 hours of heating, further heating did not result in increased yield. However, aldehyde yields up to 11% were observed in the NMR. This means that 20% of the observed yield was catalyzed by the reductant. A total of three turnovers were observed but only two of those arose from the preferred reduction pathway. The R,S trans-1,2-cyclohexanediol was tested as substrate for DODH using PPh<sub>3</sub> as reductant. This diol yielded substoichiometric amounts of 1-cyclohexene after 155 hours of heating. This was to be expected DODH typically requires R,R or S,S diols in order to afford turnover. Testing this, cis-1,2-cyclohexanediol was tested as substrate with only PPh<sub>3</sub> as reductant to test the need for R,R/S,S vicinal diols. Yields up to 30% of 1-hexene were detected after 24 hours of heating. The acyclic 1,2-octanediol showed higher activity than the cyclic diols. Initial experiments of the catalyst at 20 mM with 1,2-octanediol showed low yields after 48h, just over one turnover of catalyst. However, when the concentration of the catalyst was increased to 40 mM, the yield was increased. After 24 hours of heating the catalyst yielded 38% major product; subsequent heating was only able to push the product yield to 41% after 128 hours using PPh<sub>3</sub> as reductant. 2-propanol was the next most competent reductant; it afforded yields up to 32% C=C after 72 hours of heating. Sugar alcohols are a popular substrate for DODH due to the high amounts present in nature. Meso-erythritol did not yield the expected linear alkene but instead yielded 2,5-dihydrofuran as the major product. <sup>1</sup>H NMR analysis showed only the furan product; formation of this product suggests that after the initial DODH giving 1,4-dihydroxy-2-butene there is some dehydrating cyclization reaction happening to give the furan product. Resonances

belonging to butene were not observed in the spectra suggesting that the dehydrating cyclization is a more rapid process than the NMR timescale. The only reductants that afforded any turnover were PPh<sub>3</sub> and elemental carbon, 15% and 9%, respectively. The other reductants showed substoichiometric yield by NMR. 1,4-anhydroerythritol showed higher yields than meso-erythritol. The best reductant was PPh<sub>3</sub>, affording an average of 23% C=C after 48 hours. The other reductants afforded lower yields; the only reductants that were mildly comparable to PPh<sub>3</sub> were elemental carbon and 3-octanol.

**Table 1: Summary of Catalytic Activity of 1 at 190°C**

Diol	Reductant	t (h)	%C=C	%C=O	%PS	
	PPh <sub>3</sub>	1	49	3	21	
	PPh <sub>3</sub> <sup>a,b</sup>	6	27,69	17,4	52 <sup>a</sup> ,0 <sup>b</sup>	
	Carbon	3	31	10	-	
	Zinc	3	32	11	-	
	Na <sub>2</sub> SO <sub>3</sub>	3	29	6	-	
	3-octanol	2	12	2	-	
	2-propanol	24	23	8	-	
	1-Ph-EtOH	24	2	6	-	
		PPh <sub>3</sub>	2	44	52	-
		Carbon	2	38	49	-
Zinc		2	41	56	-	
Na <sub>2</sub> SO <sub>3</sub>		2	41	51	-	
3-octanol		2	32	55	-	
2-propanol		2	34	46	-	
1-Ph-EtOH		2	35	44	-	

**Table 1: Summary of Catalytic Activity of 1 at 190°C (cont.)**

Diol	Reductant	t (h)	%C=C	%C=O	%PS
	PPh <sub>3</sub>	24	31	0	-
	Carbon	24	17	0	-
	Zinc	48	32	0	-
	Na <sub>2</sub> SO <sub>3</sub>	24	8	0	-
	3-octanol	48	18	0	-
	2-propanol	72	32	0	-
	1-Ph-EtOH	24	10	0	-

DODH of (R,R)-(+)-hydrobenzoin, Reductant Scope.

(R,R)-(+)-hydrobenzoin proved to be non-reactive to most reductants screened. Complete conversion of substrate was observed but the DODH of this substrate exclusively follows the deformylation pathway. Aldehyde yields at or nearly at 50% coincided with an equivalent yield of trans-stilbene. The PPh<sub>3</sub> was observed to be a little active, yields of 55% were achieved, a sign that says some of the transformation occurred in part by the reduction via PPh<sub>3</sub>. Some experiments showed less than 50% yield of trans-stilbene while observing 50% aldehyde. The discrepancy lies in the hemi-acetal equilibrium previously reported for this diol. Benzaldehyde, the side product, undergoes an equilibrium with the diol forming 2,4,5-triphenyl-1,3-dioxolane. This equilibrium eventually favors the entropic outcome as the diol is consumed by the on-cycle pathway.

Kinetic Studies of 1-phenyl-1,2-ethanediol and PPh<sub>3</sub>

In-situ infrared spectroscopy was used to probe the mechanism of this particular system due to its relatively higher yields than other substrate/reductant combinations. OPPh<sub>3</sub> was used

as the kinetic handle for monitoring the reaction due its abundance at high yields. Experiments following catalytic conditions (10% catalyst loading) exhibited complex kinetics and low yields; instrument limitations led to max heating temperature of 110°C. We sought to simplify them by increasing the reductant loading to a pseudo first order regime, 100x relative to catalyst. The resulting data suggests that the growth of OPPh<sub>3</sub> is biexponential, that is, a linear combination of two exponential terms. We posit that the first exponential term is the initial generation of OPPh<sub>3</sub>. Control experiments have shown that the catalyst is readily reduced by PPh<sub>3</sub> at ambient temperature and pressure suggesting that at elevated temperatures the reduction would occur more rapidly. Additional controls have shown that, while not as rapid as the reduction, diolate condensation does occur in a heated solution of catalyst and diol, evidenced by for formation of aldehyde product. Therefore, the second exponential term must be dependent on the rate of olefin extrusion. The first reduction would generate the OPPh<sub>3</sub> and the reduced Mo(IV). The coordination of the diol was demonstrated to be facile at elevated temperature. The second exponential term is the immediate growth of OPPh<sub>3</sub> after the olefin extrusion has occurred. It has been widely reported that the olefin extrusion step is the rate determining step of DODH. If  $k_{red} \gg k_{RDS}$  then the second exponential term is approximately the rate of olefin extrusion.

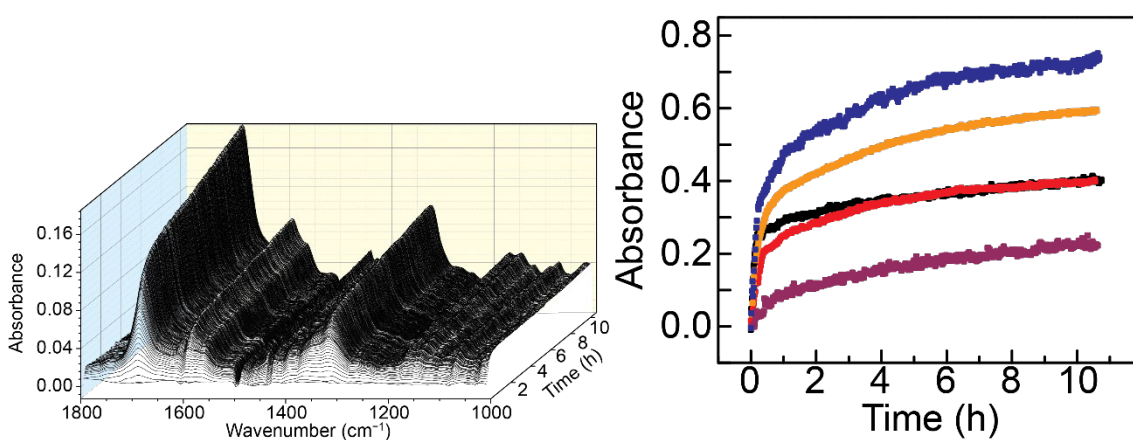


**Figure 3.** Left: Sample spectra of in-situ FTIR. Right: OPPh<sub>3</sub> reaction growth profiles as a function of time. Pseudo-first order in PPh<sub>3</sub> (blue and orange), 10% catalyst loading (red and black), Pseudo-first order in PPh<sub>3</sub> with exogenous OPPh<sub>3</sub> (purple).

Additional in-situ experiments were performed in pseudo-first order with respect to the diol. There was no product yield, no growth of  $\text{OPPh}_3$ , and only trace amounts of aldehyde were observed. This is informative of the pathway preference for this system; the catalyst catalyzes DODH by initial reduction then followed by diol condensation and then ultimately recycled by olefin extrusion. Trace aldehyde products suggest that there is formation of the oxo-diolate and mono-oxo Mo(IV) by deformylation. However, no product formation was observed when reacted with excess diol so after the C-C bond cleavage to generate the reduced species from the oxo-diolate there is some off cycle process that does not allow for useful catalysis.

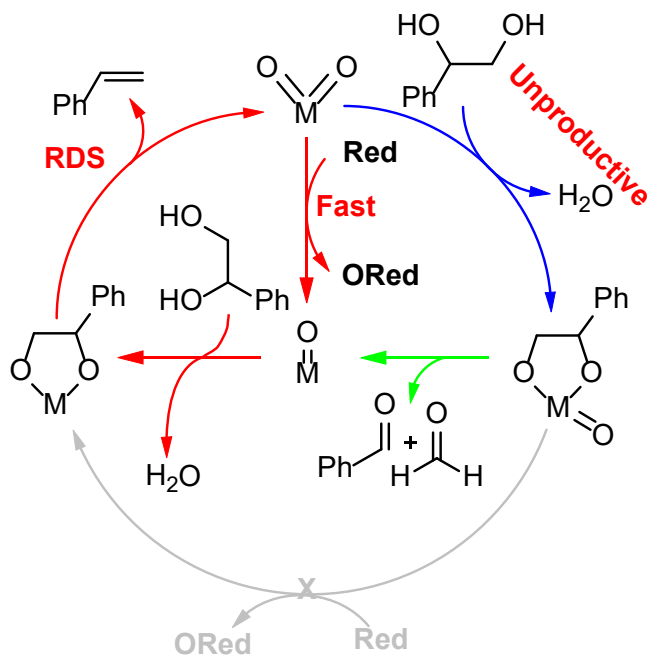


**Figure 4.** Specific mechanism of the DODH of 1-phenyl-1,2-ethanediol.

#### Kinetic Studies of (R,R)-(+)-hydrobenzoin

The kinetics of the DODH of hydrobenzoin were studied with in-situ FTIR. Regardless of reductant loading and scope, the reaction proceeded via the C-C bond cleavage path. The growth of C=O aldehyde stretches was monitored. Its growth was observed to be a linear combination of two bi-exponential processes that occur in different times of reaction. The initial rapid linear rise of C=O stretch is attributed to the rapid self-oxidation of the hydrobenzoin



## Dehydration.

Experiments testing secondary alcohols as reductants were observed to form some amount of the dehydrated reductant suggesting some ability for dehydration activity. This was observed to occur when 3-octanol and 1-phenylethanol were the reductants. 1-phenylethanol was not a competent reductant due to the relatively lower yields of major product. However, trace amounts of dehydrogenated reductant, styrene, was observed. This was also observed when 3-octanol as reductant. The dehydration product of 2-propanol, propylene, was not observed in any experiment.

## Conclusions

$\text{MoO}_2(\text{dipic})(\text{HMPA})$  was observed to be a competent DODH catalyst. It affords the modest yet selective transformation of 1-phenyl-1,2-ethanediol into styrene but is outcompeted by radical polymerization. Efforts to inhibit the polymerization while maintaining yields were successful. It affords the complete conversion of diol into trans-stilbene exclusively through the C-C bond cleavage pathway. Cis-diols were required for reactivity as shown in the E/Z-1,2-cyclohexanediol. This catalyst was shown to catalyze the transformation of aromatic diols over more traditional carbohydrate derived diols. The substrate dependent mechanism of this catalyst was studied. Styrene glycol was shown to DODH by reduction of the catalyst before diolate formation occurred. A biexponential growth was observed for  $\text{OPPh}_3$  where the second exponential component could be used to model the rate of olefin extrusion. (R,R)-(+)-hydrobenzoin was shown to only proceed by the reductant independent pathway that limits the maximum alkene product at 50%.

## Experimental Procedure

General comments: Reagents were obtained commercially and used without further purification. Solvents were obtained from Aldrich and placed over 3Å molecular sieves. All reactions were prepared in an inert nitrogen atmosphere using standard Schlenk or glovebox techniques unless otherwise noted.  $^1\text{H}$  NMR was referenced to solvent residual signals (chloroform-*d*  $\delta = 7.26$  methylenechloride-*d*<sub>2</sub>,  $\delta = 5.32$ ) and yields were determined by internal standard: (1,3,5-trimethoxybenzene,  $\delta = 3.32$  (s, 9H, OCH<sub>3</sub>)  $\delta = 6.13$  (s, 3H, aryl H)) or (hexamethylcyclotrisiloxane,  $\delta = 0.17$  (s, 18H, CH<sub>3</sub>)).

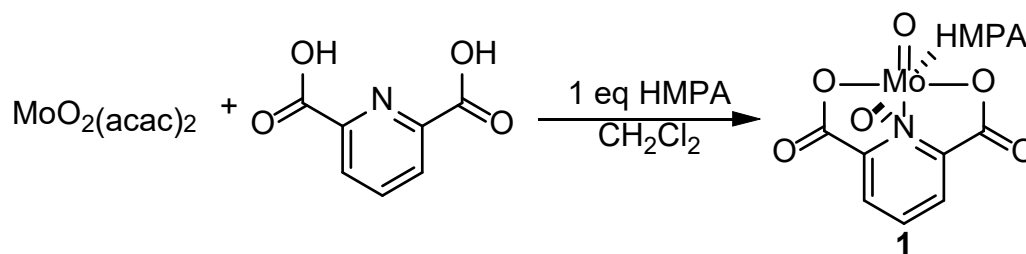


**Figure 6.** Synthesis of **1**.

Synthesis of **1**.<sup>21</sup> Equimolar amounts of  $\text{MoO}_2(\text{acac})_2$  (2157.5 mg, 6.62 mmol), pyridine-2,6-dicarboxylic acid (1107.7 mg, 6.63 mmol), and hexamethylphosphoramide (HMPA, 1.15 mL, 6.61 mmol) were suspended with dichloromethane (45 mL, 0.15 M). The solution was stirred for 24 hours at ambient temperature under inert atmosphere and then was filtered to remove any unreacted solids. Purification was done by trituration in diethyl ether. The solid was filtered and dried under vacuum resulting in white powder. (2840.1 mg, Yield: 91%) –  $^1\text{H}$  NMR (500 MHz,  $\text{CD}_2\text{Cl}_2$ ):  $\delta = 2.41$  (d,  $J = 10$  Hz, 18H, HMPA), 8.27 (d,  $J = 8$  Hz, 2H, aryl H), 2.014 (t,  $J = 8$  Hz, aryl H).

General Procedure for Catalytic Reactions. A pressure tube with threaded Teflon cap or an NMR tube equipped with a J Young valve was charged with **1**, reductant, diol, and internal standard in a stoichiometric molar ratio of 1:10:10:5. Solvent was added to reach a concentration of 40 mM. NMR spectroscopy were obtained at 298K on a Bruker DRX-500 or a

AVANCE-III-400 at 500MHz and 400MHz respectively using 1,3,5-trimethoxybenzene or hexamethylcyclotrisiloxane as an internal standard. The reaction was placed into a preheated silicon oil bath with a thermo-coupled temperature probe (190°C). The preferred substrates are PPh<sub>3</sub> and 1-phenyl-1,2-ethanediol at 190°C. Analysis of yield was done by <sup>1</sup>H NMR or GC/MS.

Kinetic Study. In-situ IR experiments were performed using a Mettler-Toledo ReactIR whose probe was equipped with a diamond tipped ATR crystal. Reactions were run at 110°C in tetrachloroethylene (TCE) and toluene. The spectral window was 4000-1000 cm<sup>-1</sup> to avoid interference from Mo=O stretches. IR experiments were run in the same concentrations as catalytic experiments and with reductant or diol in excess (approx. 100 times the catalyst). Experiments were run in 3 necked round bottom flasks under positive N<sub>2</sub> pressure. The flask necks held the IR probe, a reflux condenser, and a rubber septum. Solvent, reductant, diol, and OPPh<sub>3</sub> were added sequentially into preheated solvent (110°C). Spectra and backgrounds were taken after each addition to the flask taking care to replace the atmosphere with positive N<sub>2</sub> pressure. Reaction spectra were recorded every minute. After a few scans, the catalyst was added in with the aid of reaction solvent. The reaction was run from 12h-48h with 1 scan/minute. The growth of OPPh<sub>3</sub> was used as a handle to monitor the reaction. Analytical software separated the reaction spectra into its components and then those components were converted to relative abundance vs time plots. Kinetic treatment of the data was applied, and yields were obtained by <sup>1</sup>H NMR.

## References

- (1) United Nations Development Program. *World Energy Assessment: Energy and the Challenge of Sustainability*. United Nations, New York. 2000.
- (2) Denike, K. A.; Kilyanek, S. M. Deoxydehydration of Vicinal Diols by Homogeneous Catalysts: A Mechanistic Overview. *R. Soc. open sci.* 2019, 6, 191165.
- (3) Cook, G. K.; Andrews, M. A. Toward Nonoxidative Routes to Oxygenated Organics: Stereospecific Deoxydehydration of Diols and Polyols to Alkenes and Allylic Alcohols Catalyzed by the Metal Oxo Complex (C<sub>5</sub>Me<sub>5</sub>)ReO<sub>3</sub>. *Journal of the American Chemical Society* **1996**, 118 (39), 9448–9449. <https://doi.org/10.1021/ja9620604>.
- (4) Shiramizu, M.; Toste, F. D. Deoxygenation of Biomass-Derived Feedstocks: Oxorhenium-Catalyzed Deoxydehydration of Sugars and Sugar Alcohols. *Angew. Chem. Int. Ed.* **2012**, 51 (32), 8082–8086. <https://doi.org/10.1002/anie.201203877>.
- (5) Liu, S.; Senocak, A.; Smeltz, J. L.; Yang, L.; Wegenhart, B.; Yi, J.; Kenttämaa, H. I.; Ison, E. A.; Abu-Omar, M. M. Mechanism of MTO-Catalyzed Deoxydehydration of Diols to Alkenes Using Sacrificial Alcohols. *Organometallics* **2013**, 32 (11), 3210–3219. <https://doi.org/10.1021/om400127z>.
- (6) Ahmad, I.; Chapman, G.; Nicholas, K. M. Sulfite-Driven, Oxorhenium-Catalyzed Deoxydehydration of Glycols. *Organometallics* **2011**, 30 (10), 2810–2818. <https://doi.org/10.1021/om2001662>.
- (7) Boucher-Jacobs, C.; Nicholas, K. M. Oxo-Rhenium-Catalyzed Deoxydehydration of Polyols with Hydroaromatic Reductants. *Organometallics* **2015**, 34 (10), 1985–1990. <https://doi.org/10.1021/acs.organomet.5b00226>.
- (8) Michael McClain, J.; Nicholas, K. M. Elemental Reductants for the Deoxydehydration of Glycols. *ACS Catal.* **2014**, 4 (7), 2109–2112. <https://doi.org/10.1021/cs500461v>.
- (9) Gopaladasu, T. V.; Nicholas, K. M. Carbon Monoxide (CO)- and Hydrogen-Driven, Vanadium-Catalyzed Deoxydehydration of Glycols. *ACS Catalysis* **2016**, 6 (3), 1901–1904. <https://doi.org/10.1021/acscatal.5b02667>.
- (10) Galindo, A. DFT Studies on the Mechanism of the Vanadium-Catalyzed Deoxydehydration of Diols. *Inorganic Chemistry* **2016**, 55 (5), 2284–2289. <https://doi.org/10.1021/acs.inorgchem.5b02649>.
- (11) Chapman, G.; Nicholas, K. M. Vanadium-Catalyzed Deoxydehydration of Glycols. *Chemical Communications* **2013**, 49 (74), 8199. <https://doi.org/10.1039/c3cc44656e>.
- (12) Dethlefsen, J. R.; Lupp, D.; Oh, B. C.; Fristrup, P. Molybdenum-Catalyzed Deoxydehydration of Vicinal Diols. *ChemSusChem* **2014**, 7 (2), 425–428. <https://doi.org/10.1002/cssc.201300945>.

- (13) Dethlefsen, J. R.; Lupp, D.; Teshome, A.; Nielsen, L. B.; Fristrup, P. Molybdenum-Catalyzed Conversion of Diols and Biomass-Derived Polyols to Alkenes Using Isopropyl Alcohol as Reductant and Solvent. *ACS Catalysis* **2015**, 3638–3647. <https://doi.org/10.1021/acscatal.5b00427>.
- (14) Sandbrink, L.; Beckerle, K.; Meiners, I.; Liffmann, R.; Rahimi, K.; Okuda, J.; Palkovits, R. Supported Molybdenum Catalysts for the Deoxydehydration of 1,4-Anhydroerythritol into 2,5-Dihydrofuran. *ChemSusChem* **2017**, 10 (7), 1375–1379. <https://doi.org/10.1002/cssc.201700010>.
- (15) Beckerle, K.; Sauer, A.; Spaniol, T. P.; Okuda, J. Bis(Phenolato)Molybdenum Complexes as Catalyst Precursors for the Deoxydehydration of Biomass-Derived Polyols. *Polyhedron* **2016**, 116, 105–110. <https://doi.org/10.1016/j.poly.2016.03.053>.
- (16) Stalpaert, M.; De Vos, D. Stabilizing Effect of Bulky  $\beta$ -Diketones on Homogeneous Mo Catalysts for Deoxydehydration. *ACS Sustainable Chemistry & Engineering* **2018**, 6 (9), 12197–12204. <https://doi.org/10.1021/acssuschemeng.8b02532>.
- (17) Navarro, C. A.; John, A. Deoxydehydration Using a Commercial Catalyst and Readily Available Reductant. *Inorganic Chemistry Communications* **2019**, 99, 145–148. <https://doi.org/10.1016/j.inoche.2018.11.015>.
- (18) Tran, R.; Kilyanek, S. M. Deoxydehydration of Polyols Catalyzed by a Molybdenum Dioxo-Complex Supported by a Dianionic ONO Pincer Ligand. *Dalton Transactions* **2019**, 48 (43), 16304–16311. <https://doi.org/10.1039/C9DT03759D>.
- (19) Cudaj, M.; Cudaj, J.; Hofe, T.; Luy, B.; Wilhelm, M.; Guthausen, G. Polystyrene Solutions: Characterization of Molecular Motional Modes by Spectrally Resolved Low- and High-Field NMR Relaxation. *Macromolecular Chemistry and Physics* **2012**, 213 (17), 1833–1840. <https://doi.org/10.1002/macp.201200092>.
- (20) Tudos, Ferenc; Foldes-Bereznich, Tamara. Free-radical polymerization: Inhibition and Retardation. *Progress in Polymer Science* **1989**, 14 (6), 717-761. [https://doi.org/10.1016/0079-6700\(89\)90008-7](https://doi.org/10.1016/0079-6700(89)90008-7).
- (21) Liebeskind, L. S.; Sharpless, K. B.; Wilson, R. D.; Ibers, J. A. The First D0 Metallooxaziridines. Amination of Olefins. *Journal of the American Chemical Society* 1978, 100 (22), 7061–7063. <https://doi.org/10.1021/ja00490a047>.

## Supporting Information

### NMR characterizations

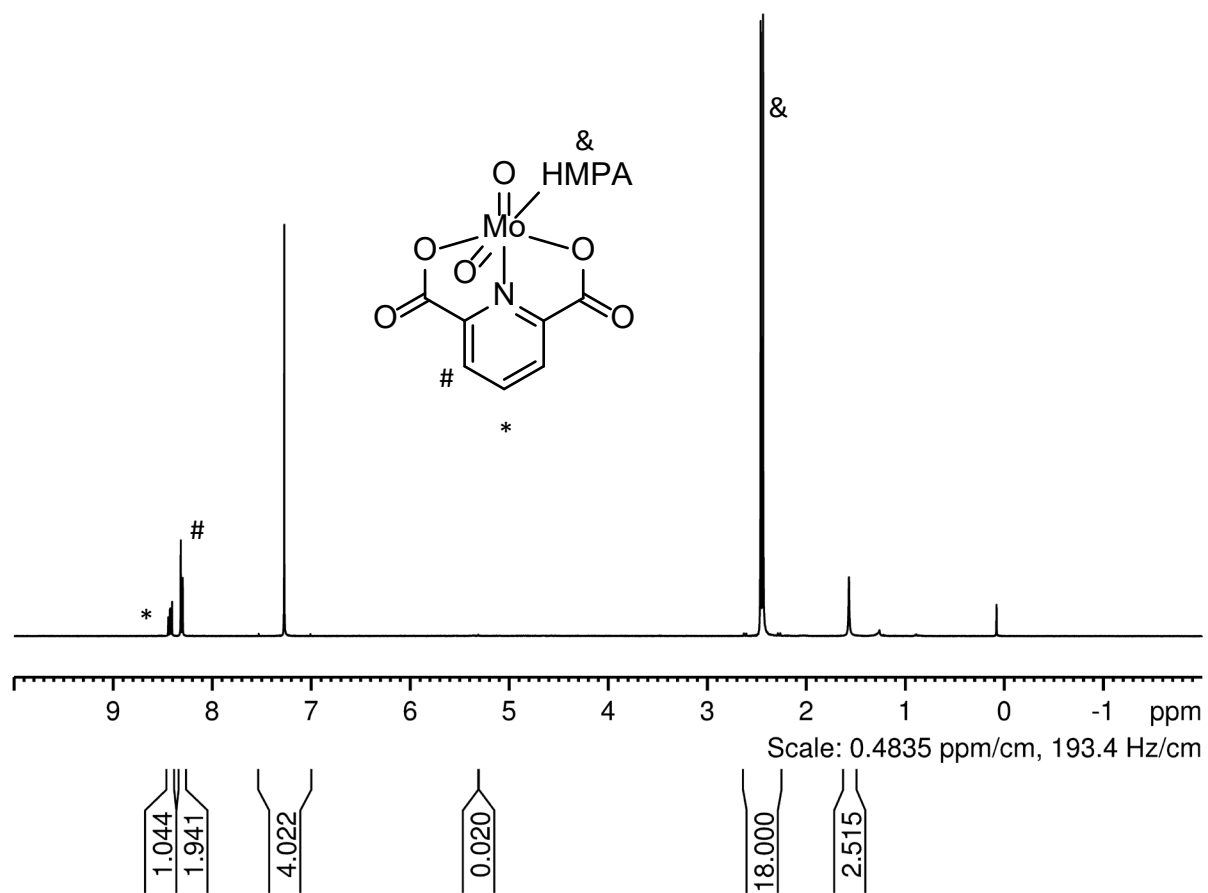
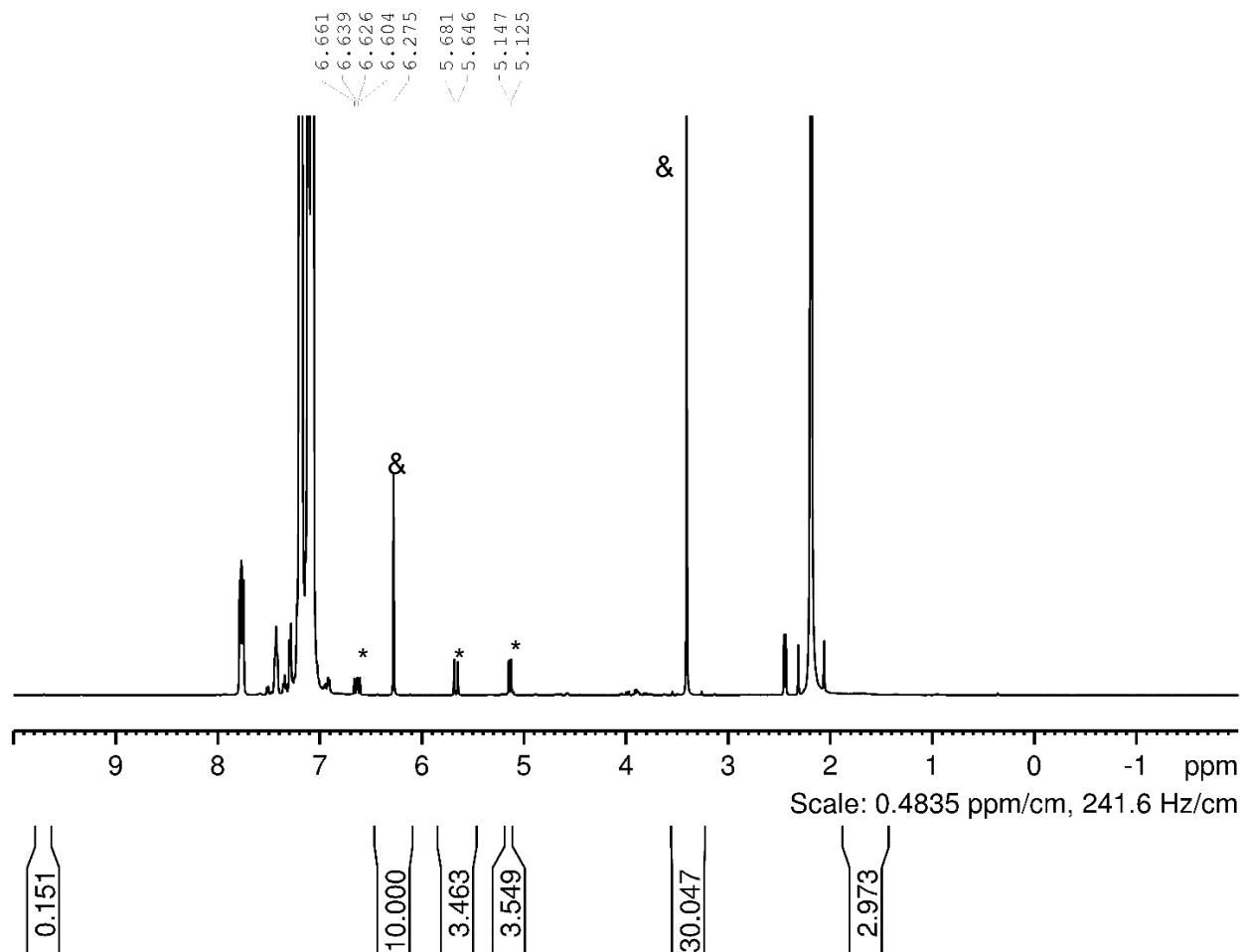


Figure S1.  $^1\text{H}$  NMR of **1**



**Figure S2. 1**, PPh<sub>3</sub>, 1-phenyl-1,2-ethanediol. Toluene, 190°C 1h

“\*” = styrene

“&” = 1,3,5-trimethoxybenzene

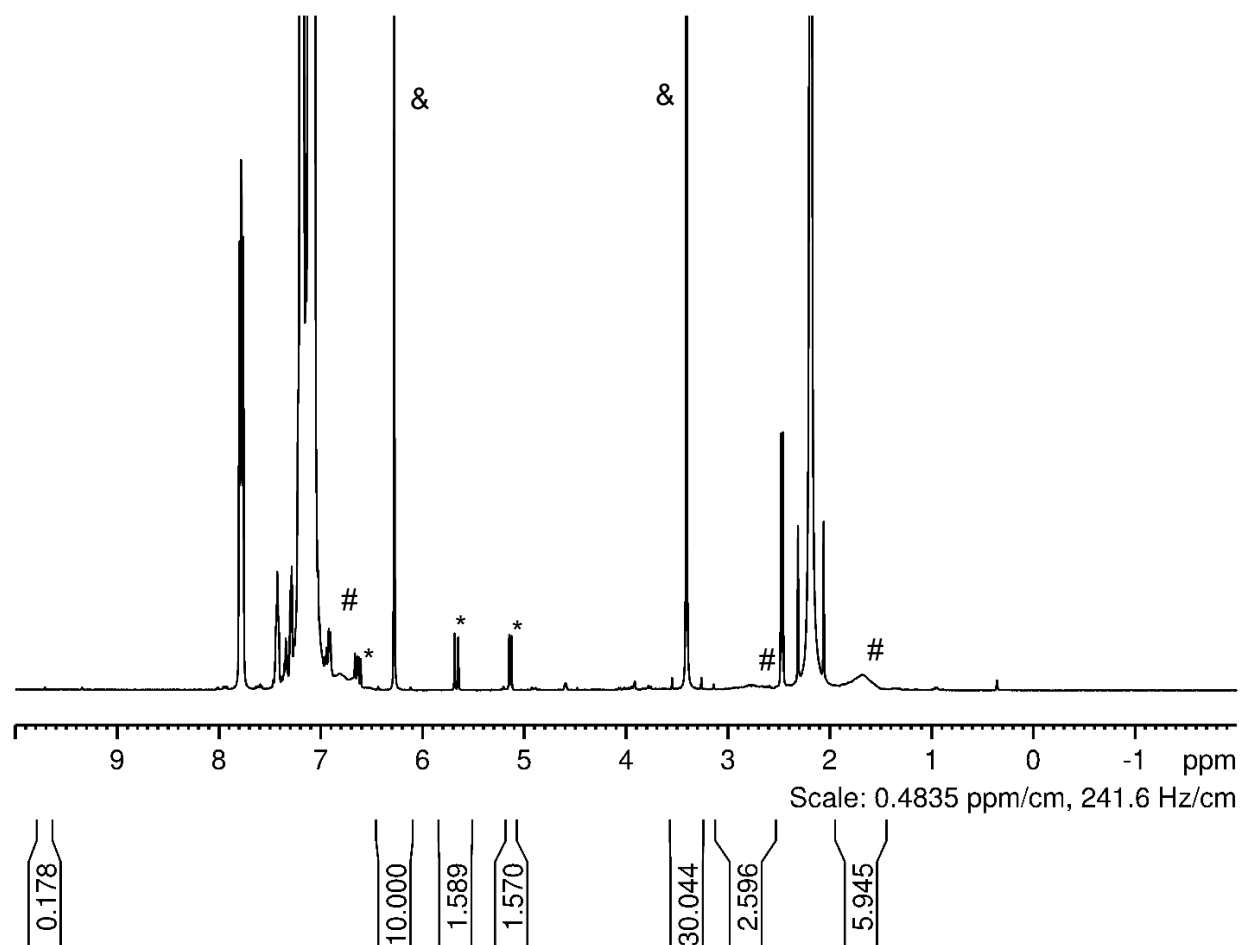


**Figure S3. 1**, PPh<sub>3</sub>, 1-phenyl-1,2-ethanediol. Toluene, 190°C 2.5h

“\*” = styrene

“&” = 1,3,5-trimethoxybenzene

“#” = polystyrene

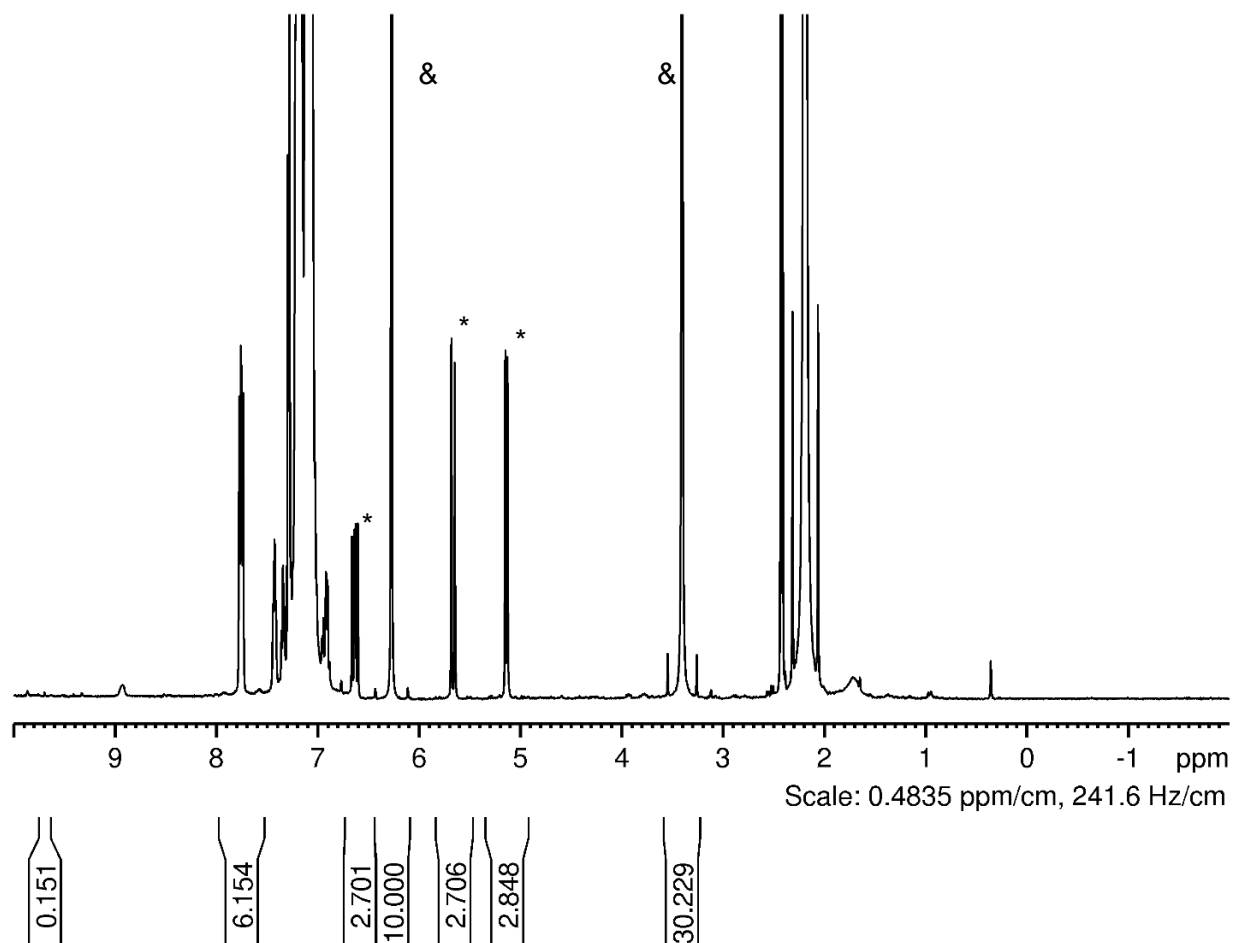


**Figure S4. 1**, PPh<sub>3</sub>, 1-phenyl-1,2-ethanediol, *p*-hydroquinone (1:10 vs cat). Toluene, 190°C 10h. Complete inhibition of polystyrene formation.

“\*” = styrene

“&” = 1,3,5-trimethoxybenzene

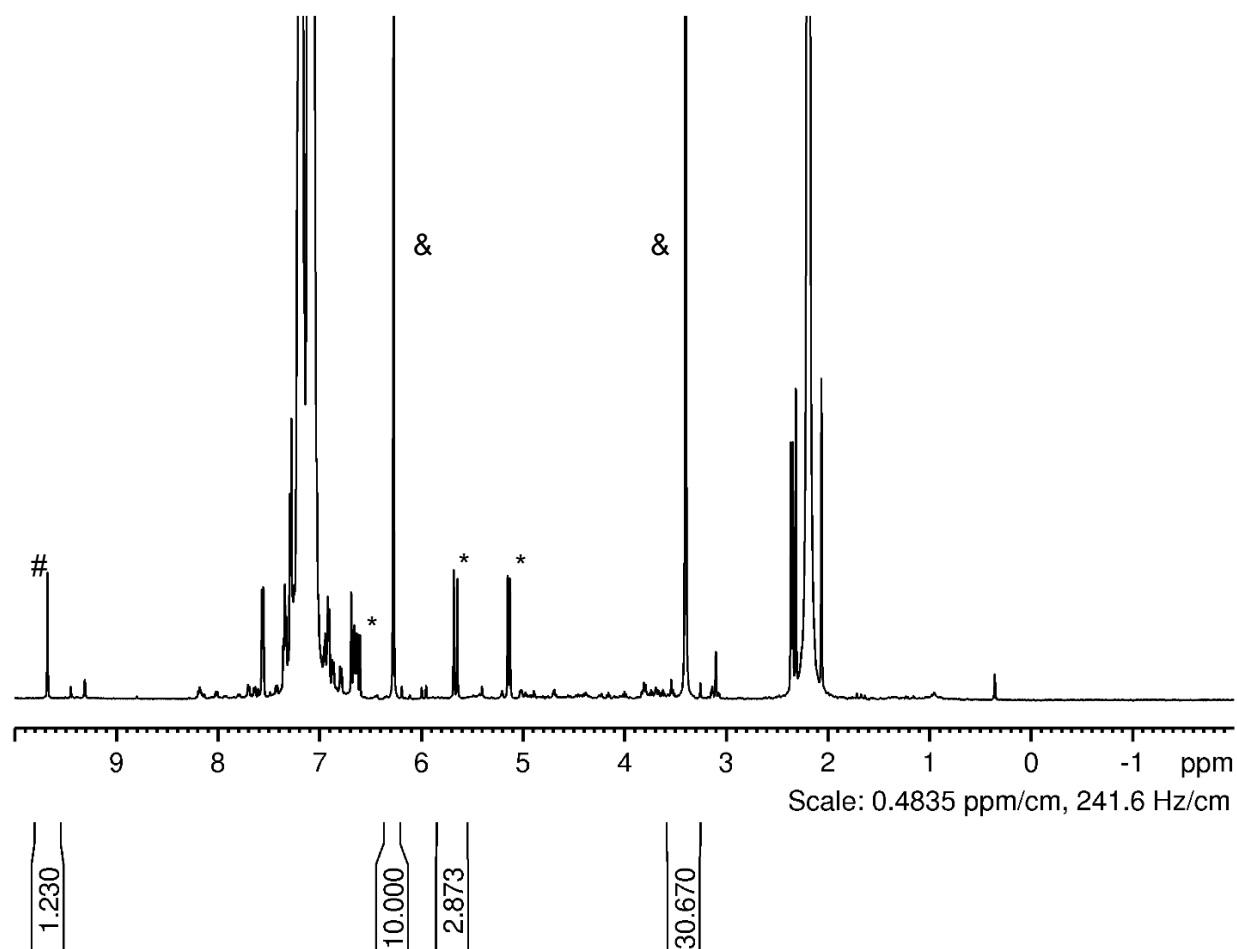


**Figure S5. 1**, 1-phenyl-1,2-ethanediol, *p*-hydroquinone (1:10 vs cat). Toluene, 190°C 1h.

"\*" = styrene

"&" = 1,3,5-trimethoxybenzene

"#" = benzaldehyde

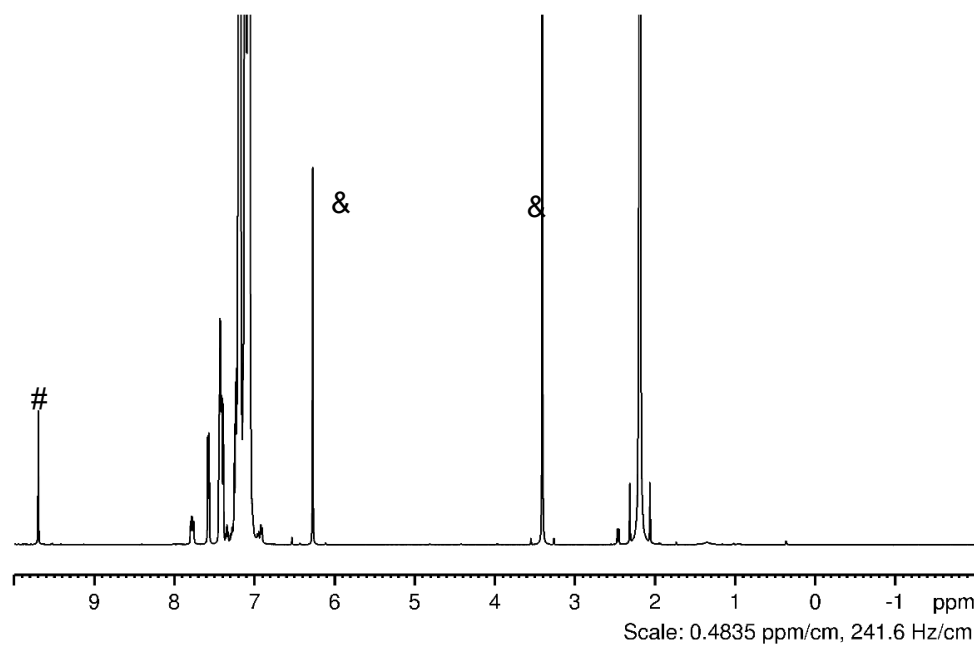
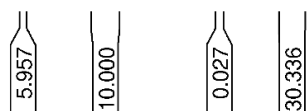
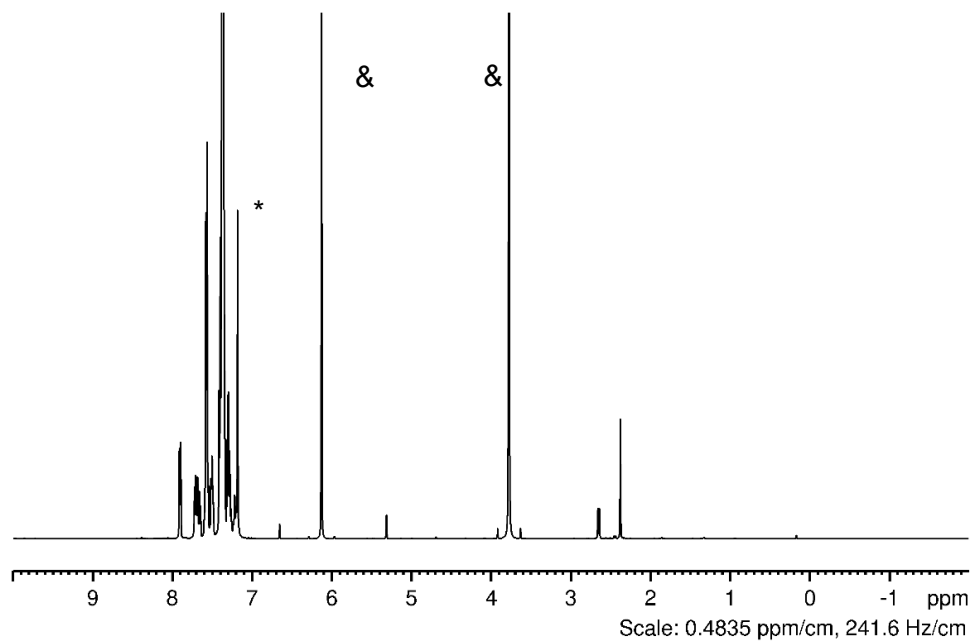
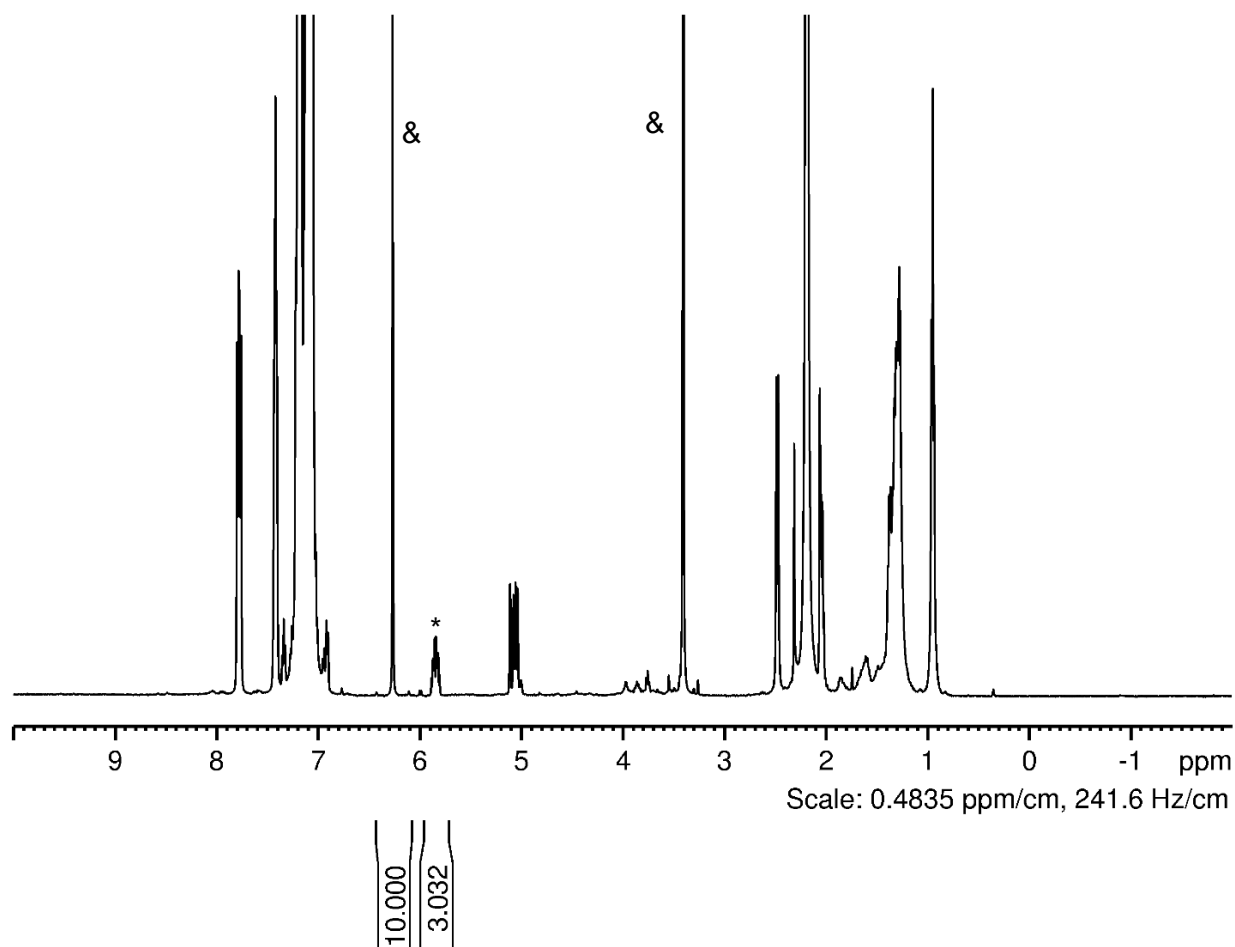


**Figure S6. 1**, PPh<sub>3</sub>, (R,R)-(+)-hydrobenzoin. Toluene, 190°C, 1h. Top: C=C Bottom: C=O.

“\*” = trans-stilbene

“&” = 1,3,5-trimethoxybenzene

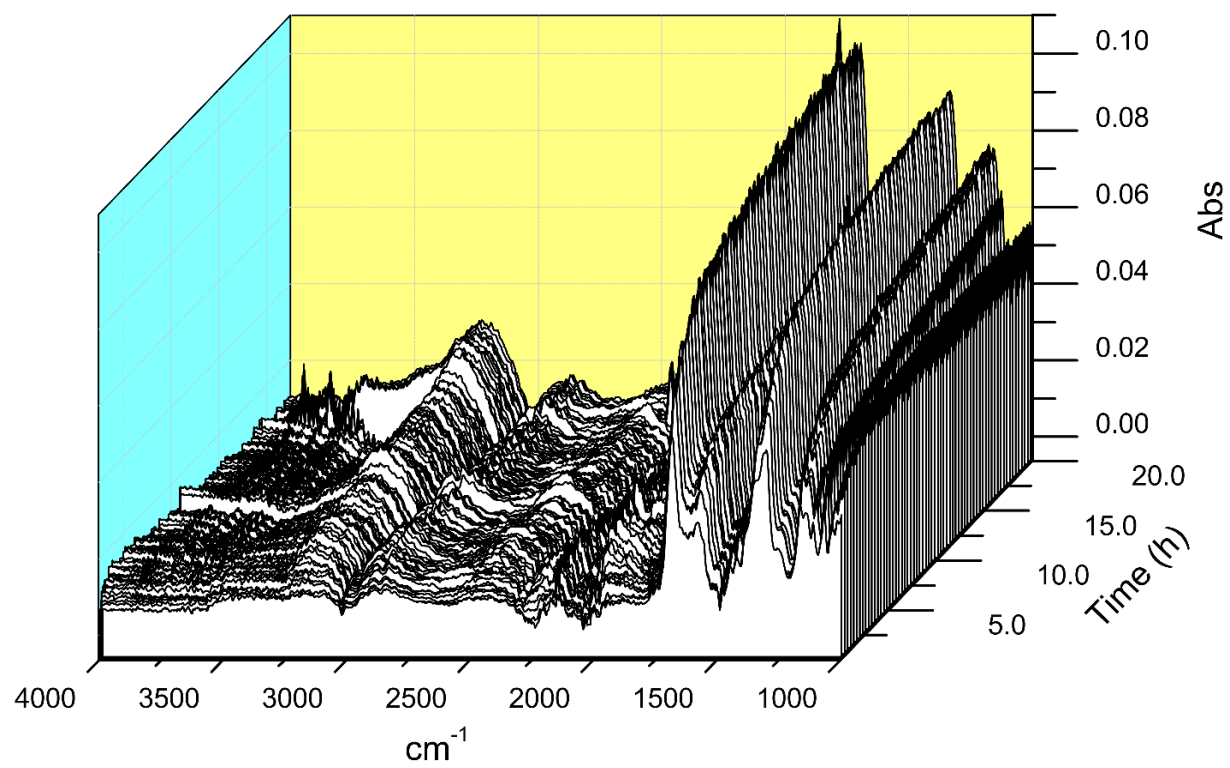
“#” = benzaldehyde

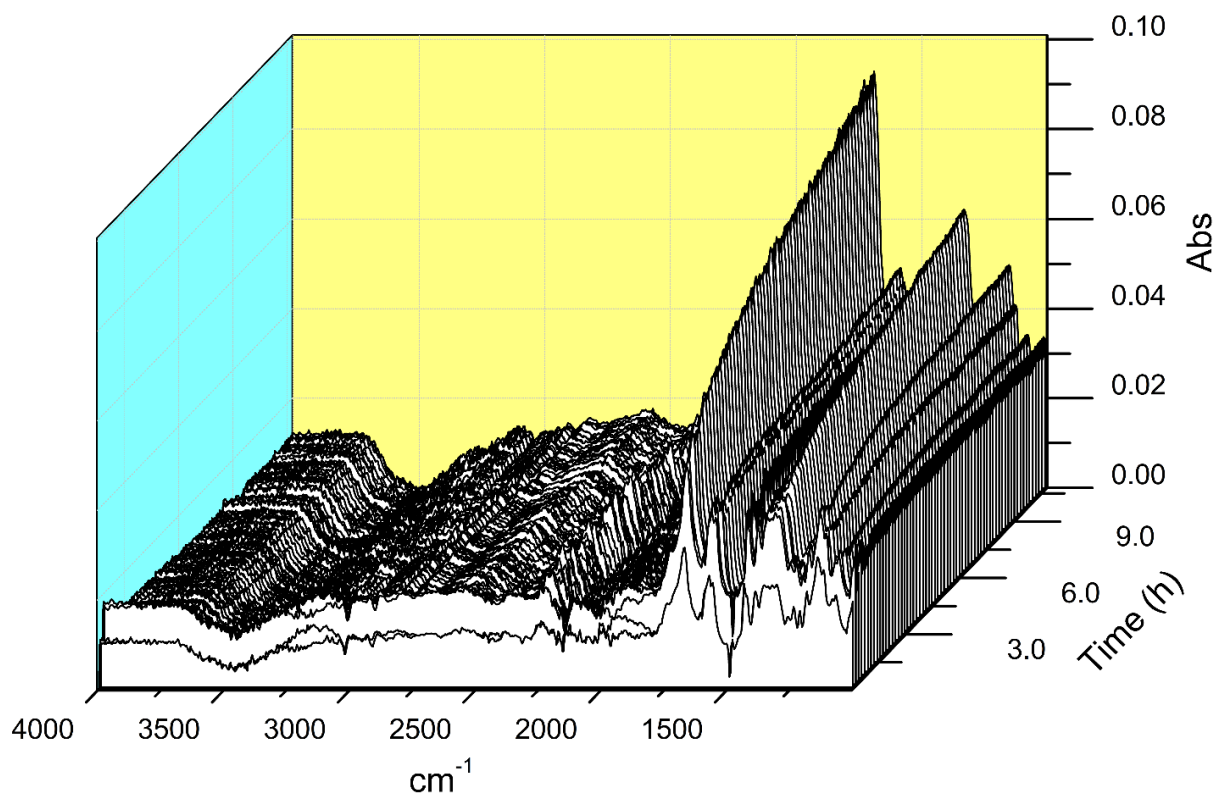


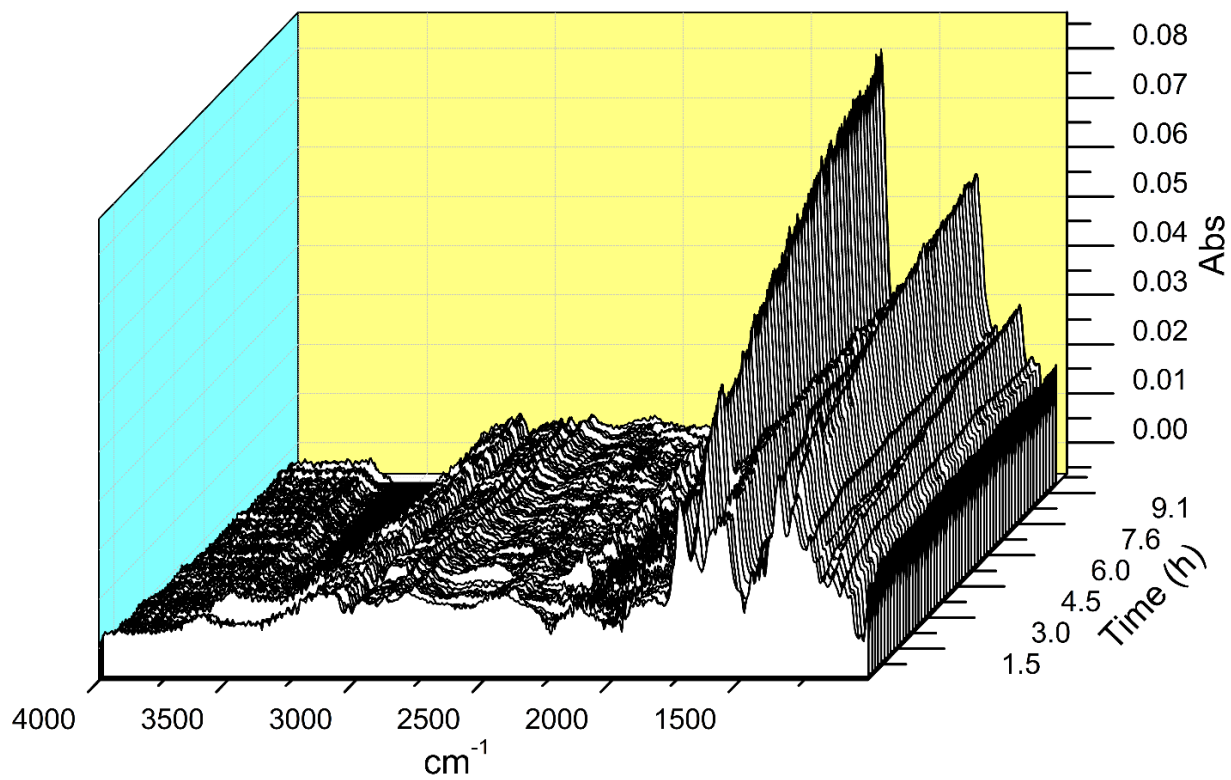
**Figure S7. 1**, PPh<sub>3</sub>, 1,2-octanediol. Toluene, 190°C, 80h

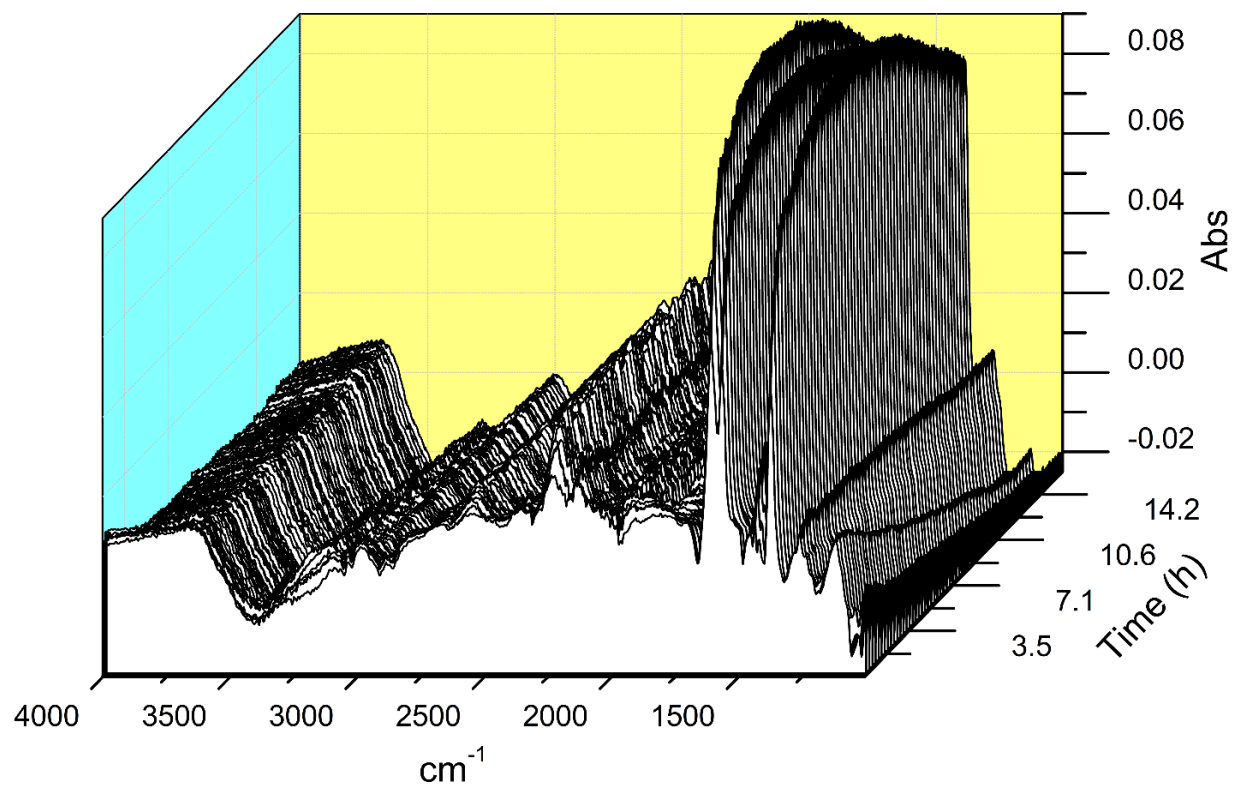
“\*” = 1-octene

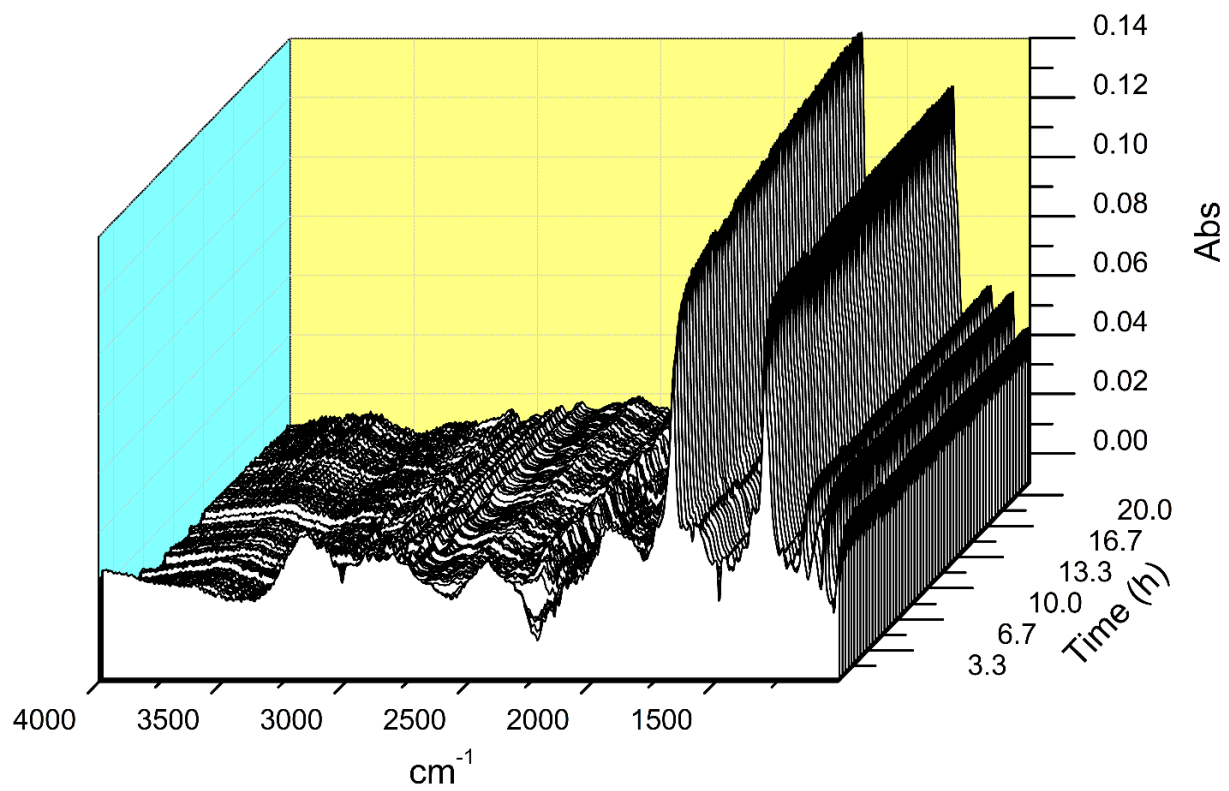
“&” = 1,3,5-trimethoxybenzene

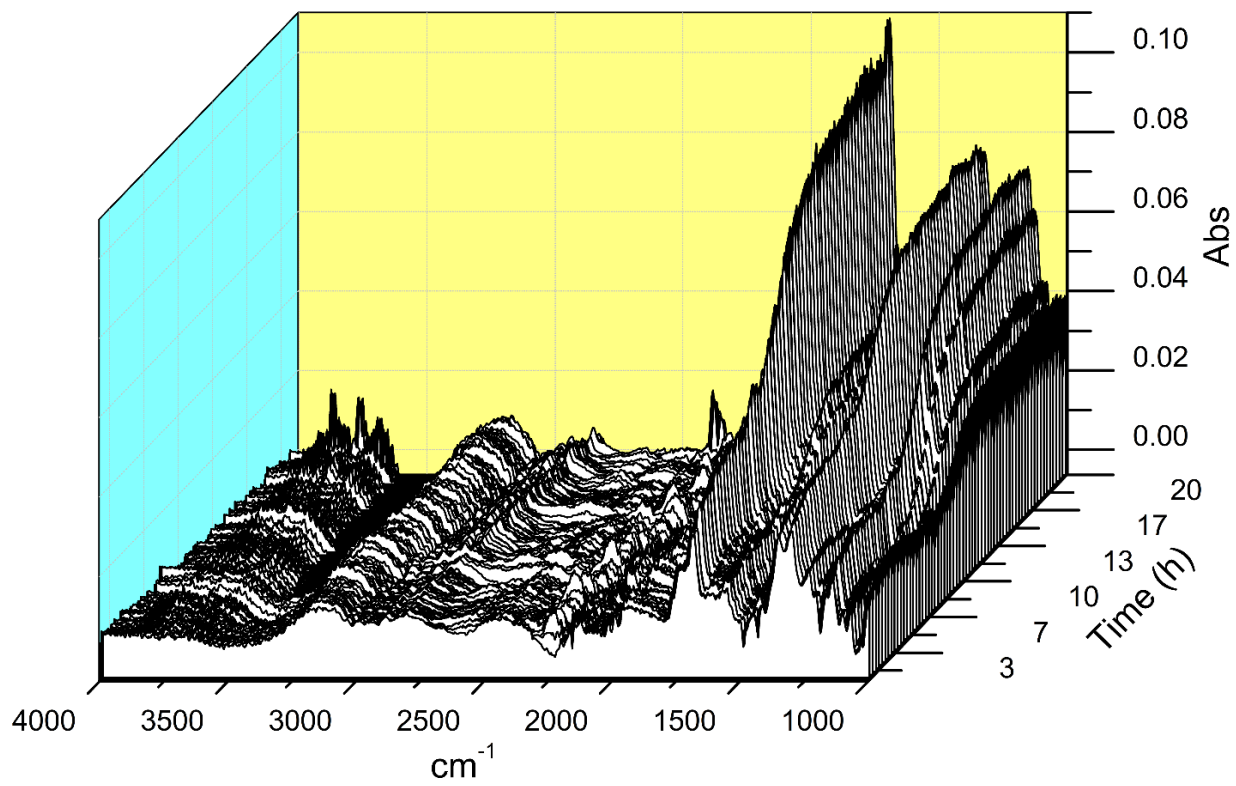












Quantitation of Yields by NMR Experiments

Table T1:1-phenyl-1,2-ethanediol DODH yields											
T(°C)	Solvent	Exp	t (h)	diol	Red	%C=C	%C=O	%PS	Total	NMR	GC
190	CIBn - 20mM	265A	48	sty-diol	PPh <sub>3</sub>	0.9	0	0	0.9		
190	CIBn - 20mM	271A	48	sty-diol	PPh <sub>3</sub>	8.1	0	0	8.1		
190	tol - 40mM	276A	0.5	sty-diol	PPh <sub>3</sub>	60.64	1.24	15.55	77.43		
			1			45.82	3.57	31.25	80.64		
			1.5			40.9	1.46	32.67	75.03	99	
190	tol - 40mM	277A	0.5	sty-diol	PPh <sub>3</sub>	45.56	0.72	0	46.28	57.83	
			1			56.53	2.46	24.26	83.25		
			1.5			41.77	2.81	40.06	84.64		
			2			31.61	3.21	48.95	83.77		
			2.5			25.79	2.31	49.3	77.4	99	99
190	tol - 40mM	278A	0.5	sty-diol	PPh <sub>3</sub>	56.7	5.17	11.56	73.43	71.52	
			1			66.31	2.58	15.41	84.3		
			1.5			69.14	2.83	28.61	100.58		
			2			40.47	3.94	31.25	75.66		99
190	tol - 40mM	280A	2	sty-diol	PPh <sub>3</sub>	25.07	1.64	38.6	65.31		99
190	mesitylene - 40mM	282A	2	sty-diol	PPh <sub>3</sub>	32.59	3.49	15.45	51.53		
			4			20.36	4	20.72	45.08		
			21			7.83	3.29	33.83	44.95		
190	tol - 40mM	289A	0.5	sty-diol	PPh <sub>3</sub>	39.73	0.8	0	40.53		
			1			41.06	2.07	11.29	54.42		

**Table T1:1-phenyl-1,2-ethanediol DODH yields (cont.)**

T(°C)	Solvent	Exp	t (h)	diol	Red	%C=C	%C=O	%PS	Total	NMR	GC
			21			16.7	4.33	66.39	87.42		
			22			13.71	2.3	50.73	66.74		
190	tol - 40mM	299A	2	sty- diol	PPh <sub>3</sub>	20.2	10.59	36.38	67.17		
	1:1 hydroquinone		3			24.37	14.85	41.78	81		
			4			25.69	19.69	46.91	92.29		
			6.5			26.5	17.06	51.95	95.51		
			9			20.38	0	39.88	60.26		
			10			27.03	14.29	53.68	95	99	99
190	tol - 40mM	300A	2	sty- diol	PPh <sub>3</sub>	64.06	2.21	15.06	81.33		
	1:10 hydroquinone		3			68.4	1.51	0	69.91		
			4			50.46	2.37	0	52.83		
			6.5			68.82	3.52	0	72.34		
			9			65.66	4.14	0	69.8		
			10			57.22	3.19	0	60.41		99
190	tol - 40mM	304A	0.5	sty- diol	PPh <sub>3</sub>	54.54	2.62	13.05	70.21		
			1			34.11	1.52	30.16	65.79		99
190	tol - 40mM	III-3A	1	sty- diol	H2quin- one	27.59	11.82	0	39.41		
190	tol - 40mM (2% cat)	III-6A	1	sty- diol	PPh <sub>3</sub>	3.99	0.43	0	4.42		
190	tol - 40mM	III-13A	0.5	sty- diol	PPh <sub>3</sub>	56.39	1.95	17.29	75.63		
			1			37.83	0.46	31.86	70.15		99

<b>Table T1:1-phenyl-1,2-ethanediol DODH yields (cont.)</b>											
<b>T(°C)</b>	<b>Solvent</b>	<b>Exp</b>	<b>t (h)</b>	<b>diol</b>	<b>Red</b>	<b>%C=C</b>	<b>%C=O</b>	<b>%PS</b>	<b>Total</b>	<b>NMR</b>	<b>GC</b>
<b>190</b>	<b>tol - 40mM</b>	<b>295A</b>	<b>1</b>	<b>sty- diol</b>	<b>Zn</b>	<b>22.51</b>	<b>6.21</b>	<b>0</b>	<b>28.72</b>		
			<b>2</b>			<b>24.03</b>	<b>7.1</b>	<b>0</b>	<b>31.13</b>		
			<b>3</b>			<b>29.1</b>	<b>10.26</b>	<b>0</b>	<b>39.36</b>		
			<b>5</b>			<b>27.16</b>	<b>15.56</b>	<b>0</b>	<b>42.72</b>		
			<b>29</b>			<b>17.63</b>	<b>9.38</b>	<b>0</b>	<b>27.01</b>		<b>99</b>
<b>190</b>	<b>tol - 40mM</b>	<b>III-50A</b>	<b>3</b>	<b>sty- diol</b>	<b>Zn</b>	<b>35.85</b>	<b>11.2</b>		<b>47.05</b>		
			<b>15</b>			<b>24.4</b>	<b>9.63</b>		<b>34.03</b>		
			<b>24</b>			<b>29.83</b>	<b>11.18</b>		<b>41.01</b>		
			<b>36</b>			<b>23.63</b>	<b>8.77</b>		<b>32.4</b>		<b>99</b>
<b>190</b>	<b>tol - 40mM</b>	<b>294A</b>	<b>0.5</b>	<b>sty- diol</b>	<b>C</b>	<b>21.45</b>	<b>2.5</b>	<b>0</b>	<b>23.95</b>	<b>64</b>	
			<b>2</b>			<b>27.2</b>	<b>6.5</b>	<b>0</b>	<b>33.7</b>		
			<b>3</b>			<b>25.47</b>	<b>10.86</b>	<b>0</b>	<b>36.33</b>		
			<b>4</b>			<b>24.57</b>	<b>15.55</b>	<b>0</b>	<b>40.12</b>		<b>99</b>
<b>190</b>	<b>tol - 40mM</b>	<b>III-49A</b>	<b>3</b>	<b>sty- diol</b>	<b>C</b>	<b>36.17</b>	<b>9.87</b>		<b>46.04</b>		
			<b>15</b>			<b>21.96</b>	<b>8.79</b>		<b>30.75</b>		
			<b>24</b>			<b>20.75</b>	<b>8.93</b>		<b>29.68</b>		
			<b>36</b>			<b>15.91</b>	<b>7.16</b>		<b>23.07</b>		<b>99</b>
<b>190</b>	<b>tol - 40mM</b>	<b>296A</b>	<b>1</b>	<b>sty- diol</b>	<b>Na<sub>2</sub>SO<sub>3</sub></b>	<b>22.55</b>	<b>3.88</b>		<b>26.43</b>		
			<b>2</b>			<b>19.13</b>	<b>4.85</b>		<b>23.98</b>		
			<b>3</b>			<b>22.03</b>	<b>4.75</b>		<b>26.78</b>		
			<b>5</b>			<b>26.2</b>	<b>9.92</b>		<b>36.12</b>		
			<b>29</b>			<b>8.94</b>	<b>4.15</b>		<b>13.09</b>		<b>99</b>

**Table T1:1-phenyl-1,2-ethanediol DODH yields (cont.)**

T(°C)	Solvent	Exp	t (h)	diol	Red	%C=C	%C=O	%PS	Total	NMR	GC
190	tol - 40mM	III-51A	3	sty- diol	Na <sub>2</sub> SO <sub>3</sub>	35.52	7.8		43.32		
			15			20.35	5.84		26.19		
			24			24.49	7.52		32.01		
			36			21.44	12.18		33.62		99
190	tol - 40mM	III-52A	3	sty- diol	2- propanol	29.71	8.27		37.98		
			24			25.57	8.7		34.27		99
190	tol - 40mM	III-53A	3	sty- diol	2- propanol	30.62	7.53		38.15		
			24			19.61	6.38		25.99		99
190	3oct solvent - 40mM	281A	2	sty- diol	3- octanol	13.44	1.77		15.21	58.45	99
190	3oct solvent - 40mM	297A	1	sty- diol	3- octanol	22.13	2.44		24.57	50.94	
			2			11.51	1.23				
			3			14.14	2.83				
			4			6.08	1.73				
			29			3.73	0.74				
190	tol - 40mM	III-107A	3	sty- diol	1-ph- EtOH	4.88	5.08				
			24			2.66	4.42				
190	tol - 40mM	III-108A	3	sty- diol	1-ph- EtOH	4.57	4.88				
			24			2.1	7.36				

Table T2: 1,2-octanediol DODH yields								
odd T	solvent	NMR	t(h)	substrate	reductant	%C=C	%C=O	Total
190	CIBn - 20mM	259A	48	octene	PPh <sub>3</sub>	11.68	0	11.68
190	CIBn - 20mM	260A	48	octene	PPh <sub>3</sub>	10.81	0	10.81
190	CIBn - 20mM	266A	48	octene	PPh <sub>3</sub>	13.88	0	13.88
190	Mesitylene - 40mM	285A	1	octene	PPh <sub>3</sub>	2.05	0	2.05
			2			7.59	0	7.59
190	tol - 40mM	290A	0.5	octene	PPh <sub>3</sub>	2.74	0	2.74
			1			4.75	0	4.75
			2			7.26	0	7.26
			4			12.96	0	12.96
			24			37.52	0	37.52
190	tol - 40mM	292A	24	octene	PPh <sub>3</sub>	26.24	0	26.24
			41			24.44	0	24.44
			63			35.03	0	35.03
			80			40.78	0	40.78
			128			40.08	0	40.08
			147			39.9	0	39.9
			165			37.93	0	37.93
190	tol - 40mM	III-27A	24	octene	C	19.78	0	19.78
			48			22.89	0	22.89
190	tol - 40mM	III-28A	24	octene	C	14.66	0	14.66
190	tol - 40mM	III-44A	24	octene	3-octanol	6.25		6.25
			48			16.54		16.54
190	tol - 40mM	III-45A	24	octene	3-octanol	8.72		8.72
			48			19.19		19.19

Table T2: 1,2-octanediol DODH yields (cont.)								
odd T	solvent	NMR	t(h)	substrate	reductant	%C=C	%C=O	Total
190	tol - 40mM	III-25A	24	octene	Zn	15.66	0	15.66
			48			36.47	0	36.47
190	tol - 40mM	III-26A	24	octene	Zn	12.7	0	12.7
			48			26.58	0	26.58
190	tol - 40mM	III-30A	24	octene	Na <sub>2</sub> SO <sub>3</sub>	8.12	0	8.12
190	tol - 40mM	III-31A	24	octene	Na <sub>2</sub> SO <sub>3</sub>	6.92	0	6.92
190	tol - 40mM	III-32A	24	octene	IPA (10eq)	27.92	0	27.92
odd T	solvent	NMR	t(h)	substrate	reductant	%C=C	%C=O	Total
			72			33.47	0	33.47
			96			25.1	0	25.1
190	tol - 40mM	III-33A	24	octene	IPA (10eq)	26.33	0	26.33
			72			31.3	0	31.3
			96			27.49	0	27.49
190	tol - 40mM	III-111A	24	octene	1-ph-EtOH	9.41	0	
190	tol - 40mM	III-112A	24	octene	1-ph-EtOH	11.46	0	

<b>T (°C)</b>	<b>solvent</b>	<b>NMR</b>	<b>t(h)</b>	<b>substrate</b>	<b>reductant</b>	<b>%C=C</b>	<b>%C=O</b>	<b>total</b>
190	tol - 40mM	II-286A		hydrobenzoin	PPh <sub>3</sub>	44.07	52.3	96.37
190	tol - 40mM			hydrobenzoin	PPh <sub>3</sub>			0
190	tol - 40mM	III-97A	2	hydrobenzoin	Zn	38.01	56.4	94.41
190	tol - 40mM	III-98A	2	hydrobenzoin	Zn	43.95	56.86	100.81
190	tol - 40mM	III-99A	2	hydrobenzoin	Na <sub>2</sub> SO <sub>3</sub>	40.91	54.34	95.25
190	tol - 40mM	III-100A	2	hydrobenzoin	Na <sub>2</sub> SO <sub>3</sub>	40.97	47.89	88.86
190	tol - 40mM	III-105A	2	hydrobenzoin	C	35.53	50.99	86.52
190	tol - 40mM	III-106A	2	hydrobenzoin	C	40.77	46.09	86.86
190	tol - 40mM	III-103A	2	hydrobenzoin	IPA	33.26	46.12	79.38
190	tol - 40mM	III-104A	2	hydrobenzoin	IPA	34.66	46.08	80.74
190	3octanol	III-101A	2	hydrobenzoin	3octanol	37.22	70.54	107.76
190	3octanol	III-102A	2	hydrobenzoin	3octanol	26.86	39.48	66.34
190	tol - 40mM	III-109A	2	hydrobenzoin	1-ph-EtOH	36.08	42.35	78.43
190	tol - 40mM	III-110A	2	hydrobenzoin	1-ph-EtOH	33.51	45.86	79.37

<b>Table T4: trans-1,2-cyclohexanediol DODH yields</b>								
<b>T (°C)</b>	<b>solvent</b>	<b>NMR</b>	<b>t(h)</b>	<b>substrate</b>	<b>reductant</b>	<b>%C=C</b>	<b>%C=O</b>	<b>total</b>
190	tol - 20mM	267A	48	E-cycloC6diol	PPh <sub>3</sub>	3.58	0	3.58
190	tol - 40mM	291A	1	E-cycloC6diol	PPh <sub>3</sub>	0	0	0
			18			1.41	0	1.41
			35			1.99	0	1.99
			36			1.7	0	1.7
			53			2.88	0	2.88
			70			3.61	0	3.61
			118			5.59	0	5.59
			137			5.21	0	5.21
			155			6.6	0	6.6
190	tol - 40mM	III-34A	24	E-cycloC6diol	PPh <sub>3</sub>	4.51	0	4.51
190	tol - 40mM	III-35A	24	E-cycloC6diol	C	4.19		4.19

Table T5: Meso-erythritol DODH yields								
T (°C)	solvent	NMR	t(h)	substrate	reductant	C=C	C=O	total
190	tol - 40mM	III-38A	1	meso-erythritol	PPh <sub>3</sub>	0.19		
			24			3.02		
190	tol - 40mM	III-39A	1	meso-erythritol	PPh <sub>3</sub>	0.13		
			24			16.35		
190	tol - 40mM	III-41A	1	meso-erythritol	C	0.02		
			24			10.35		
190	tol - 40mM	III-96A	24	meso-erythritol	C	8.28		
			48			8.53		
190	tol - 40mM	III-92A	24	meso-erythritol	Zn	3.15		
			48			3.93		
190	tol - 40mM	III-93A	24	meso-erythritol	Zn	4.89		
			48			4.94		
190	tol - 40mM	III-94A	24	meso-erythritol	Na <sub>2</sub> SO <sub>3</sub>	0.25		
			48			0.6		
190	tol - 40mM	III-95A	24	meso-erythritol	Na <sub>2</sub> SO <sub>3</sub>	0.26		
			48			0.28		
190	tol - 40mM	III-42A	24	meso-erythritol	3-octanol			
190	tol - 40mM	III-43A	24	meso-erythritol	3-octanol			
190	tol - 40mM	III-54A	24	meso-erythritol	2propanol	4.73		
190	tol - 40mM	III-55A	24	meso-erythritol	2propanol	2.99		
190	tol - 40mM	III-113A	24	meso-erythritol	1-ph-EtOH	2.76		
190	tol - 40mM	III-114A	24	meso-erythritol	1-ph-EtOH	1.56		

Table T6: 1,4-anhydroerythritol DODH yields							
T (°C)	solvent	NMR	t(h)	substrate	reductant	%C=C	%C=O
190	tol - 40mM	III-80A		1,4-anhydroerythritol	PPh <sub>3</sub>	unobs	
190	tol - 40mM	III-81A	24	1,4-anhydroerythritol	PPh <sub>3</sub>	20.96	
			48			23.15	
190	tol - 40mM	III-88A	24	1,4-anhydroerythritol	PPh <sub>3</sub>	21.24	
			48			23.57	
190	tol - 40mM	III-83A	24	1,4-anhydroerythritol	C	15.88	
			48			17.15	
190	tol - 40mM	III-89A	24	1,4-anhydroerythritol	C	12.93	
			48			15.27	
190	tol - 40mM	III-84A	24	1,4-anhydroerythritol	Zn	5.8	
			48			6.76	
190	tol - 40mM	III-85A	24	1,4-anhydroerythritol	Zn	6.28	
			48			12.89	
190	tol - 40mM	III-87A	24	1,4-anhydroerythritol	Na <sub>2</sub> SO <sub>3</sub>	0.73	
			48			0.66	
190	tol - 40mM	III-90A	24	1,4-anhydroerythritol	Na <sub>2</sub> SO <sub>3</sub>	0.39	
			48			0.59	
190	tol - 40mM	III-78A	24	1,4-anhydroerythritol	3octanol	20.05	
			48			26.77	
190	tol - 40mM	III-79A	24	1,4-anhydroerythritol	3octanol	11.81	
			48			9.22	
190	tol - 40mM	III-76A	24	1,4-anhydroerythritol	IPA	7.04	
			48			19.86	
190	tol - 40mM	III-77A	24	1,4-anhydroerythritol	IPA	4.1	
			48			9.72	

<b>Table T6: 1,4-anhydroerythritol DODH yields (cont.)</b>							
<b>T (°C)</b>	<b>solvent</b>	<b>NMR</b>	<b>t(h)</b>	<b>substrate</b>	<b>reductant</b>	<b>%C=C</b>	<b>%C=O</b>
<b>190</b>	<b>tol - 40mM</b>	<b>III-117A</b>	<b>24</b>	<b>1,4-anhydroerythritol</b>	<b>1-ph-EtOH</b>	<b>7.77</b>	
<b>190</b>	<b>tol - 40mM</b>	<b>III-118A</b>	<b>24</b>	<b>1,4-anhydroerythritol</b>	<b>1-ph-EtOH</b>	<b>6.92</b>	

### Determination of Yields for Catalytic Reactions

$$\frac{\text{int } P}{\text{int std}} * \frac{H \text{ std}}{H P} * \frac{\text{mmol std}}{\text{sample}} * \frac{\text{vol reaction}}{\text{vol aliquot}} = \text{mmol } P$$

Int:	description	int H's	std int:	std H's	mmol P	adjusted mmol	% Yield vs diol
					0.00028845	0.00824167	
2.9078	styrene	1	10	3	9	4	0.8025%
22.514					0.01340109	0.38288838	
9	acetone	6			4	9	37.2824%
					0.00022437	0.00641069	
1.1309	formyl	2			4	5	0.6242%

Sample calculation of Catalytic Yields

### Chapter 3

#### Deoxydehydration of Polyols Catalyzed by a Molybdenum Dioxo-Complex Supported by a Dianionic ONO Pincer Ligand.

This chapter was adapted from

Tran, R.; Kilyanek, S. M. Deoxydehydration of Polyols Catalyzed by a Molybdenum Dioxo-Complex Supported by a Dianionic ONO Pincer Ligand. *Dalton Trans.* **2019**, *48*, 16304. DOI:10.1039/C9DT03759D

Biomass deoxygenation and up-conversion have gained popularity as a method to produce commodity chemicals currently produced by the petrochemical industry.<sup>1</sup> Deoxydehydration (DODH) is a promising route for converting biomass-derived diols and polyols into alkenes and dienes. The reaction converts vicinal diols into alkenes typically using high oxidation state metal-oxo complexes as catalysts and reductants such as PPh<sub>3</sub> or a secondary alcohol (**Figure 1**).

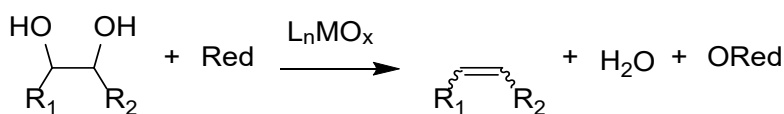


**Figure 1.** Generalized DODH reaction

DODH was first reported by Cook and Andrews.<sup>2</sup> Cp\*ReO<sub>3</sub> was used as a precatalyst to convert 1-phenyl-1,2-ethanediol to styrene with PPh<sub>3</sub> as oxo acceptor and reductant. Toste and coworkers have demonstrated that MeReO<sub>3</sub> is an excellent catalyst using secondary alcohols as a reductant.<sup>3</sup> Other studies in the literature have shown that a wide variety of reductants can be used.<sup>4-10</sup> Recently, molybdenum complexes have been shown to be active for DODH at high temperatures and pressures.<sup>11-13</sup> The most notable being ammonium heptamolybdate ((NH<sub>4</sub>)<sub>6</sub>Mo<sub>7</sub>O<sub>24</sub> · 4H<sub>2</sub>O, AHM) reported by Frstrup is an active catalyst using secondary alcohols as sacrificial reductant. However, the yields were relatively low (46 %) while requiring relatively harsh conditions (210 °C and 60-90 bar for 13h).

The proposed catalytic cycle for DODH involves three steps: (1) reduction of the metal / oxo abstraction (2) condensation of a metal oxo with vicinal diol to form a metal-diolate and water (3) olefin extrusion of the alkene product regenerating a metal dioxo species. Mechanistic studies of  $\text{MeReO}_3$  by Abu Omar and co-workers show that a reduced dioxo species is the active form of the catalyst.<sup>5</sup> The mechanism of DODH likely varies with reductant and catalyst, for example, oxo abstraction / reduction and metal-diolate formation could happen in any order. Additionally, reduction of the metal could occur by deformylation of the metal-diolate species.<sup>11</sup> **Figure 2** summarizes the possible mechanisms of DODH.

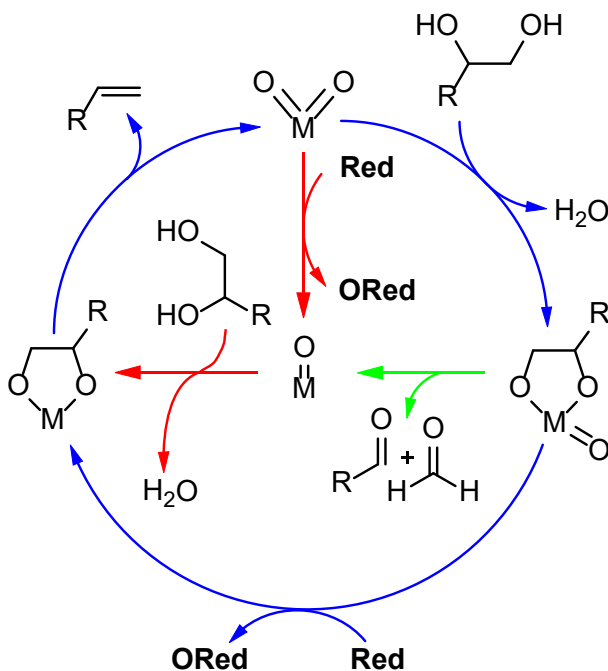


**Figure 2.** Possible competing mechanisms of DODH. The dioxomolybdenum catalyst can be first reduced or condense the diol to form the reduced mono-oxo or mono-oxo diolate, respectively.

Abu-Omar found that one of the off-cycle components of the  $\text{MeReO}_3$  catalyst system was the formation of oxo-bridged-Re dimers. We chose a bulky ligand scaffold to discourage catalyst dimerization and deactivation by comproportionation. Recent work has shown that manipulating the ligand environment can substantially improve the yields of Mo-catalyzed DODH beyond the simple salts reported in the literature.<sup>14,15</sup> The relative low cost of Mo

compared to Re owing to its greater earth abundance led us to choose a Mo complex when designing our catalyst system. To date, the ligand environments of cis-dioxo-Mo based DODH catalysts have been six coordinate systems. To the best of our knowledge, this report is the first example of a five coordinate/coordinatively unsaturated cis-dioxo-Mo system active for DODH. The primary interest in cis-dioxo-Mo(VI) systems lie in potential as models for oxo-transferase enzymes.<sup>16-18</sup> Currently a handful of five coordinate systems are known.<sup>19-24</sup> Berg and Holm reported the first example of a five coordinate cis-dioxo.<sup>19</sup> Recently, Stylianou and co have studied the aqueous coordination chemistry of *N,N*-di-substituted-bis(hydroxylamido)-1,3,5-triazine ligands affording a five coordinate species.<sup>25</sup> Osborn and co have isolated five coordinate cis-dioxo units that were base-free and dimeric where the sixth coordination site at each octahedral Mo is occupied by a bridging O of the adjacent Mo=O bond.<sup>26</sup> Coordinatively saturated systems have dominated the literature. Acylpyrazolonate-based systems are the first examples of Mo-catalyzed DODH in the literature.<sup>27</sup> Hills and co have found conversions of 60-99% with yields between 10-55% of alkene.<sup>27</sup> Okuda and co studied tetradentate OSSO type ligands showing that phenolate-based systems are competent DODH catalysts.<sup>28</sup> Aside from the simple molybdate salts, Fristrup and co examined common six coordinate cis-dioxo-Mo compounds including the synthetically convenient [MoO<sub>2</sub>X<sub>2</sub>] (X = Cl, Br, Me). These compounds were also found to be competent DODH systems, affording complete conversion of the diol with alkene yields between 10-45%. A common motif of Mo DODH systems is the reliance on high temperature and pressures during reaction. A downside to this is the inherent difficulty in identification of the catalytically active species because numerous Mo species can be formed at high temperatures.

DFT has been leveraged to study the DODH reaction. They assume that the active catalytic species is a simple MoO<sub>3</sub> fragment or a MoO<sub>2</sub>(diolate) type species.<sup>12,29</sup> Consistent with literature of DODH catalyzed by other metals, these studies showed that the olefin extrusion is

the rate determining step of reaction.<sup>29</sup> Additional DFT calculations show that the RDS proceeds through formation of metal-oxetane species consistent with the work of Gable and co on Re(V)-diolate systems.<sup>30-33</sup>

We synthesized and screened a new Mo(VI)-dioxo-pincer complex for DODH activity. Treatment of  $\text{MoO}_2(\text{acac})_2$  in methylene chloride with equimolar amounts of 2,6-bis-(3,4-di-tertbutyl-2-phenol)pyridine (L) in the presence of various ancillary ligands yields compounds **1-3** (Figure 3) in good yield.

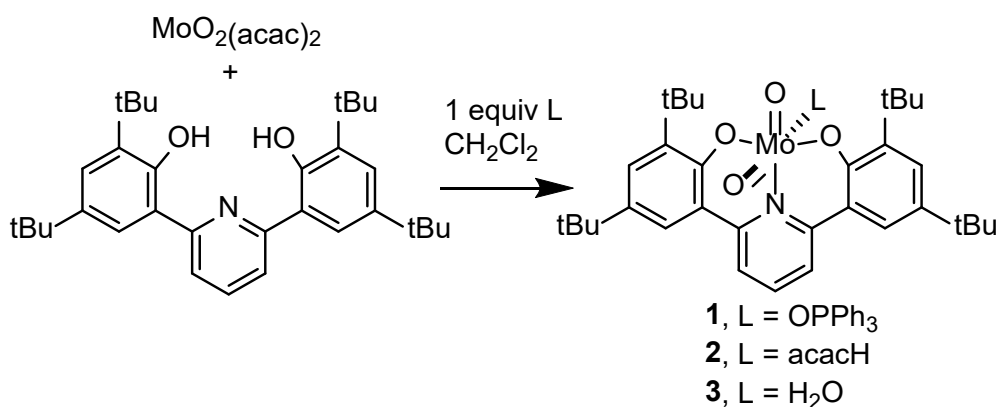


**Figure 3.** Synthesis of Mo(VI)-dioxo-pincer supported by various ancillary ligands.

X-Ray crystallography revealed that **1-3** all bear a cis-dioxo-Mo fragment supported within pincer L. **1** and **3** adopt octahedral geometries around the Mo center. Upon crystallization, **2** was isolated as a base free complex showing a trigonal bipyramidal structure at the Mo center with the oxo-ligands occupying the equatorial plane of the complex. (Figure 1 and 2). Elemental analysis of **1** shows the presence of water in the pure compound owing to the complex's hygroscopic nature. X-ray analysis of **3** demonstrates that at ambient temperature the  $\text{LMoO}_2$  fragment is stable to water (supporting information).  $^{31}\text{P}$  NMR of **1** shows no signal for the bound  $\text{OPPh}_3$  likely due to the signal being broadened into the baseline.  $^1\text{H}$  NMR shows broadened aryl peaks for both the phenolate ligand and  $\text{OPPh}_3$ . This data implies that  $\text{OPPh}_3$  is weakly bound to the Mo center in solution and the rate of dissociation / reassociation is approximately that of the NMR time scale. Broad peaks are also observed for  $\text{acacH}$  in the  $^1\text{H}$  NMR of **2**.

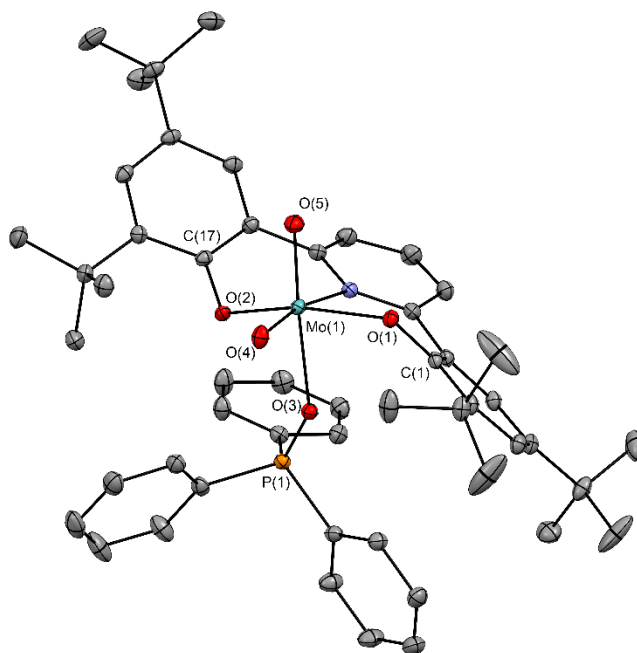


**Figure 4.** X-ray Crystal structure of **1** shows an octahedral cis-dioxo bipyramidal Mo center. Selected bond lengths (Å) and angles (deg): Mo=O4 = 1.714, Mo=O5 = 1.701, Mo-O1 = 1.961, Mo-O2 = 1.963, M-N = 2.341;  $\angle$ O4-Mo-O5 = 104.46,  $\angle$ O1-Mo-O2 = 154.85.

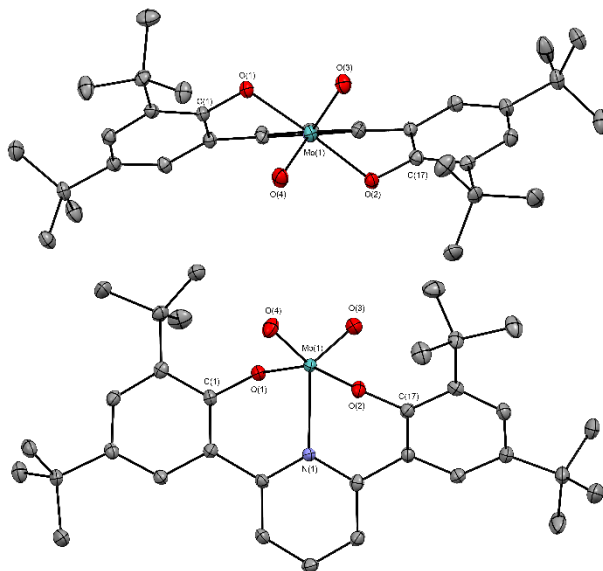


**Figure 5.** X-ray Crystal structure of five coordinate compound **2** shows a trigonal bipyramidal Mo center. Selected bond lengths (Å) and angles (deg): Mo=O3 = 1.689, Mo=O4 = 1.693, Mo-O1 = 1.951, Mo-O2 = 1.947, Mo-N = 2.223;  $\angle$ O3-Mo-O4 = 111.68,  $\angle$ O1-Mo-O2 = 156.69.

DODH Catalyzed by **1** and **2**.

The catalytic activity of **1** and **2** were screened using 10 mol % catalyst at 150°C for 48h. Catalytic reactions of **1** with 1-phenyl-1,2-ethanediol as substrate gave appreciable yields using a variety of reductants. PPh<sub>3</sub> showed lower yields (45%) compared to sulfite and the elemental reductants (Zn, C). <sup>1</sup>H NMR analysis of the product revealed that **1** has good selectivity for alkene formation, only 10% aldehyde side product yield was detected. Elemental zinc and carbon showed the best yield for styrene when catalyzed by **1**. (R,R)-(+)-hydrobenzoin showed poor yields for the major product (trans-stilbene) using **1** and PPh<sub>3</sub> as reductant. Isopropyl alcohol also performed poorly for DODH yielding only trace amounts of alkene when catalyzed by **1**. When DODH of 1-phenyl-1,2-ethanediol is catalyzed by **2**, the styrene yield increases to 49%. The higher yields using isopropyl alcohol were surprising given that PPh<sub>3</sub> has been shown consistently to be an excellent reductant for Re systems. Use of activated carbon as reductant under these mild conditions with catalyst **2** seems to result in the highest yield of styrene.

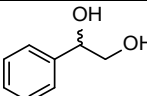
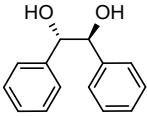
In reactions where isopropyl alcohol was used as the reductant with **1**, large amounts of acetone were observed (the side product of catalyst reduction) relative to the DODH products (alkenes and aldehydes) observed. When **1** is reduced by isopropyl alcohol in the presence of 1-phenyl-1,2-ethanediol we observed acetone corresponding to ~3 turnovers of the catalyst. However, only trace DODH products were observed in solution. When **1** is reduced by isopropyl alcohol in the presence of (R,R)-(+)-hydrobenzoin we observed acetone corresponding to ~20 turnovers of catalyst when the corresponding DODH products indicated only 2 catalyst turnovers. Notably **1** can perform sub-stoichiometric DODH of 1-phenyl-1,2-ethanediol in the absence of reductant. This demonstrates that a metal diolate derived from **1** can react via deformylation to close the DODH cycle (**Figure 2** green path).

**1** and **2** show poor catalytic conversion of aliphatic diols (1,2-octanediol and cis-1,2-cyclohexanediol) to alkenes (supporting information Table S1). (L)-(+)-diethyltartrate was examined as a model substrate for DODH incorporating functional groups similar to biomass

starting materials (Table S1). The largest yield ,29%, was obtained using PPh<sub>3</sub> as reductant. Elemental Zn and C yielded 16% and 13% respectively. Sodium sulfite exhibited the worst yield (7%). These results demonstrate that **1** and **2** prefer aromatic substrates rather than aliphatic substrates.

**1** and **2** were found to be sensitive to water under catalytic conditions. Crystallographic data shows that when **2** is recrystallized in atmosphere a stable inner sphere hydrate is formed (supporting information). However, over the course of a catalytic reaction, protonated free ligand is detected by <sup>1</sup>H NMR. Addition of water to a toluene solution of **1** at elevated temperature shows partial decomposition of **1** and formation of free ligand. Use of common desiccants such as molecular sieves, P<sub>2</sub>O<sub>5</sub> and MgSO<sub>4</sub> in the catalytic reaction did not afford product formation.

**Table 1. Summary of catalytic activity of 1 and 2**

Substrate	Reductant	Yield <sup>a</sup> Cat 1	Yield <sup>a</sup> Cat 2
	PPh <sub>3</sub>	45%	34%
	Na <sub>2</sub> SO <sub>3</sub>	52%	51%
	iPr-OH	<1%	49%
	Zinc	56%	42%
	Carbon	56%	57%
	Diol	4%	-
	PPh <sub>3</sub>	33%	58%
	Na <sub>2</sub> SO <sub>3</sub>	51%	47%
	iPr-OH	19%	-
	Zinc	51%	38%
	Carbon	36%	35%
	PPh <sub>3</sub>	45%	34%

<sup>a</sup>Yields reported are an average of two reactions. Yields were determined by <sup>1</sup>H NMR using an internal standard (supporting information).

Solutions of **1** or **2** in aromatic solvent are light yellow to light green in color. Upon heating in the presence of PPh<sub>3</sub> and substrate at catalytic concentrations, these solutions become deep purple. The purple color is characteristic of a paramagnetic species. However, <sup>1</sup>H NMR of these solutions only show diamagnetic components. Since no paramagnetic species

were observed via  $^1\text{H}$  NMR we hypothesize that an anti-ferromagnetically coupled dimer may be present. After longer reaction times, the reaction changed from purple to an intense orange color. Further studies are underway to examine the identity of species in solution during catalysis.

#### Preliminary Kinetics:

Preliminary kinetics studies were performed via  $^1\text{H}$  NMR by monitoring the formation of the major product, styrene, and the consumption of 1-phenyl-1,2-ethanediol substrate. The growth of styrene shows an early relatively rapid non-linear growth of product. After 15 hours, we observe the concentration of styrene plateau. The profile of the concentration of diol vs time shows an apparent zero-order dependence on diol during this period. The profile of styrene production during this period does not correspond to a first or second order production of styrene. This implies several species may be competent catalysts for DODH and that the rate of production is not dependent solely on the concentration of reductant and catalyst (supporting information). This suggests more complicated kinetics are present in this reaction, but further studies are underway to better understand the mechanism of DODH in these systems.

In conclusion we have synthesized  $d^0$  Mo-dioxo catalysts that are active for deoxydehydration. It has been shown that these catalysts are active for DODH for a wide variety of reductants. They afford modest yields for aromatic diols while aliphatic diols can only be converted in trace amounts.  $\text{PPh}_3$  is a competent oxo acceptor to catalyze these reactions but greener reductants including isopropyl alcohol also show good yields when used with these catalysts. Better yields could likely be achieved if the catalyst could be protected from water. Current efforts are underway to explore the mechanism of reaction and better understand the possible reaction pathways.

## Experimental Procedure

General comments: Reagents were obtained commercially and used without further purification. Solvents were obtained anhydrous from Aldrich and placed over 3Å molecular sieves. All reactions were performed under inert atmosphere using standard Schlenk or glovebox techniques unless otherwise noted. The preparation of the ligand is a modified version of literature.<sup>1</sup> <sup>1</sup>H NMR was referenced to solvent residual signals (chloroform-*d* δ = 7.26 methylenechloride-*d*<sub>2</sub>, δ = 5.32) and yields were determined by internal standard: (1,3,5-trimethoxybenzene, δ = 3.32 (s, 9H, OCH<sub>3</sub>) δ = 6.13 (s, 3H, aryl H)) or (hexamethylcyclotrisiloxane, δ = 0.17 (s, 18H, CH<sub>3</sub>)). Elemental analysis was performed by CENTC Elemental Analysis Facility at the University of Rochester.

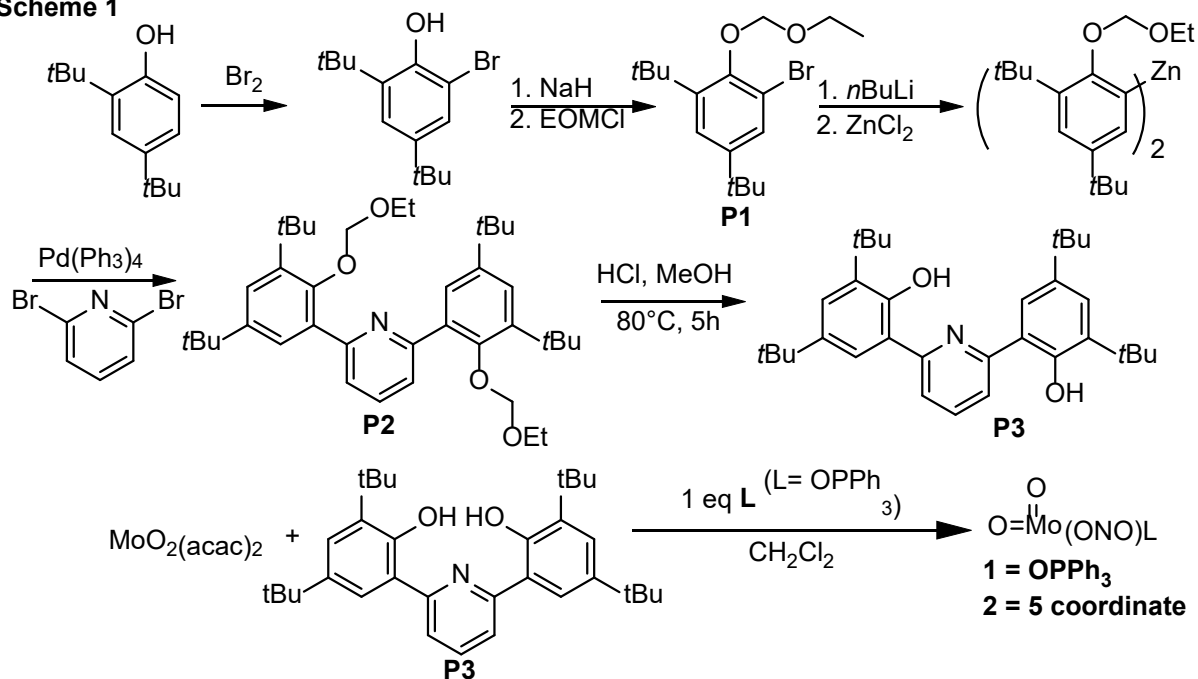
## General procedure for catalytic reactions

A pressure tube with threaded teflon cap was charged with catalyst, reductant, diol, and internal standard. The reaction was placed stirring in a pre-heated oil bath. NMR spectroscopy were obtained on a Bruker DRX-500 or a AVANCE-III-400 at 500MHz and 400MHz respectively using 1,3,5-trimethoxybenzene as an internal standard.

## Ligand synthesis

The synthesis of the dianionic ONO pincer ligand is shown in Scheme 1.

**Scheme 1**



Synthesis of O-methoxyethyl-2,4-di-tert-butyl-6-bromophenoxide, P1. 2,4-di-tert-butylphenol (2090.3 mg, 10.13 mmol) was dissolved in CH<sub>2</sub>Cl<sub>2</sub> (DCM, 26 mL). Bromine (0.5 mL, 10.14 mmol) was added via syringe; upon addition, the bromine became colorless. The organic mixture was washed with water, dried by MgSO<sub>4</sub>, and filtered. The solution was dried via rotary evaporation resulting in golden oil. Under inert atmosphere, this oil was dissolved in dry tetrahydrofuran (THF, 30 mL) and deprotonated with sodium hydride (NaH, 270.1 mg, 11.26 mmol). This reaction stirred for 1 hour at room temperature and the chloromethyl ethyl ether (EOMCl, 1.1 mL, 11.86 mmol) was added via syringe. Then the reaction was stirred for 9 hours at room temperature followed by an aqueous workup: quenched with H<sub>2</sub>O, concentrated in vacuo, extracted with DCM thrice, dried with MgSO<sub>4</sub>, and dried in vacuo overnight resulting in a viscous oil. 87% yield. <sup>1</sup>H NMR (400 Mhz, CDCl<sub>3</sub>) δ = 1.31 (s, 9H, t-butyl), 1.35 (t, 3H, CH<sub>3</sub>, J = 7.1 Hz), 1.43 (s, 9H, t-butyl), 3.95 (q, 2H, CH<sub>2</sub>, J = 7.1 Hz), 5.25 (s, 2H, OCH<sub>2</sub>O), 7.30 (s, 1H, aryl H, J = 2.4 Hz), 7.39 (s, 1H, aryl H, J = 2.4 Hz).

Synthesis of EOM2(ONO), P2. P1 (3409.5 mg, 9.93 mmol) was dissolved in THF (16 mL) in a threaded Teflon-capped Schlenk tube and alongside n-butyllithium (nBuLi, 8.34 mL, 20.86 mmol) in hexanes, was chilled in a -35°C freezer. When chilled, the THF solution was vigorously stirred and the nBuLi was added dropwise via a syringe. The solution would bubble slightly as the nBuLi was added. A clear layer formed between the THF and the hexanes. After it was fully added, it was more thoroughly mixed with a stirring rod. This was done because of the layering of the solvent and the long Schlenk tube making it difficult for the stir bar to diffuse everything together. The lithiation mixture was stirred for 3 hours; white precipitate would appear during it and the solution would be shaken to disturb the solid. Meanwhile, ZnCl<sub>2</sub> (947.7 mg, 6.95 mmol), 2,6-dibromopyridine (1058.7 mg, 4.47 mmol), and Pd(PPh<sub>3</sub>)<sub>4</sub> (114.8 mg, 0.10 mmol) were measured out separately into scintillation vials. After stirring, ZnCl<sub>2</sub> was added with the aid of THF and stirred for 30 minutes. Upon addition of the zinc reagent, the white precipitate immediately went back into solution. Then 2,6-dibromopyridine and Pd(PPh<sub>3</sub>)<sub>4</sub> was added with aid from THF. This reaction was promptly placed into a preheated 75°C oil bath and stirred for 16 hours. The reaction was quenched with water and the volatiles were removed. Additional water was added and then the product was extracted thrice with Et<sub>2</sub>O. The fractions were combined and dried with MgSO<sub>4</sub>, filtered, and then solvent pumped off. This residue was suspended in methanol and chilled to -25°C. The result was a white precipitate that was collected via filtration and washed with cold methanol. 75% yield. <sup>1</sup>H NMR (400 MHz, CDCl<sub>3</sub>) δ = 1.15 (t, 3H, CH<sub>3</sub>, J = 7 Hz), 1.35 (s, 18H, t-butyl, J = 10 Hz), 1.50 (s, 18H, t-butyl, J = 10 Hz), 3.62 (q, 4H, CH<sub>2</sub>, J = 7 Hz), 4.66 (s, 4H, OCH<sub>2</sub>O), 7.43 (s, 2H, aryl-H, J = 2.5 Hz), 7.58 (s, 2H, aryl-H, J = 2.5 Hz), 7.71-7.80 (m, 3H, pyr-H).

Synthesis of H2(ONO), P3. The final step is deprotection of the phenol groups. P2 was suspended in a 1:1 solution of methanol and hydrochloric acid; this mix was stirred and heated at 80°C for 5 hours. Volatiles were pumped off and then dried under Schlenk line. 80% yield. <sup>1</sup>H NMR (400 MHz, CD<sub>2</sub>Cl<sub>2</sub>) δ = 1.37 (s, 18H, t-butyl), 1.47 (s, 18H, t-butyl), 7.44 (s, 2H, aryl H, J =

2.4 Hz), 7.51 (s, 2H, aryl H, J = 2.4 Hz), 7.75 (d, 2H, pyr H, J = 8 Hz), 8.05 (t, 1H, pyr H, J = 8 Hz).

Preparation of Catalyst. Equimolar amounts of  $\text{MoO}_2(\text{acac})_2$ , P3, and an auxiliary ligand (L) were measured out into a round bottom flask and dichloromethane was added (0.15M). This solution was stirred for 48 hours at room temperature. Then it was filtered to remove trace unreacted solids and the solution was dried under vacuum resulting in a green to yellow solid. This solid can then be purified by trituration in pentane and recrystallized in neat acetonitrile (L=OPPh<sub>3</sub>) or layering dichloromethane and pentane (L=acacH / 5-coordinate). Crystallization in ambient atmosphere yields the hydrate complex. <sup>1</sup>H NMR (400 MHz, CH<sub>2</sub>Cl<sub>2</sub>) (L = OPPh<sub>3</sub>) δ = 1.32 (s, 18H, C(CH<sub>3</sub>)<sub>3</sub>), 1.36 (s, 18H, C(CH<sub>3</sub>)<sub>3</sub>), 7.28 (br s, 15H, OPPh<sub>3</sub>), 7.39 (s, 2H, aryl H), 7.52 (s, 2H, aryl H), 7.61 (d, 2H, pyr H, J = 8 Hz), 7.74 (t, 1H, pyr H, J = 8 Hz). <sup>13</sup>C{<sup>1</sup>H} NMR (CDCl<sub>3</sub>, 500 MHz) δ 30.2 (C(CH<sub>3</sub>)<sub>3</sub>), 31.8 (C(CH<sub>3</sub>)<sub>3</sub>), 34.6 (C(CH<sub>3</sub>)<sub>3</sub>), 35.5 (C(CH<sub>3</sub>)<sub>3</sub>) 122.8, 123.8, 126.3, 128.5, 132.1, 132.5, 138.3, 141.7, 154.9, 155.1, 160.5 (aryl). Anal. Calcd. for C<sub>51</sub>H<sub>58</sub>MoNO<sub>5</sub>P (891.96 g/mol) : C, 68.68%; H, 6.55%; N, 1.57%. Found: C, 66.208%; H, 6.40%; N, 1.41%. Elemental analysis was attempted 6 times and in each case the sample was found to absorb water from the environment in transit. Anal Calcd. for C<sub>51</sub>H<sub>58</sub>MoNO<sub>5</sub>P \* 2H<sub>2</sub>O (910 g/mol) C, 66.19%; H, 6.80%; N, 1.67%. Found: C, 66.208%; H, 6.40%; N, 1.41%. (L = 5-coordinate) δ = 1.41 (s, 18H, C(CH<sub>3</sub>)<sub>3</sub>), 1.44 (s, 18H, C(CH<sub>3</sub>)<sub>3</sub>), 7.64 (s, 2H, aryl H), 7.66 (s, 2H, aryl H), 7.93 (d, 2H, pyr H, J = 8 Hz), 8.20 (t, 1H, pyr H, J = 8 Hz). <sup>13</sup>C{<sup>1</sup>H} NMR (CD<sub>2</sub>Cl<sub>2</sub>, 500 MHz) δ 29.9 (C(CH<sub>3</sub>)<sub>3</sub>), 30.1 (C(CH<sub>3</sub>)<sub>3</sub>), 31.7 (C(CH<sub>3</sub>)<sub>3</sub>), 34.8 (C(CH<sub>3</sub>)<sub>3</sub>), 35.6 (C(CH<sub>3</sub>)<sub>3</sub>), 104.9, 123.1, 123.6, 124.9, 128.5, 138.0, 140.6, 143.8, 154.2 (aryl). Anal. Calcd. for C<sub>33</sub>H<sub>43</sub>MoNO<sub>4</sub> (615.22 g/mol) : C, 64.59%; H, 7.06%; N, 2.28%. Found: C, 62.066%; H, 7.115%; N, 1.839%. Elemental analysis was attempted 4 times and in each case the sample was found to absorb water from the environment in transit. Anal Calcd. for C<sub>33</sub>H<sub>43</sub>MoNO<sub>4</sub> \* 1H<sub>2</sub>O \* 1C<sub>5</sub>H<sub>8</sub>O<sub>2</sub> (731.78 g/mol) C, 62.36%; H, 7.30%; N, 1.91%. Found: C, 62.066%; H, 7.115%; N, 1.839%.

Preliminary Kinetics Study. Reactions were carried out in J. Young high-pressure NMR tubes. The reactions were measured out to be 1:10:10 molar concentrations of catalyst:reductant:substrate. The tubes were charged with the starting materials and toluene-d<sub>8</sub> was added to achieve a concentration of 0.01M catalyst. 1,3,5-trimethoxybenzene was used as an internal standard and triphenylphosphine was used as an external standard for <sup>31</sup>P NMR measurements.

## References

- (1) Gallezot, P. Conversion of Biomass to Selected Chemical Products. *Chem. Soc. Rev.* **2012**, *41* (4), 1538. <https://doi.org/10.1039/c1cs15147a>.
- (2) Cook, G. K.; Andrews, M. a. Toward Nonoxidative Routes to Oxygenated Organics: Stereospecific Deoxydehydration of Diols and Polyols to Alkenes and Allylic Alcohols Catalyzed by the Metal Oxo Complex (C 5 Me 5 )ReO 3. *J. Am. Chem. Soc.* **1996**, *118* (39), 9448–9449. <https://doi.org/10.1021/ja9620604>.
- (3) Shiramizu, M.; Toste, F. D. Deoxygenation of Biomass-Derived Feedstocks: Oxorhenium-Catalyzed Deoxydehydration of Sugars and Sugar Alcohols. *Angew. Chem. - Int. Ed.* **2012**, *51* (32), 8082–8086. <https://doi.org/10.1002/anie.201203877>.
- (4) Shiramizu, M.; Toste, F. D. Expanding the Scope of Biomass-Derived Chemicals through Tandem Reactions Based on Oxorhenium-Catalyzed Deoxydehydration. *Angew. Chem. - Int. Ed.* **2013**, *52* (49), 12905–12909. <https://doi.org/10.1002/anie.201307564>.
- (5) Liu, S.; Senocak, A.; Smeltz, J. L.; Yang, L.; Wegenhart, B.; Yi, J.; Kenttämaa, H. I.; Ison, E. a.; Abu-Omar, M. M. Mechanism of MTO-Catalyzed Deoxydehydration of Diols to Alkenes Using Sacrificial Alcohols. *Organometallics* **2013**, *32* (11), 3210–3219. <https://doi.org/10.1021/om400127z>.
- (6) Ahmad, I.; Chapman, G.; Nicholas, K. M. Sulfite-Driven, Oxorhenium-Catalyzed Deoxydehydration of Glycols. *Organometallics* **2011**, *30* (10), 2810–2818. <https://doi.org/10.1021/om2001662>.
- (7) Boucher-Jacobs, C.; Nicholas, K. M. Catalytic Deoxydehydration of Glycols with Alcohol Reductants. *ChemSusChem* **2013**, *6* (4), 597–599. <https://doi.org/10.1002/cssc.201200781>.
- (8) Boucher-Jacobs, C.; Nicholas, K. M. Oxo-Rhenium-Catalyzed Deoxydehydration of Polyols with Hydroaromatic Reductants. *Organometallics* **2015**, No. Table 1, 150508090015007. <https://doi.org/10.1021/acs.organomet.5b00226>.
- (9) Denning, A. L.; Dang, H.; Liu, Z.; Nicholas, K. M.; Jentoft, F. C. Deoxydehydration of Glycols Catalyzed by Carbon-Supported Perrhenate. *ChemCatChem* **2013**, *5* (12), 3567–3570. <https://doi.org/10.1002/cctc.201300545>.
- (10) Raju, S.; Moret, M.; Klein Gebbink, R. J. M. Rhenium-Catalyzed Dehydration and Deoxydehydration of Alcohols and Polyols: Opportunities for the Formation of Olefins from Biomass. *ACS Catal.* **2014**, 281–300. <https://doi.org/10.1021/cs501511x>.
- (11) Dethlefsen, J. R.; Lupp, D.; Oh, B. C.; Fristrup, P. Molybdenum-Catalyzed Deoxydehydration of Vicinal Diols. *ChemSusChem* **2014**, *7* (2), 425–428. <https://doi.org/10.1002/cssc.201300945>.
- (12) Dethlefsen, J. R.; Lupp, D.; Teshome, A.; Nielsen, L. B.; Fristrup, P. Molybdenum-Catalyzed Conversion of Diols and Biomass-Derived Polyols to Alkenes Using Isopropyl Alcohol as Reductant and Solvent. *ACS Catal.* **2015**, 3638–3647. <https://doi.org/10.1021/acscatal.5b00427>.

- (13) Beckerle, K.; Sauer, A.; Spaniol, T. P.; Okuda, J. Bis(Phenolato)Molybdenum Complexes as Catalyst Precursors for the Deoxydehydration of Biomass-Derived Polyols. *Polyhedron* **2016**, *116*, 105–110. <https://doi.org/10.1016/j.poly.2016.03.053>.
- (14) Navarro, C. A.; John, A. Deoxydehydration Using a Commercial Catalyst and Readily Available Reductant. *Inorganic Chemistry Communications* **2018**, *99*, 145–148. <https://doi.org/10.1016/j.inoche.2018.11.015>.
- (15) Stalpaert, M.; De Vos, D. Stabilizing Effect of Bulky  $\beta$ -Diketones on Homogeneous Mo Catalysts for Deoxydehydration. *ACS Sustainable Chemistry & Engineering* **2018**, *6* (9), 12197–12204. <https://doi.org/10.1021/acssuschemeng.8b02532>.
- (16) Heinze, Katja. Bioinspired Functional Analogs of the Active Site of Molybdenum Enzymes: Intermediates and Mechanisms. *Coord. Chem. Rev.* **2015**, *300*, 121–141. <https://doi.org/10.1016/j.ccr.2015.04.010>.
- (17) Majumdar, Amit. Structural and Functional Models in Molybdenum and Tungsten Bioinorganic Chemistry: Description of Selected Model Complexes, Present Scenario and Possible Future Scopes. *Dalton Trans.* **2014**, *43*, 8990–9003. <https://doi.org/10.1039/c4dt00631c>.
- (18) Majumdar, A.; Sarkar, Sabyasachi. Bioinorganic Chemistry of Molybdenum and Tungsten Enzymes: A Structural-Functional Modeling Approach. *Coord. Chem. Rev.* **2011**, *255*, 1039–1054. <https://doi.org/10.1016/j.ccr.2010.11.027>.
- (19) Berg, J. M.; Holm, R. H. Synthetic Approach to the Mononuclear Active Sites of Molybdoenzymes: Catalytic Oxygen Atom Transfer Reactions by Oxomolybdenum(IV,VI) Complexes with Saturation Kinetics and without Molybdenum(V) Dimer Formation. *J. Am. Chem. Soc.* **1984**, *106*, 3035–3036. <https://doi.org/10.1021/ja00322a050>.
- (20) Berg, J. M.; Holm, R. H. Model for the Active Site of Oxo-Transfer Molybdoenzymes: Synthesis, Structure, and Properties. *J. Am. Chem. Soc.* **1985**, *107*, 917–925. <https://doi.org/10.1021/ja00290a029>.
- (21) Hawkins, J. M.; Dewan, J. C.; Sharpless, K. B. Dioxomolybdenum(VI)-Substituted 2,6-Pyridinedimethanol Complexes: New Five-Coordinate Species. *Inorg. Chem.* **1986**, *25* (9), 1501–1503. <https://doi.org/10.1021/ic00229a041>.
- (22) Most, K.; Koepke, S.; Dall'Antonia, F.; Moesch-Zanetti, N. C. The First Molybdenum Dioxo Compounds with H<sub>2</sub>-Pyrazolate Ligands: Crystal Structure and Oxo Transfer Properties. *Chem. Commun. (Cambridge, U. K.)* **2002**, 1676–1677. <https://doi.org/10.1039/B205420E>.
- (23) Dinda, R.; Sengupta, P.; Ghosh, S.; Sheldrick, W. S. Synthesis, Structure, and Reactivity of a New Mononuclear Molybdenum(VI) Complex Resembling the Active Center of Molybdenum Oxotransferases. *Eur. J. Inorg. Chem.* **2003**, 363–369. <https://doi.org/10.1002/ejic.200390049>.
- (24) Pedrosa, M. R.; Escribano, J.; Aguado, R.; Sanz, R.; Díez, V.; Arnáiz, F. J. Synthesis, Crystal Structure and Reactivity of a New Pentacoordinated Chiral Dioxomolybdenum(VI) Complex. *Polyhedron* **2010**, *29* (2), 841–849. <https://doi.org/10.1016/j.poly.2009.09.022>.

- (25) Stylianou, M.; Nikolakis, V. A.; Chilas, G. I.; Jakusch, T.; Vaimakis, T.; Kiss, T.; Sigalas, M. P.; Keramidis, A. D.; Kabanos, T. A. Molybdenum(VI) Coordination Chemistry of the N,N-Disubstituted Bis(Hydroxylamido)-1,3,5-Triazine Ligand, H<sub>2</sub>bihyat. Water-Assisted Activation of the MoVI=O Bond and Reversible Dimerization of Cis-[Mo(VI)O<sub>2</sub>(Bihyat)] to [MoVI<sub>2</sub>O<sub>4</sub>(Bihyat)<sub>2</sub>(H<sub>2</sub>O)<sub>2</sub>]. *Inorg. Chem.* **2012**, *51* (24), 13138–13147. <https://doi.org/10.1021/ic301282q>.
- (26) Bellemin-Laponnaz, S.; Coleman, K. S.; Dierkes, P.; Masson, J.-P.; Osborn, J. A. Synthesis and Coordination of the New Chiral Tridentate O,N,O Ligand 2,6-Bis[(1S,2S,5R)-1-Hydroxy-(-)-Menthyl]pyridine to Molybdenum(VI) and Vanadium(V) Oxo Complexes: Crystal Structures of [(2,6-Bis{1-Hydroxy-(-)-Menthyl}pyridine)MoO<sub>2</sub>] and [(2,6-Bis{1-Hydroxy-(-)-Menthyl}pyridine)VO]<sub>2</sub>(μ-O). *Eur. J. Inorg. Chem.* **2000**, All Rights Reserved., 1645–1649. [https://doi.org/10.1002/1099-0682\(200007\)2000:7](https://doi.org/10.1002/1099-0682(200007)2000:7)
- (27) Hills, L.; Moyano, R.; Montilla, F.; Pastor, A.; Galindo, A.; Álvarez, E.; Marchetti, F.; Pettinari, C. Dioxomolybdenum(VI) Complexes with Acylpyrazolonate Ligands: Synthesis, Structures, and Catalytic Properties. *Eur. J. Inorg. Chem.* **2013**, No. 19, 3352–3361. <https://doi.org/10.1002/ejic.201300098>.
- (28) Beckerle, K.; Sauer, A.; Spaniol, T. P.; Okuda, J. Bis(Phenolato)Molybdenum Complexes as Catalyst Precursors for the Deoxydehydration of Biomass-Derived Polyols. *Polyhedron* **2016**, 3–8. <https://doi.org/10.1016/j.poly.2016.03.053>.
- (29) Lupp, D.; Christensen, N. J.; Dethlefsen, J. R.; Fristrup, P. DFT Study of the Molybdenum-Catalyzed Deoxydehydration of Vicinal Diols. *Chemistry (Weinheim an der Bergstrasse, Germany)* **2015**, *21* (8), 3435–3442. <https://doi.org/10.1002/chem.201405473>.
- (30) Gable, K. P.; AbuBaker, A.; Zientara, K.; Wainwright, A. M. Cycloreversion of Rhenium(V) Diolates Containing the Hydridotris(3,5-Dimethylpyrazolyl)Borate Ancillary Ligand. *Organometallics* **1999**, *18* (2), 173–179. <https://doi.org/10.1021/om980807o>.
- (31) Gable, K. P.; Phan, T. N. Extrusion of Alkenes from Rhenium(V) Diolates: Energetics and Mechanism. *J. Am. Chem. Soc.* **1994**, *116* (3), 833–839. <https://doi.org/10.1021/ja00082a002>.
- (32) Gable, K. P.; Juliette, J. J. J. Hammett Studies on Alkene Extrusion from Rhenium(V) Diolates and an MO Description of Metal Alkoxide–Alkyl Metal Oxo Interconversion. *J. Am. Chem. Soc.* **1996**, *118* (11), 2625–2633. <https://doi.org/10.1021/ja952537w>.
- (33) Gable, K. P.; Juliette, J. J. J. Extrusion of Alkenes from Rhenium(V) Diolates: The Effect of Substitution and Conformation. *J. Am. Chem. Soc.* **1995**, *117* (3), 955–962. <https://doi.org/10.1021/ja00108a012>.

## Supporting Information

X-Ray Crystallography for 1. (L = OPPh<sub>3</sub>) A green, block-shaped crystal of dimensions 0.09 x 0.10 x 0.36 mm was selected for structural analysis. Intensity data for this compound were collected using a diffractometer with a Bruker APEX ccd area detector<sup>2</sup> and graphite-monochromated Mo K $\alpha$  radiation ( $\lambda = 0.71073 \text{ \AA}$ ). The sample was cooled to 100(2) K. Cell parameters were determined from a least-squares fit of 9381 peaks in the range  $2.25 < \theta < 25.37^\circ$ . A total of 34540 data were measured in the range  $1.393 < \theta < 25.737^\circ$  using  $\phi$  and  $\omega$  oscillation frames. The data were corrected for absorption by the empirical method<sup>3</sup> giving minimum and maximum transmission factors of 0.6603 and 0.7453. The data were merged to form a set of 9608 independent data with  $R(\text{int}) = 0.0393$  and a coverage of 99.9 %.

The orthorhombic space group  $P2_12_12_1$  was determined by systematic absences and statistical tests and verified by subsequent refinement. The structure was solved by direct methods and refined by full-matrix least-squares methods on  $F^2$ .<sup>4</sup> The positions of hydrogens were initially determined by geometry and were refined using a riding model. Non-hydrogen atoms were refined with anisotropic displacement parameters. Hydrogen atom displacement parameters were set to 1.2 (1.5 for methyl) times the isotropic equivalent displacement parameters of the bonded atoms. A total of 586 parameters were refined against 18 restraints and 9608 data to give  $wR(F^2) = 0.0971$  and  $S = 0.999$  for weights of  $w = 1/[\sigma^2(F^2) + (0.0600 P)^2 + 3.3000 P]$ , where  $P = [F_o^2 + 2F_c^2] / 3$ . The final  $R(F)$  was 0.0376 for the 8826 observed,  $[F > 4\sigma(F)]$ , data. The largest shift/s.u. was 0.001 in the final refinement cycle. The final difference map had maxima and minima of 0.482 and -0.795 e/ $\text{\AA}^3$ , respectively. The absolute structure was determined by refinement of the Flack parameter<sup>5</sup>.

X-Ray Crystallography for 2. (L = 5-coordinate) A yellow, needle-shaped crystal of dimensions 0.031 x 0.034 x 0.252 mm was selected for structural analysis. Intensity data for this compound were collected using a D8 Quest diffractometer with a Bruker Photon II cpad area

detector<sup>2</sup> and an Incoatec I $\mu$ s microfocus Mo K $\alpha$  source ( $\lambda = 0.71073 \text{ \AA}$ ). The sample was cooled to 100(2) K. Cell parameters were determined from a least-squares fit of 9975 peaks in the range  $2.21 < \theta < 27.07^\circ$ . A total of 52,537 data were measured in the range  $2.208 < \theta < 27.135^\circ$  using  $\phi$  and  $\omega$  oscillation frames. The data were corrected for absorption by the empirical method<sup>3</sup> giving minimum and maximum transmission factors of 0.6042 and 0.6941. The data were merged to form a set of 6820 independent data with  $R(\text{int}) = 0.0742$  and a coverage of 99.9 %.

The monoclinic space group  $P2_1/c$  was determined by systematic absences and statistical tests and verified by subsequent refinement. The structure was solved by direct methods and refined by full-matrix least-squares methods on  $F^2$ .<sup>4</sup> The positions of hydrogens bonded to carbons were initially determined by geometry and were refined using a riding model. Non-hydrogen atoms were refined with anisotropic displacement parameters. Hydrogen atom displacement parameters were set to 1.2 (1.5 for methyl) times the isotropic equivalent displacement parameters of the bonded atoms. A total of 364 parameters were refined against 6820 data to give  $wR(F^2) = 0.1013$  and  $S = 1.003$  for weights of  $w = 1/[\sigma^2(F^2) + (0.0500 P)^2 + 2.9200 P]$ , where  $P = [F_o^2 + 2F_c^2] / 3$ . The final  $R(F)$  was 0.0342 for the 5132 observed,  $[F > 4\sigma(F)]$ , data. The largest shift/s.u. was 0.001 in the final refinement cycle. The final difference map had maxima and minima of 0.446 and -0.686 e/ $\text{\AA}^3$ , respectively.

## NMR characterizations

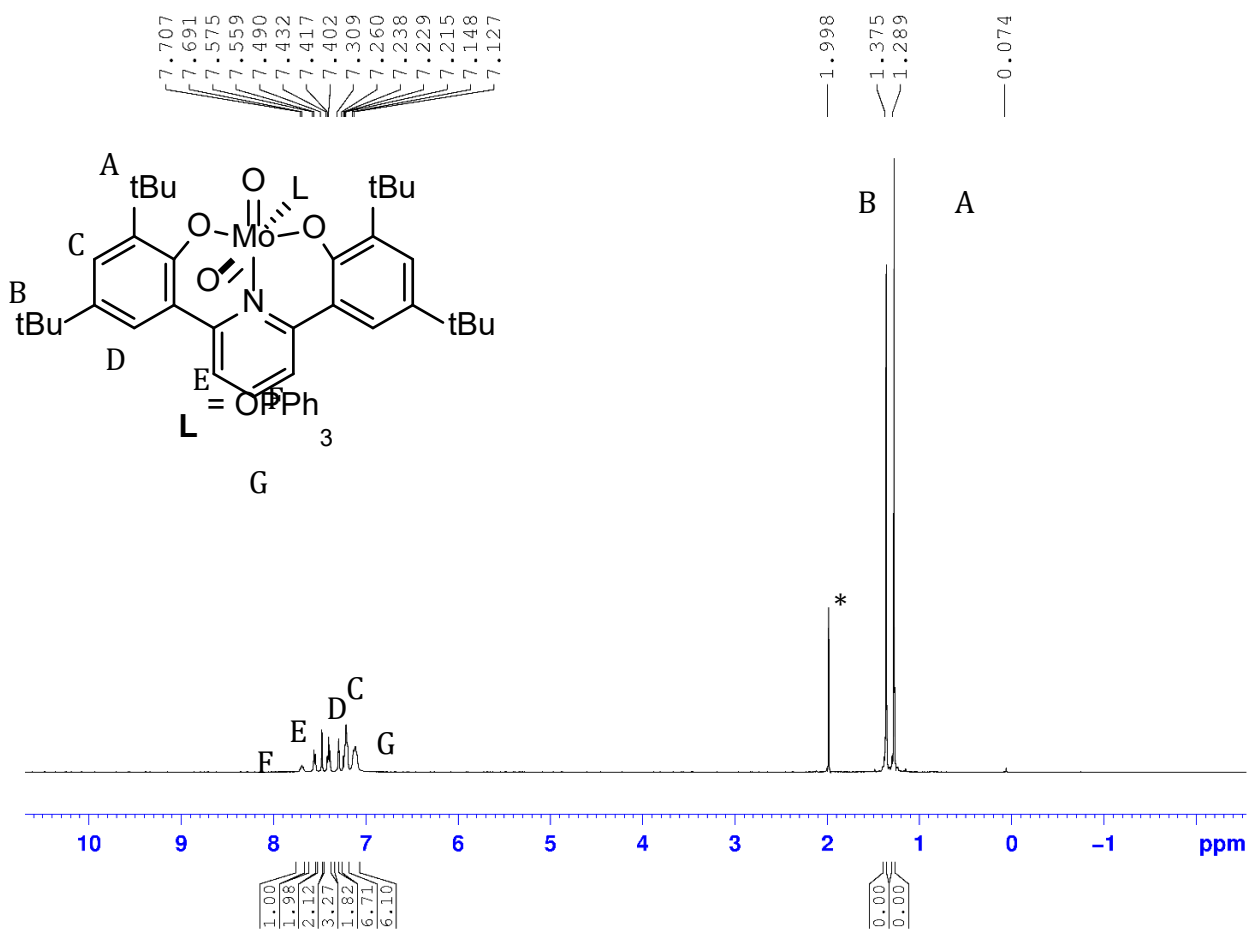


**Figure S1.** Catalyst L = OPPh<sub>3</sub> (<sup>1</sup>H, 500 MHz, CDCl<sub>3</sub>) The OPPh<sub>3</sub> is weakly bound in solution and the rate of dissociation/association is approximately that of the NMR timescale.

“\*” = acetonitrile

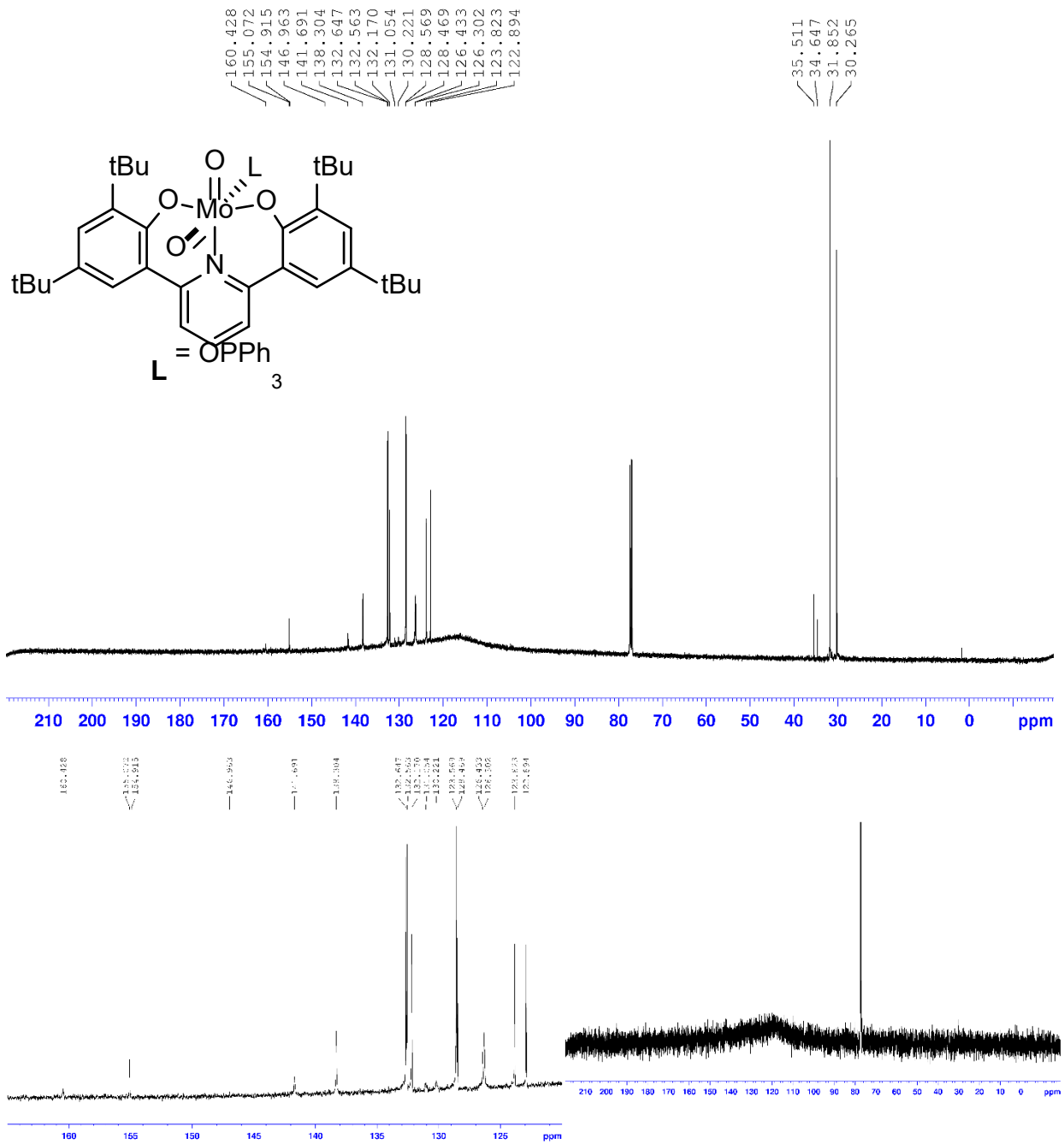
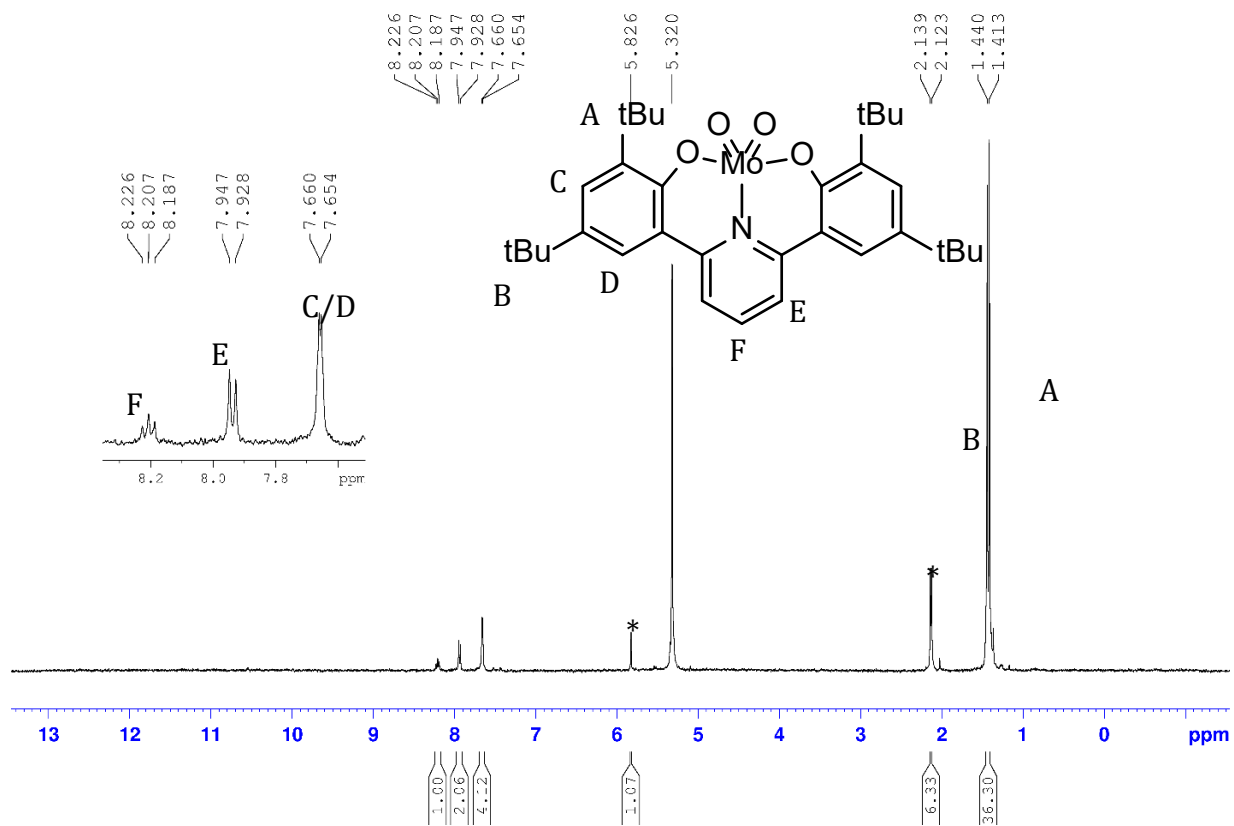


Figure S2. Catalyst L = OPPh<sub>3</sub> (<sup>13</sup>C{<sup>1</sup>H}, 500 MHz, CDCl<sub>3</sub>) Bottom: aryl region



**Figure S3.** Catalyst 5-coordinate (1H, 500 MHz, CDCl<sub>3</sub>)

\* = acetylacetone



## Quantitation of Yields by NMR Experiments

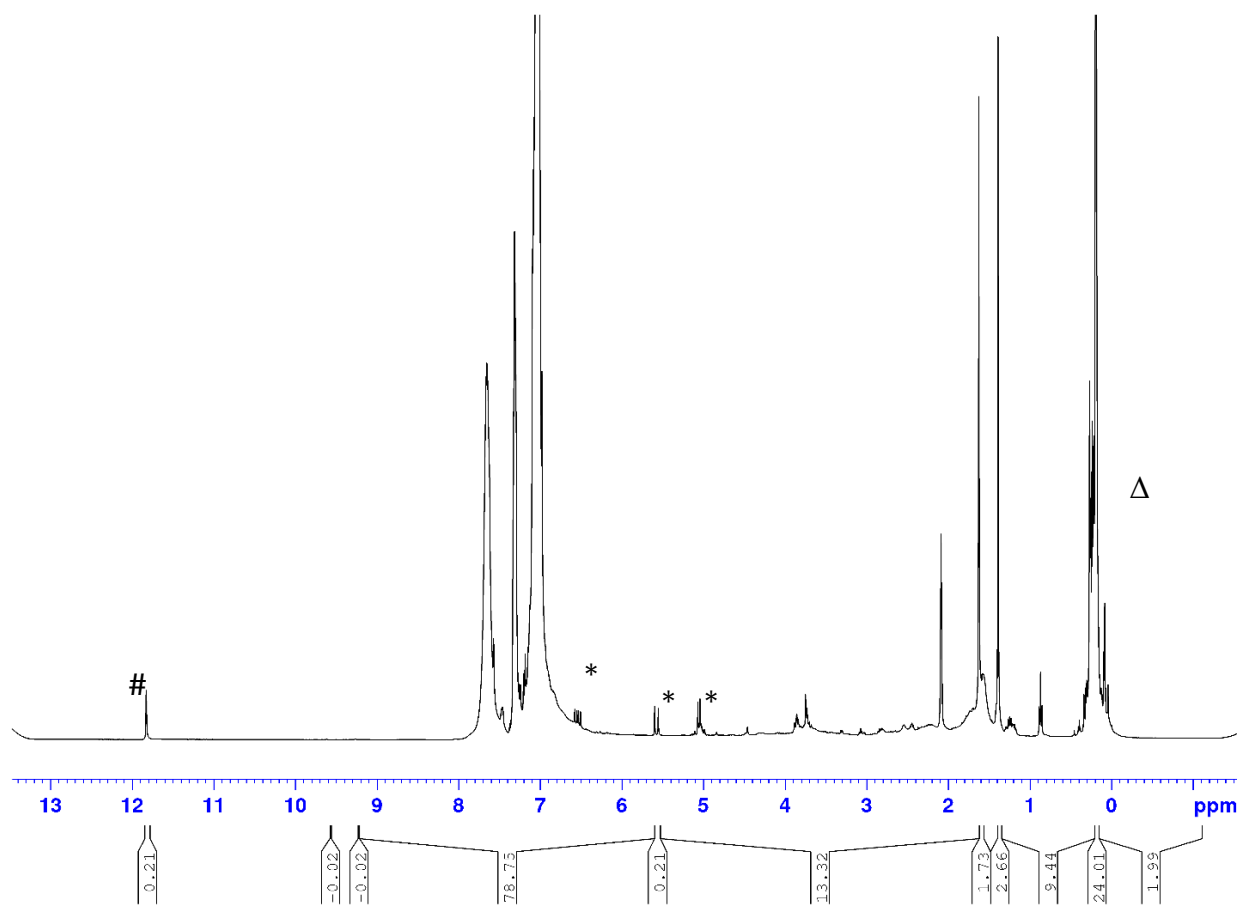


**Figure S5.** Catalyst 1 L = OPh<sub>3</sub>, PPh<sub>3</sub>, 1-phenyl-1,2-ethanediol, hexamethylcyclotrisiloxane  
48h 150°C 1H NMR (1H, 500 MHz, toluene-d<sub>8</sub>)

“\*” denotes styrene resonances tracked

“#” denotes free ligand (P3)

“Δ” denotes internal standard

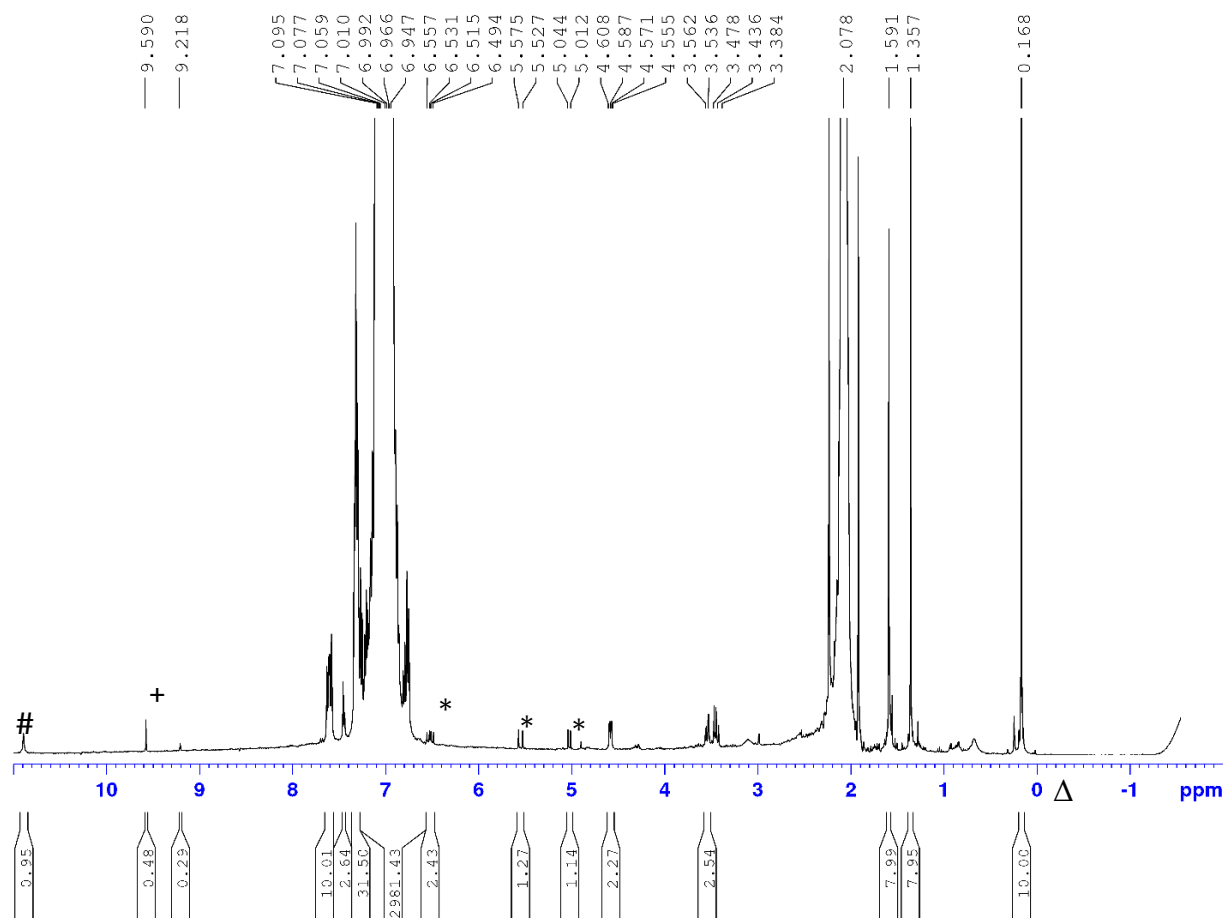


**Figure S6.** Catalyst 2 L = none, PPh<sub>3</sub>, 1-phenyl-1,2-ethanediol, hexamethylcyclotrisiloxane 48h 150°C (1H, 500 MHz, toluene-d<sub>8</sub>)

“\*” denotes styrene resonances tracked

“#” denotes free ligand (P3)

“+” denotes aldehyde

“Δ” denotes internal standard

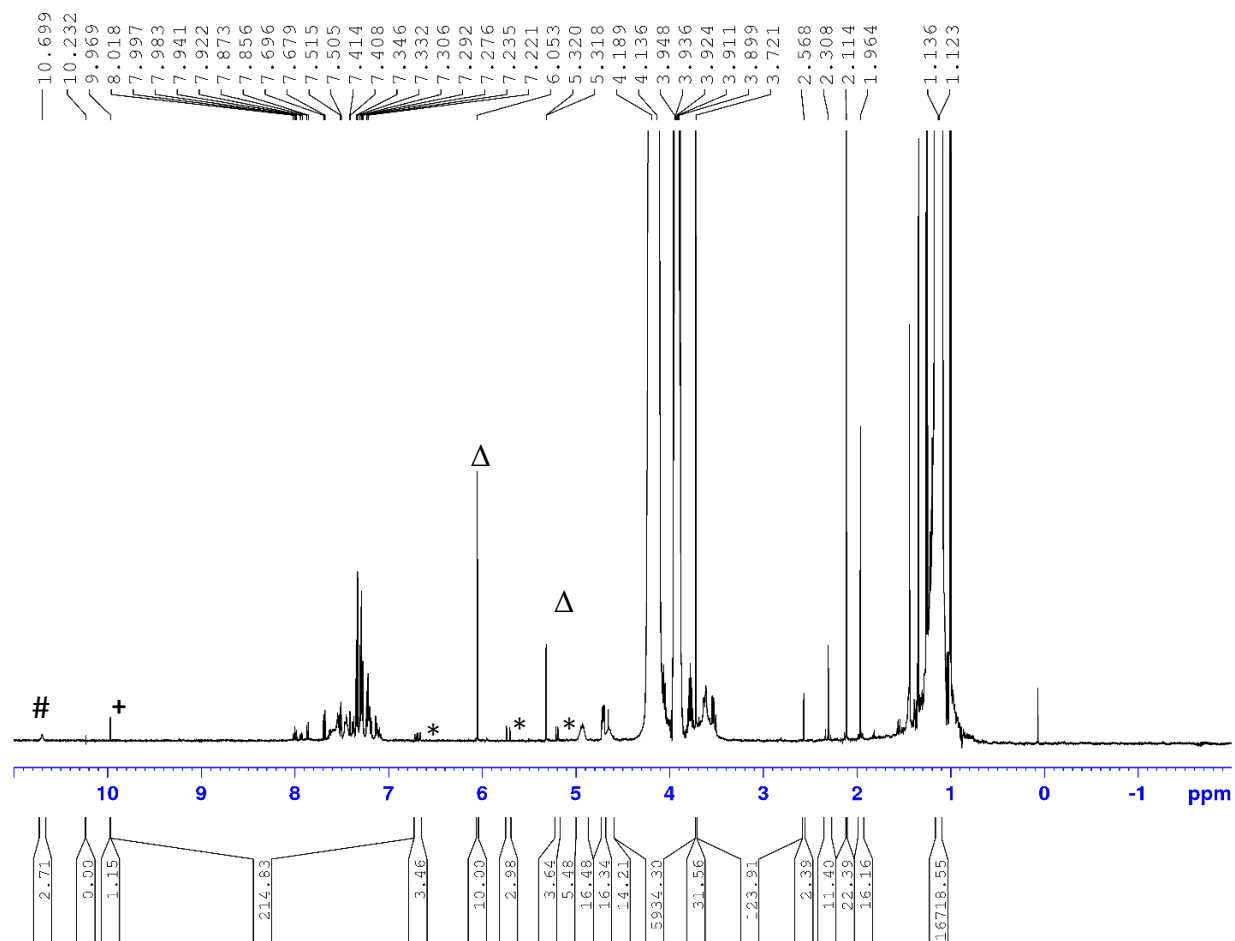


**Figure S7.** Catalyst 1 L = OPh<sub>3</sub>, PPh<sub>3</sub>, 1-phenyl-1,2-ethanediol, 1,3,5-trimethoxybenzene 48h 150°C (1H, 500 MHz, CD<sub>2</sub>Cl<sub>2</sub>)

“\*” denotes styrene resonances tracked

“#” denotes free ligand (P3)

“+” denotes aldehyde

“Δ” denotes internal standard

### Kinetics Studies

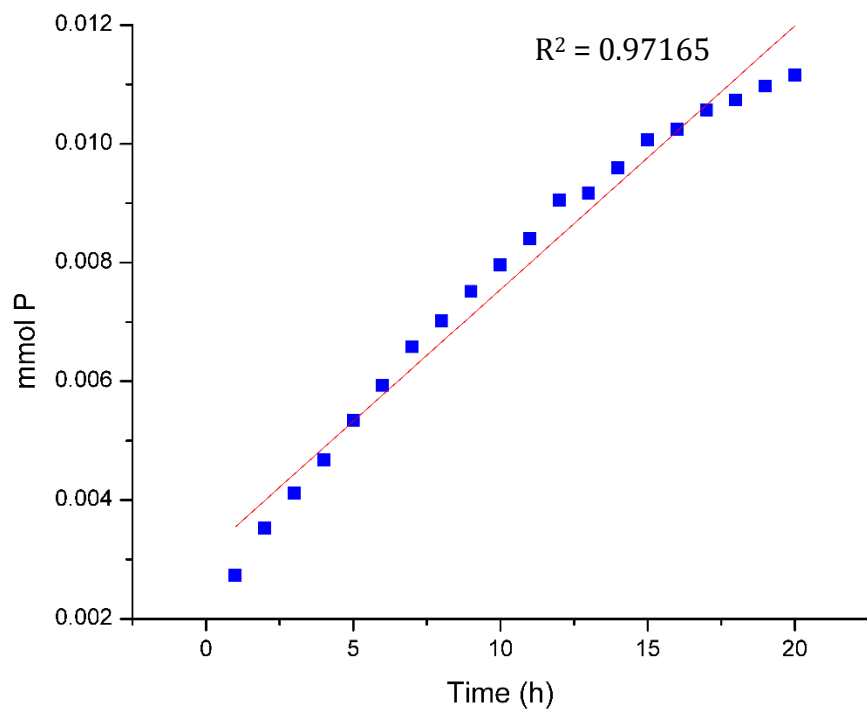


**Figure S8.** Monitored growth of styrene versus time.

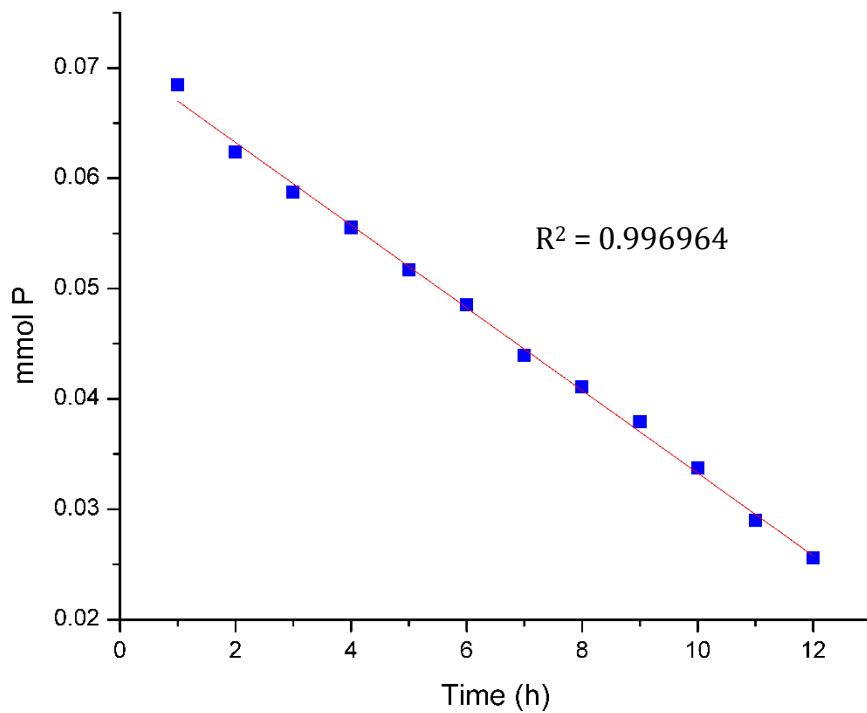


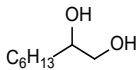
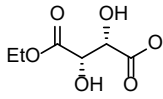
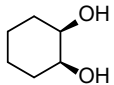
**Figure S9.** Monitored consumption of diol vs time.

## Determination of Yields for Catalytic Reactions

$$\frac{\text{int } P}{\text{int std}} * \frac{H \text{ std}}{H P} * \frac{\text{mmol std}}{\text{sample}} * \frac{\text{vol reaction}}{\text{vol aliquot}} = \text{mmol } P$$

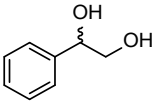
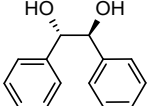
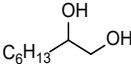
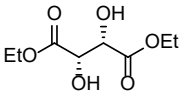
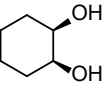
Int:	description	int H's	mmol P	adjusted mmol	% Yield vs diol
2.9078	styrene	1	0.000288459	0.008241674	0.8025%
22.5149	acetone	6	0.013401094	0.382888389	37.2824%
1.1309	formyl	2	0.000224374	0.006410695	0.6242%

Sample calculation of Catalytic Yields

<b>Table T1. DODH of aliphatic and biomass diols by 1 and 2</b>			
Substrate	Reductant	Yield Cat 1	Yield Cat2
	PPh <sub>3</sub>	Trace	Trace
	Na <sub>2</sub> SO <sub>3</sub>	Trace	Trace
	iPr-OH	Trace	Trace
	Zinc	Trace	Trace
	Carbon	Trace	Trace
	PPh <sub>3</sub>	29%	-
	Na <sub>2</sub> SO <sub>3</sub>	7%	-
	iPr-OH	10%	-
	Zinc	13%	-
	Carbon	16%	-
	PPh <sub>3</sub>	Trace	-
	Na <sub>2</sub> SO <sub>3</sub>	Trace	-
	iPr-OH	Trace	-
	Zinc	Trace	-
	Carbon	Trace	-

Reactions were run for 48 hours at 150°C.

**Table of All Reactions Before Averaging**

<b>Table T2</b>					
Substrate	Reductant	1 L = OPPh <sub>3</sub>		2 L = 5-coordinate	
	PPh <sub>3</sub>	45%	47.8%	34%	33%
	Na <sub>2</sub> SO <sub>3</sub>	52%	50%	51%	55%
	iPr-OH	0.84%	0.80%	49%	47%
	Zinc	56%	64%	42%	35%
	Carbon	56%	68.8%	57%	60.6%
	PPh <sub>3</sub>	33%	32%	58%	55%
	Na <sub>2</sub> SO <sub>3</sub>	51%	50%	47%	49%
	iPr-OH	18.7%	18.4%	-	-
	Zinc	52%	34%	38%	40. %8
	Carbon	36%	44%	35%	52%
	PPh <sub>3</sub>	Trace	Trace	Trace	Trace
	Na <sub>2</sub> SO <sub>3</sub>	Trace	Trace	Trace	Trace
	iPr-OH	Trace	Trace	Trace	Trace
	Zinc	Trace	Trace	Trace	Trace
	Carbon	Trace	Trace	Trace	Trace
	PPh <sub>3</sub>	27.5%	30.3%	-	-
	Na <sub>2</sub> SO <sub>3</sub>	8.7%	5.4%	-	-
	iPr-OH	-	-	-	-
	Zinc	12.8%	12.4%	-	-
	Carbon	15.9%	16.6%	-	-
	PPh <sub>3</sub>	Trace	Trace	Trace	Trace
	Na <sub>2</sub> SO <sub>3</sub>	Trace	Trace	Trace	Trace
	iPr-OH	Trace	Trace	Trace	Trace
	Zinc	Trace	Trace	Trace	Trace
	Carbon	Trace	Trace	Trace	Trace

## X-ray crystallography

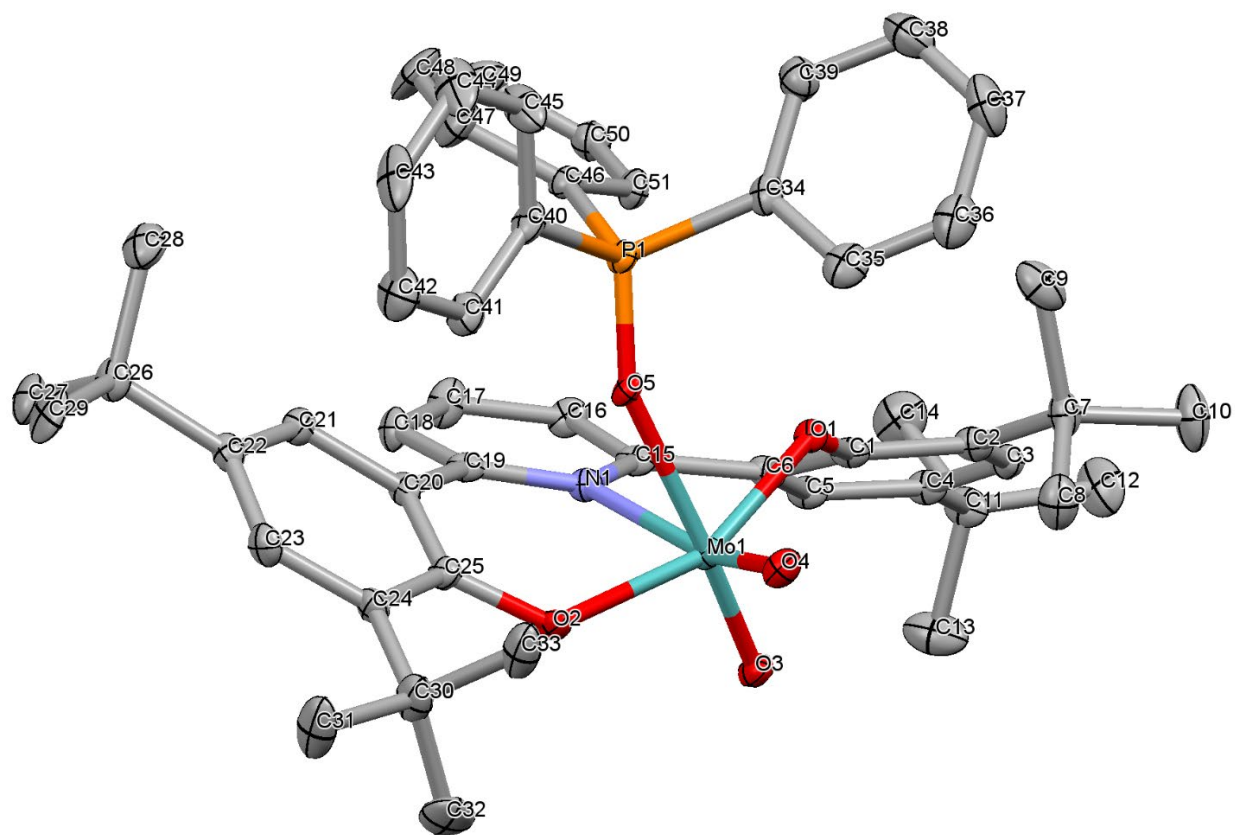


**Figure S10.** X-ray structure of **1** L=OPPh<sub>3</sub>. The displacement ellipsoids are drawn at 50% probability level. Hydrogen atoms were omitted for clarity.

**Table T3.** Crystal data and structure refinement for **1 L = OPPh<sub>3</sub>**.

Empirical formula	(C <sub>51</sub> H <sub>58</sub> Mo N O <sub>5</sub> P) · 2(C <sub>2</sub> H <sub>3</sub> N)	
	C <sub>55</sub> H <sub>64</sub> Mo N <sub>3</sub> O <sub>5</sub> P	
Formula weight	974.00	
Crystal system	orthorhombic	
Space group	<i>P</i> 2 <sub>1</sub> 2 <sub>1</sub> 2 <sub>1</sub>	
Unit cell dimensions	<i>a</i> = 10.6148(11) Å	α = 90°
	<i>b</i> = 17.2317(19) Å	β = 90°
	<i>c</i> = 27.584(4) Å	γ = 90°
Volume	5045.4(11) Å <sup>3</sup>	
Z, Z'	4, 1	
Density (calculated)	1.282 Mg/m <sup>3</sup>	
Wavelength	0.71073 Å	
Temperature	100(2) K	
<i>F</i> (000)	2048	
Absorption coefficient	0.341 mm <sup>-1</sup>	
Absorption correction	semi-empirical from equivalents	
Max. and min. transmission	0.7453 and 0.6603	
Theta range for data collection	1.393 to 25.737°	
Reflections collected	34540	
Independent reflections	9608 [R(int) = 0.0393]	
Data / restraints / parameters	9608 / 18 / 586	
<i>wR</i> ( <i>F</i> <sup>2</sup> all data)	<i>wR</i> 2 = 0.0971	
<i>R</i> ( <i>F</i> obsd data)	<i>R</i> 1 = 0.0376	
Goodness-of-fit on <i>F</i> <sup>2</sup>	0.999	
Observed data [ <i>I</i> > 2σ( <i>I</i> )]	8826	
Absolute structure parameter	-0.017(12)	
Largest and mean shift / s.u.	0.001 and 0.000	
Largest diff. peak and hole	0.482 and -0.795 e/Å <sup>3</sup>	

-----

$$wR2 = \{ \sum [w(F_o^2 - F_c^2)^2] / \sum [w(F_o^2)^2] \}^{1/2}$$

$$R1 = \sum ||F_o| - |F_c|| / \sum |F_o|$$

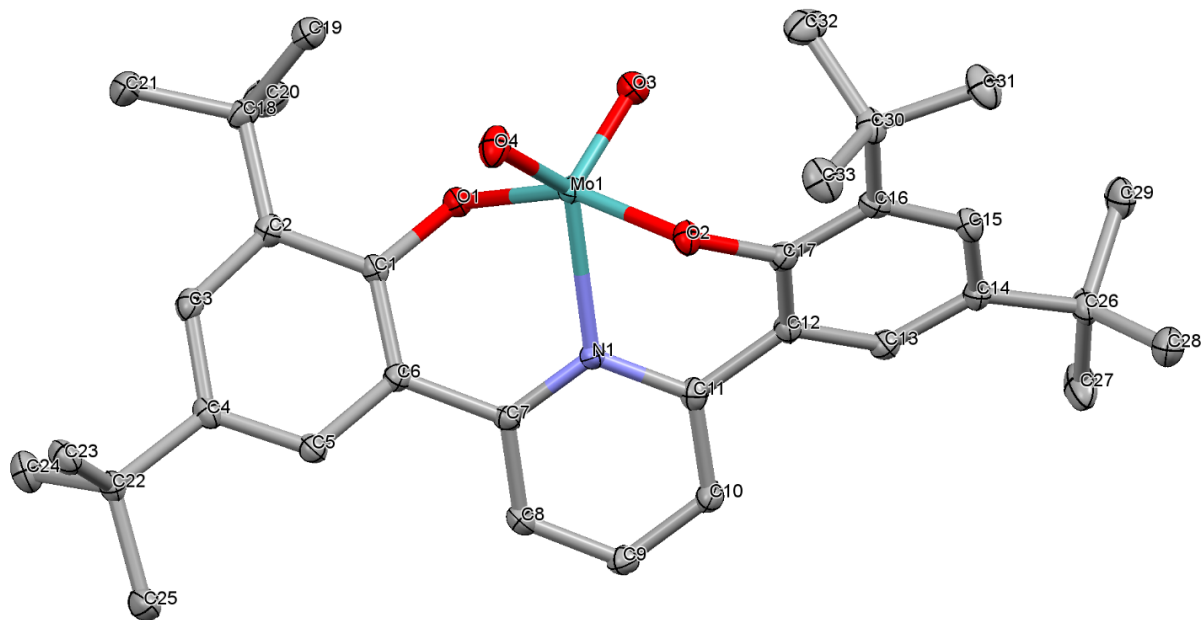


**Figure S11.** X-ray structure of **2** L=5-coordinate. The displacement ellipsoids are drawn at 50% probability level. Hydrogen atoms were omitted for clarity.

**Table T4.** Crystal data and structure refinement for **2 L = 5-coordinate.**

Empirical formula	$C_{33} H_{43} Mo N O_4$	
Formula weight	613.62	
Crystal system	monoclinic	
Space group	$P2_1/c$	
Unit cell dimensions	$a = 17.6718(6) \text{ \AA}$	$\alpha = 90^\circ$
	$b = 11.7729(4) \text{ \AA}$	$\beta = 118.4751(14)^\circ$
	$c = 16.8857(6) \text{ \AA}$	$\gamma = 90^\circ$
Volume	$3088.05(19) \text{ \AA}^3$	
Z, Z'	4, 1	
Density (calculated)	$1.320 \text{ Mg/m}^3$	
Wavelength	$0.71073 \text{ \AA}$	
Temperature	$100(2) \text{ K}$	
$F(000)$	1288	
Absorption coefficient	$0.461 \text{ mm}^{-1}$	
Absorption correction	semi-empirical from equivalents	
Max. and min. transmission	0.6941 and 0.6042	
Theta range for data collection	$2.208$ to $27.135^\circ$	
Reflections collected	52537	
Independent reflections	6820 [R(int) = 0.0742]	
Data / restraints / parameters	6820 / 0 / 364	
$wR(F^2 \text{ all data})$	$wR2 = 0.1013$	
$R(F \text{ obsd data})$	$R1 = 0.0342$	
Goodness-of-fit on $F^2$	1.003	
Observed data [ $ I  > 2\sigma(I)$ ]	5132	
Largest and mean shift / s.u.	0.001 and 0.000	
Largest diff. peak and hole	0.446 and $-0.686 \text{ e/\AA}^3$	

-----

$$wR2 = \{ \sum [w(F_o^2 - F_c^2)^2] / \sum [w(F_o^2)^2] \}^{1/2}$$

$$R1 = \sum ||F_o| - |F_c|| / \sum |F_o|$$

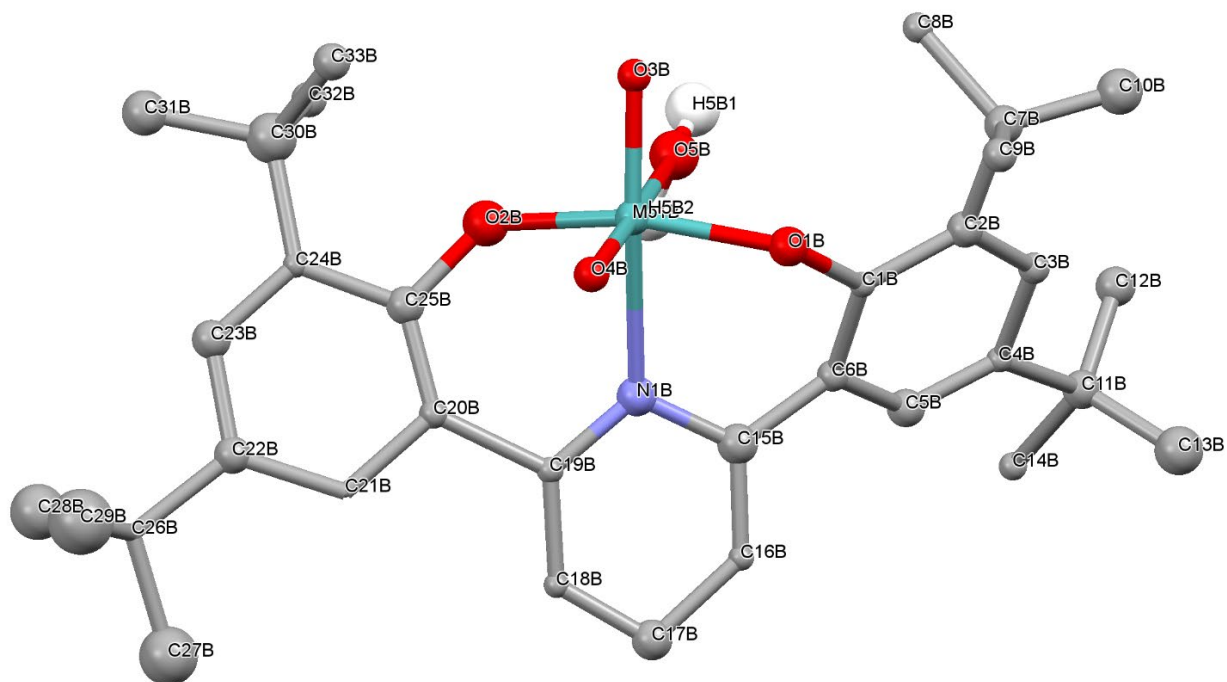


**Figure S12.** X-ray structure of **3** L=H<sub>2</sub>O. The displacement ellipsoids are drawn at 50% probability level. Hydrogen atoms were omitted for clarity.

**Table T5.** Crystal data and structure refinement for **3 L = H<sub>2</sub>O**.

Empirical formula	C33 H47 Mo N O6	
Formula weight	649.65	
Crystal system	triclinic	
Space group	$P\bar{1}$	
Unit cell dimensions	$a = 11.896(17) \text{ \AA}$	$\alpha = 65.73(3)^\circ$
	$b = 15.96(3) \text{ \AA}$	$\beta = 84.21(3)^\circ$
	$c = 18.68(3) \text{ \AA}$	$\gamma = 82.87(3)^\circ$
Volume	3203(9) $\text{\AA}^3$	
Z, Z'	4, 2	
Density (calculated)	1.347 Mg/m <sup>3</sup>	
Wavelength	0.71073 $\text{\AA}$	
Temperature	100(2) K	
$F(000)$	1368	
Absorption coefficient	0.452 mm <sup>-1</sup>	
Absorption correction	semi-empirical from equivalents	
Max. and min. transmission	0.982 and 0.843	
Theta range for data collection	1.198 to 16.793 $^\circ$	
Reflections collected	23495	
Independent reflections	3591 [R(int) = 0.0969]	
Data / restraints / parameters	3591 / 12 / 333	
$wR(F^2 \text{ all data})$	$wR2 = 0.2705$	
$R(F \text{ obsd data})$	$R1 = 0.1002$	
Goodness-of-fit on $F^2$	1.027	
Observed data [ $ I  > 2\sigma(I)$ ]	1965	
Largest and mean shift / s.u.	0.000 and 0.000	
Largest diff. peak and hole	1.052 and -1.468 e/ $\text{\AA}^3$	

$$wR2 = \{ \sum [w(F_o^2 - F_c^2)^2] / \sum [w(F_o^2)^2] \}^{1/2}$$

$$R1 = \sum ||F_o| - |F_c|| / \sum |F_o|$$

## **Acknowledgements**

The authors thank the National Science Foundation (grant CHE-0130835) and the University of Oklahoma for funds to purchase of the X-ray instrument and computers. This structure was determined by Douglas R. Powell.

## References

- (1) Fu, R.; Bercaw, J. E.; Labinger, J. A. Intra- and Intermolecular C–H Activation by Bis(Phenolate)Pyridineiridium(III) Complexes. *Organometallics* **2011**, *30* (24), 6751–6765. <https://doi.org/10.1021/om201069k>.
- (2) (a) Data Collection: APEX2 (2007) Bruker AXS Inc., Madison, Wisconsin, USA. (b) Data Reduction: SAINT (2007) Bruker AXS Inc., Madison, Wisconsin, USA.
- (3) L. Krause, R. Herbst-Irmer, G. M. Sheldrick, and D. Stalke (2015). *J. Appl. Cryst.*, *48*, 3-10.
- (4) (a) G. M. Sheldrick (2015). *Acta Cryst.*, *A71*, 3-8. (b) G. M. Sheldrick (2015). *Acta Cryst.*, *C71*, 3-8.
- (5) S. Parsons, H. D. Flack, and T. Wagner (2013). *Acta Cryst.*, *B69*, 249-259.

## Chapter 4

### Electrochemical Investigation of a Bisphenylatopyridyl Dioxomolybdenum Complex

#### Introduction

The global problem facing inhabitants of the 21<sup>st</sup> century, rising CO<sub>2</sub> emissions, must be addressed. The environmental effects of rising CO<sub>2</sub> emissions are well documented. One major source of emissions lies in the industrial chemical sector; current industry standards utilize various harsh methods and rare-earth metals to deoxygenate high oxygen compounds to access the target carbon compounds. Alternative methods to generate these compounds are actively pursued. Deoxydehydration (DODH) serves as a potential method to combat and alleviate the rising emissions. DODH can synthesize the important industrial commodity chemicals from agricultural-derived diols and polyols at relatively milder conditions. Early work on this process revolved around rhenium but recent work has explored abundant earth alternatives such as vanadium and molybdenum. Chapters 2 and 3 explored molybdenum oxo catalysts as potential candidates for DODH. They exhibited appreciable and distinct activity, but is it still limited to the lab bench. As outlined in chapter 1, the poly-oxo catalyst must be reduced to its active species to catalyze DODH typically by way of chemical reductant. This active reduced species condenses with the diol substrate and then regenerates the poly-oxo catalyst by extruding the deoxygenated substrate. DODH is not currently industrially viable for a variety of reasons: 1) the relative prohibitive cost and low earth abundance of rhenium ores 2) the use chemical reductants such as phosphines and the concomitant formation of chemical waste 3) the reported over reduction of rhenium catalysts resulting in catalyst death and catalyst dimerization also resulting in catalyst death. There has been a body of work reported in recent years detailing researcher's efforts in addressing these issues. Vanadium and molybdenum have been shown to be active for DODH. Various "green" alternative reductants have been proposed such as secondary alcohols, elemental reductants, and gases. Modulation of the

ligand environment of the catalyst has worked to lessen the effects of catalyst dimerization and aid in increasing the rate of the rate determining step. The problem this work seeks to address is the reliance on chemical reductants the concomitant generation of chemical waste. There are a few answers to this problem, such as coupling a reductive process to the DODH to regenerate the chemical reductant, but this brings its own challenges as additional energy inputs are required. An alternative method to generate the reduced species without the concomitant generation of waste chemical is to electrochemically reduce the metal catalyst.<sup>1</sup> This sidesteps any thermal need to reduce the catalyst and is a greener alternative to directly access the catalytically active species. Generation of the electrons needed for reduction are supplied by the electrode and the charge balancing protons are supplied by Brønsted-Lowry acids. The conjugate bases formed are more easily handled than the waste reductants.

This method requires a fundamental understanding of how the poly-oxo catalyst behaves in proton transfer (PT) and electron transfer (ET) reactions. These fundamental proton and electron transfers are contained in a body of work known as proton coupled electron transfer (PCET). It refers to the stepwise transfer of either the electron or proton followed by the other. PCET lies in the heart of small molecule transformations as multiproton and multielectron processes.<sup>2,3</sup> The proton and the electron start from different orbitals and are transferred to different atomic orbitals. What would be expected for PCET of this this octahedral molybdenum system is the electron occupies the  $t_{2g}$  d-orbitals on the metal center while the proton adds to the oxo group, forming a hydroxy moiety.<sup>4-6</sup> A second PCET cycle would then generate the high spin Mo(IV)  $d^2$  aquo complex where the aquo group can facilely disassociate ultimately leading to the reduced mono-oxo active species for DODH. The electrode provides the electron for an outer sphere transfer and the Brønsted-Lowry acids supply the proton. PCET is the sum of a proton transfers (PT) and electron transfer (ET); it can be stepwise or concerted (CPET).<sup>7-9</sup> Thermodynamically, the concerted process is favored because it avoids the formation of high

energy intermediates. A deep understanding of PT and ET processes will allow for fine control of redox events via modulation of pKa (PT) or potential (ET).<sup>10</sup> The PCET chemistry of molybdenum has been explored in other contexts. Chang et al<sup>11</sup> discusses PCET in the context of hydrogen evolution (HER) using a molecular molybdenum-oxo catalyst.

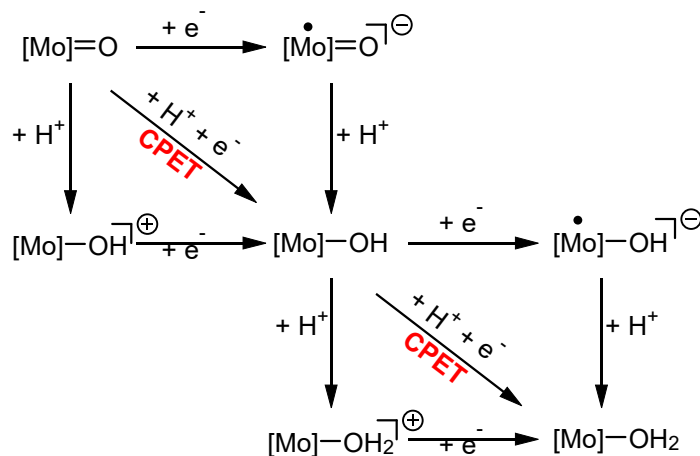


**Figure 1.** Competing mechanisms for the transfer of protons and electrons via PCET or CPET.

## Results and Discussion

### Cyclic Voltammetry

All voltammograms are referenced to the ferrocene/ferrocene<sup>+</sup> couple and all voltammograms of **2** in the presence and absence of proton donor were shown to exhibit linear responses to varying scan rate and no surface modification at the electrode was occurring. The voltammogram of phenolate ligand shows three reductive and three oxidative events. The quasi-reversible redox at  $E = -0.528$  V is attributed to the one electron oxidation of the phenolate to the still bound quinoidal monoanionic species and the following redox at  $E = 0.583$  V is attributed to the further oxidation of the other phenolate ring.<sup>4</sup> The redox behavior near -3 V is then characterized as being pyridine based. The voltammogram of **2** exhibits three quasi-reversible redox processes and three oxidations. The redox at  $E = -1.867$  V corresponds to the one electron Mo<sup>VI/IV</sup> couple. The subsequent redox at  $E = 2.51$  V corresponds to the subsequent

Mo<sup>VI/V</sup> couple. Coulometry data confirms the consecutive one electron reductions at E<sub>VI/V</sub> and E<sub>V/IV</sub>. The redox at -3.1 V is attributed to a combination of the pyridine ligand and OPPh<sub>3</sub> redox features.<sup>5</sup> The oxidation at -0.537V is assigned as the one electron oxidation of the phenolate as mentioned above for the ligand alone. This feature was observed to be coupled to the redox event at -3.1 V; if the polarity was switched prior to reaching this redox couple, the oxidations do not occur.

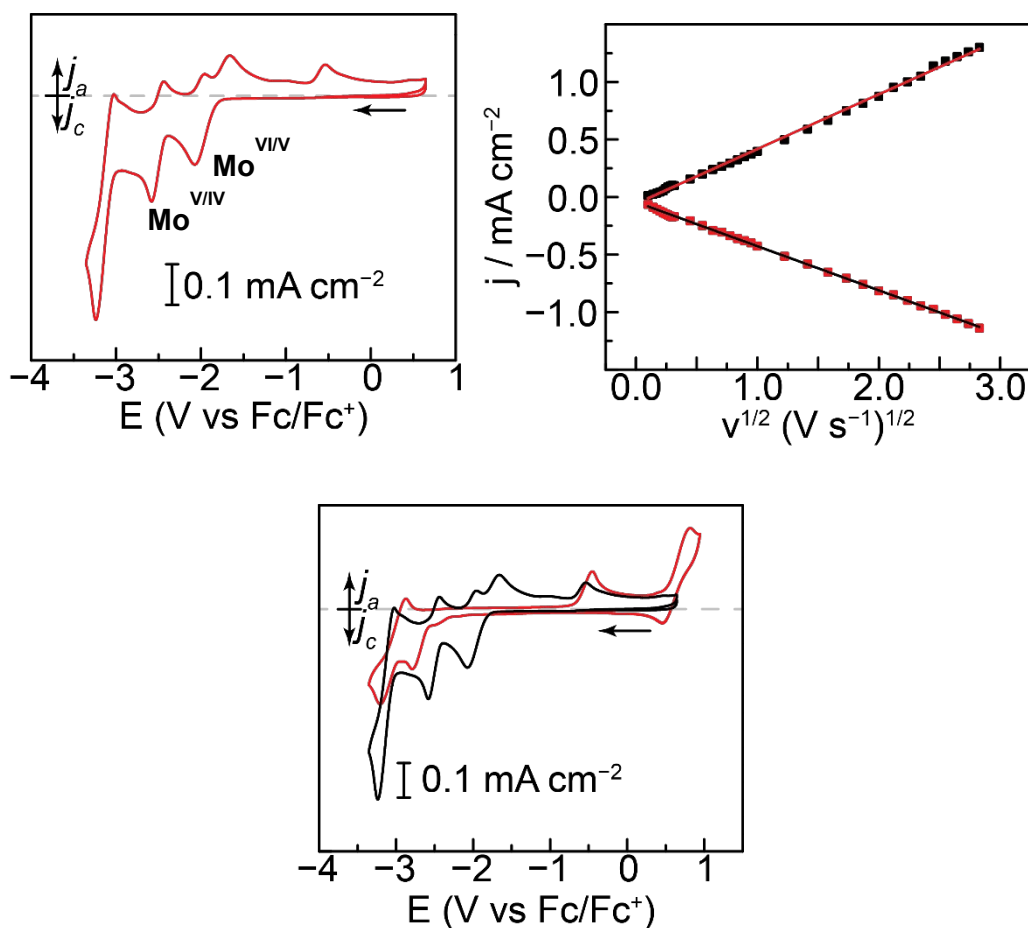


**Figure 2.** Left: voltammogram of catalyst. Right: Linear peak response to the square root of the scan rate. Bottom: Overlaid voltammograms of ligand (black) and **2** (red).

The voltammogram response was shown to be first order with respect to molybdenum. Measured current response to a variety of acid donor strength allows for a measure of PT kinetics. Foot of the wave (FOTW) analysis at E<sub>VI/V</sub> was done in the presence of varying proton

donor strength. Calculated diffusion constant in the absence of proton donor was shown to be  $8.19 \times 10^{-6} \text{ cm}^2/\text{s}$ .

Table 1. Selected pKa's of acids in THF. <sup>6,7</sup>	
Brønsted-Lowry Acid	pKa(THF)
p-toluenesulfonic acid (TsOH)	9*
3,4-dichlorobenzoic acid	23
2,4-dichlorobenzoic acid	22
2-iodobenzoic acid	24
2,6-dihydroxybenzoic acid	19
benzoic acid	25.11
4-methoxyphenol	~32

\*pKa for TsOH is reported in acetonitrile.

The weakest proton donor tested, 4-methoxyphenol, an initial non-linear growth in the current as a function to acid concentration was observed until a time dependent process occurred and loss of signal at the expected potential happened. This is rationalized as likely being some chemical process that occurred to the catalyst that changed its electroactive potential. The most likely case thus far is the displacement of  $\text{OPPh}_3$  as the ancillary ligand; this would serve to lower the steric strain of the catalyst due to the 4-methoxyphenol being smaller than  $\text{OPPh}_3$ . The NMR supports the presence of a p-substituted benzene in solution as evidenced by the appearance of a second order AA'BB' feature distinct from free p-methoxyphenol.

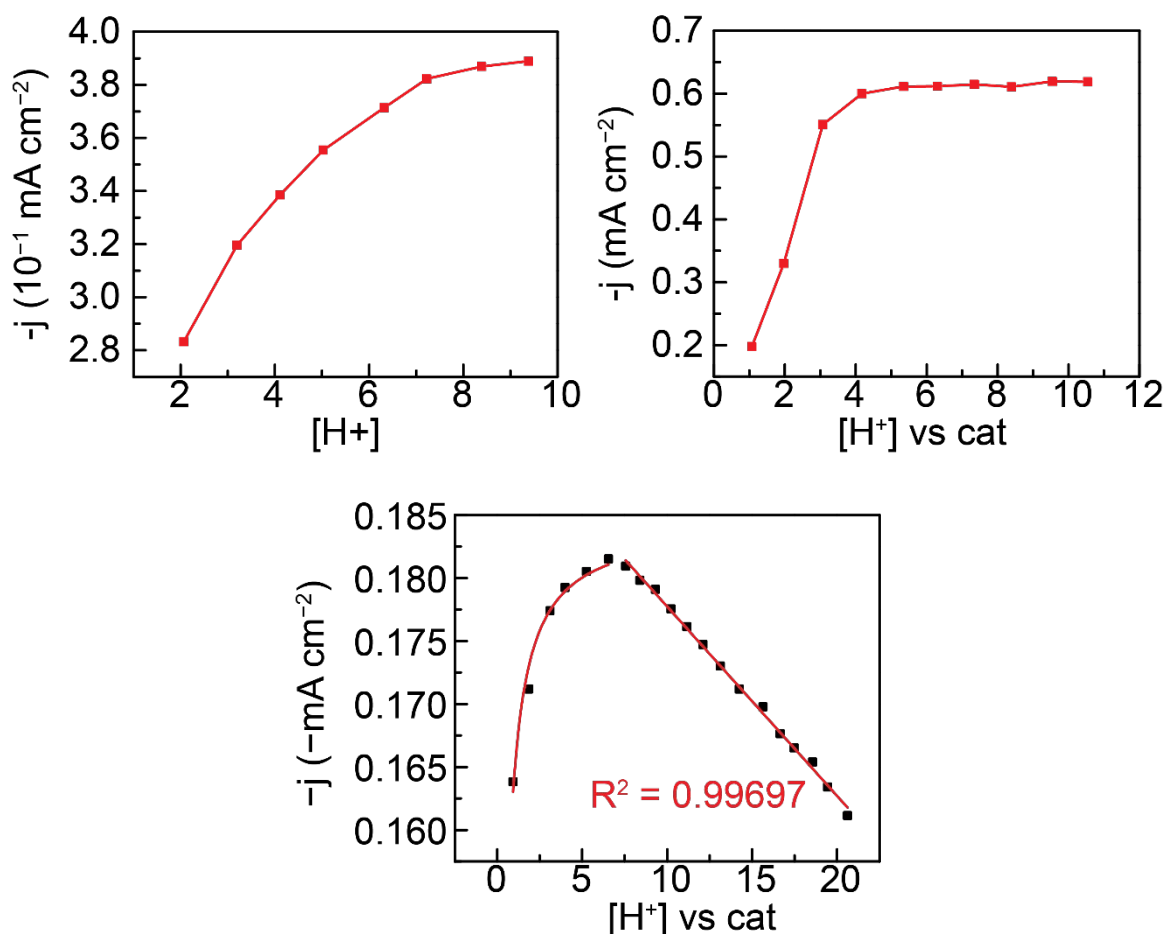


**Figure 3.** Voltammogram current response to increasing proton concentration. Top left: 2,4-dichlorobenzoic acid. Top right: p-toluenesulfonic acid monohydrate. Bottom: 4-methoxyphenol

Benzoic acid and its halogenated derivatives exhibited similar behavior. The current grew in a Michaelis-Menten enzyme saturation kinetic regime as a function of acid concentration. This occurred until a certain equivalence of acid was reached, dependent on the relative strength of the acid, after which there was a noted rapid decrease in current. The possible reason why this occurred was that a film was formed on the surface of the electrode in the experiments where the decrease in current signal was observed, however the acid concentration at current decrease was dependent on the relative strength of proton donor. For the more acidic halogenated benzoic acids, 2,4-dichlorobenzoic acid, 3,4-dichlorobenzoic acid, 2-iodobenzoic acid, and 2,6-dihydroxybenzoic acid, ~15-18 equivalents of acid were required before loss of current signal was observed. The chemical process that occurs is relatively slow

versus the CV timescale; 15 equivalents of 2-iodobenzoic acid showed no decrease in current yet if the solution were allowed to sit and stir for 15 minutes, the current decreased dramatically. Current decrease was not observed at one equivalent of any proton source, showing that the catalyst is temporally stable to low equivalents of acid and that the decrease in current signal is reliant on larger amounts of proton donor. 2,6-dihydroxybenzoic acid as a proton source did not follow the Michaelis-Menten kinetic regime; it showed a linear increase in current signal with increasing concentration. However, side reactions occurred that interfered with the proton transfer observed, resulting in large changes in current that are more than simple proton transfer. Michaelis-Menten fitting allowed for extraction of some kinetic parameters. Application of the Michaelis-Menten model to this electrochemical system is represented by the initial equilibrium of the catalyst and proton followed by the quasi-reversible (kinetically slow) reduction at the electrode. Leveraging Le Chatelier's principle, the equilibrium can be "pushed" toward the right with the addition of excess proton. This is summarized in Figure 4.

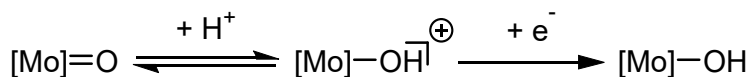


**Figure 4.** Initial equilibrium of proton addition to the catalyst. Excess proton can push the equilibrium to the right via Le Chatelier's principle. This is followed by the irreversible electron transfer.

#### Tafel Analysis

Onset potentials is defined here as the potential at 25% of the peak height. This puts the potential in the mixed control region. Tafel analysis of catalyst behavior in the presence of increasing concentrations of benzoic acid showed an apparent tafel slope of 75 mV/dec. 2,4-dichlorobenzoic acid showed a tafel slope of 77 mV/dec. 3,4-dichlorobenzoic acid showed a tafel slope of 213 mV/dec while 2-iodobenzoic acid's tafel slope was 214 mV/dec. TsOH exhibited the largest tafel slope of 790 mV/dec. Tafel analysis was also done at steady state currents using chronoamperometry. In the absence of proton donor, the apparent tafel slope

was observed to be  $180 \text{ mV dec}^{-1}$ . This corresponds to a charge transfer coefficient of 0.32 suggesting a  $< 1$  electron transfer occurring. Subsequent increases in proton donor strength changed the observed tafel slope to 241, 335, and  $371 \text{ mV dec}^{-1}$  for 10x benzoic acid, 10x TsOH, and 100x TsOH, respectively.

Exchange current densities varied in the absence or presence of proton donor. In the absence of proton, exchange currents were calculated to be on the order of magnitude of  $10^{-15}$  at  $\text{Mo}^{\text{VI/V}}$  while that increases by 10 orders of magnitude when in the presence of excess TsOH.

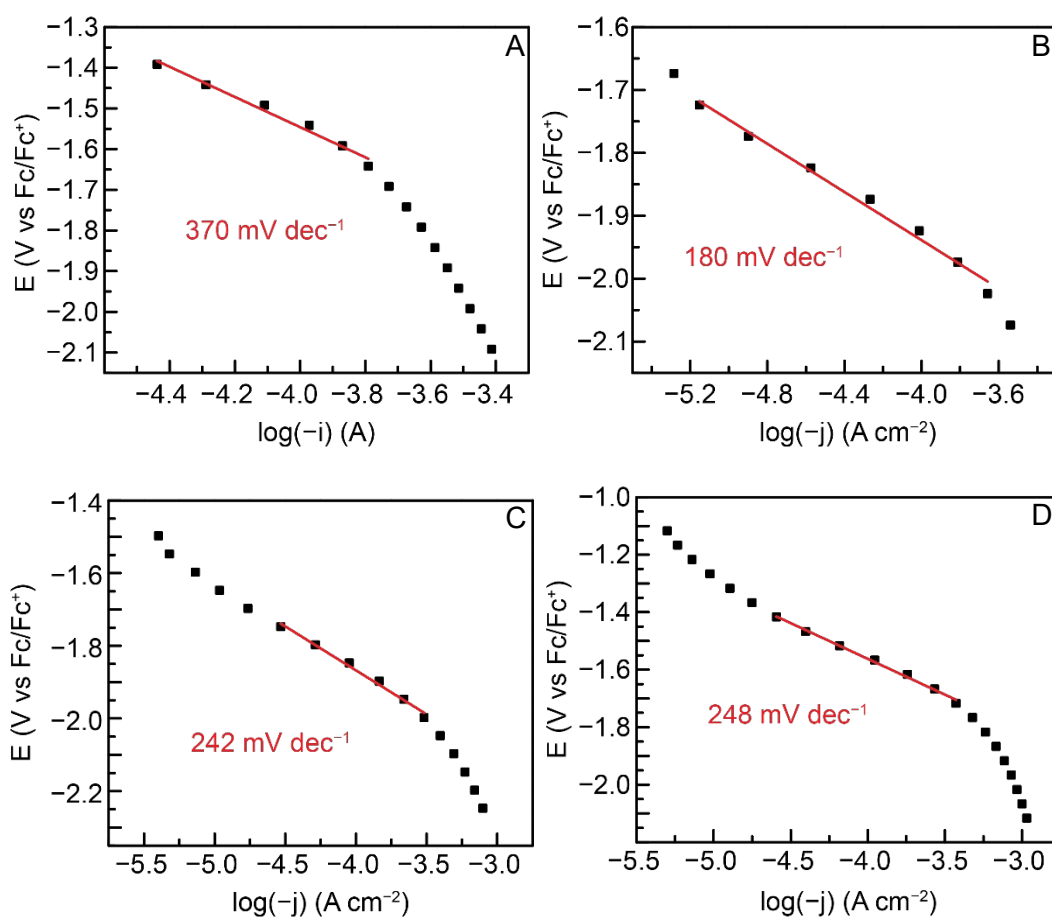


**Figure 5.** (A): 100x TsOH. (B): no proton donor. (C): 10x benzoic acid. (D): 10x TsOH

<b>Table 2. Exchange currents, Tafel slopes, and CTC in different conditions at an RDE at 1500 rpm.</b>			
<b>Conditions</b>	<b>Exchange Current Density (A/cm<sup>2</sup>) CA</b>	<b>Tafel slope (mV dec<sup>-1</sup>)</b>	<b>a, CTC (b = 2.3RT/aF)</b>
No proton	1.8947 x 10 <sup>-15</sup>	180	0.328296
100x TsOH	3.4602 x 10 <sup>-8</sup>	307	0.159281
10x TsOH	3.2259 x 10 <sup>-9</sup>	302	0.176398
10x benzoic acid	1.9117 x 10 <sup>-12</sup>	242	0.2452

### Linear Sweep Voltammetry (LSV)

Koutecky-Levich (KL) analysis was done with LSV experiments. Plots of  $A^{-1}$  vs  $\omega^{-1/2}$  yield linear responses from which important parameters may be extracted, such as the kinetic current,  $i_k$ , from the intercept of the KL plot. The heterogeneous electron rate transfer coefficient,  $k_h$ , may be calculated from  $i_k$ . It was shown that  $k_h$  in the absence of proton donor was  $-6.77 \times 10^{-2}$  cm/s while in the presence of 10 equivalents of strong proton donor, TsOH, it was considerably slower at  $-2.39 \times 10^{-2}$  cm/s. Tafel plots were also derived from KL analysis. The potentials were plotted against the kinetic currents calculated from the KL analysis in various conditions. The resulting plots show large increases in the apparent tafel slope up to 2824 mV dec<sup>-1</sup> when in the presence of 10 equivalents of TsOH. Kinetic current is the observed current in the absence of mass transport limitations and so the increasing apparent tafel slopes in these plots inform that the proton addition is the chemically limiting step of PCET. Therefore, it is highly probable that this molybdenum catalyst system undergoes a PTET mechanism for PCET.

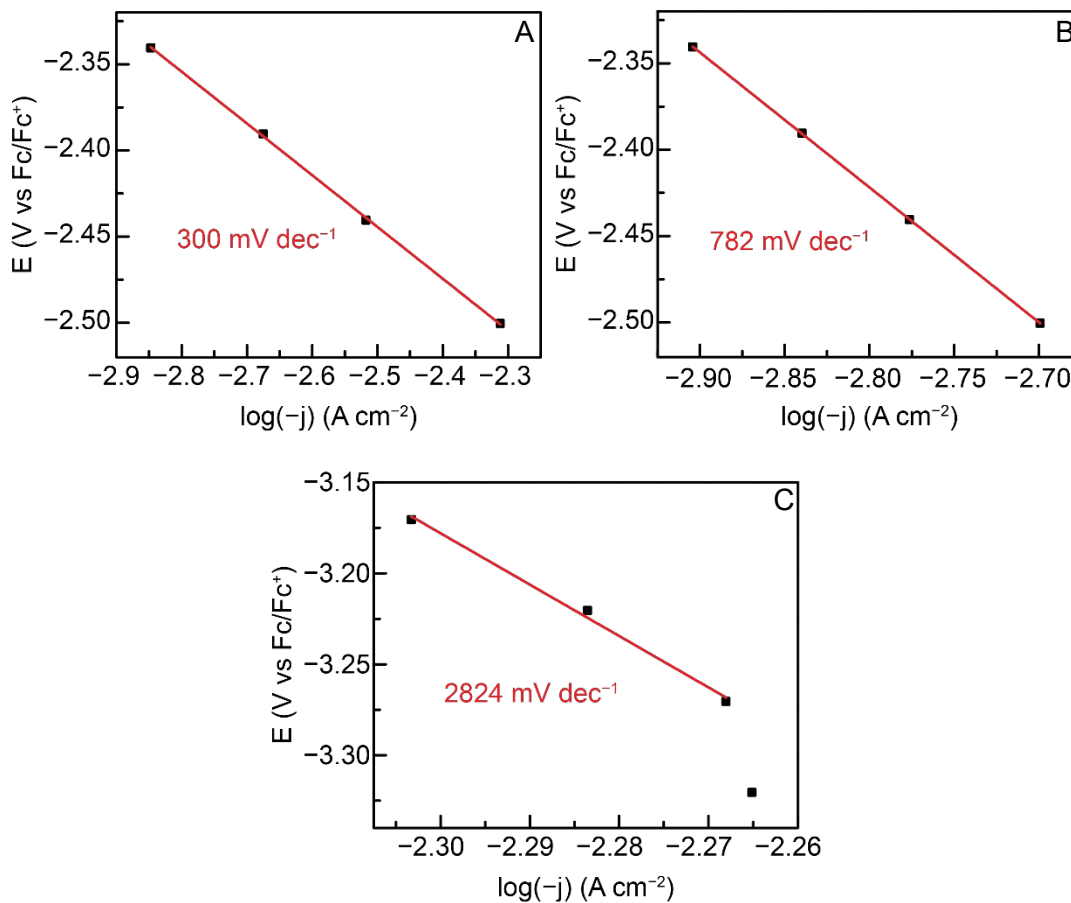


**Figure 6.** (A) Catalyst only (B) 10x benzoic acid (C) 10x TsOH. Tafel plots derived from the pure kinetic current ( $i_k$ ) calculated from Koutecky-Levich analysis. This removes the mass-transport limitations in the Tafel plot. The large increasing Tafel slope in the presence of strong proton donor and absence of mass-transport limitations are informative of the proton addition being the limiting step of the PCET.

## Conclusions

The direct electrochemical reduction of  $MoO_2(L)$  to access the catalytically active species for DODH is an approach towards reducing the chemical waste generated in DODH when relying on chemical reductants. An electrochemical characterization and understanding of the PCET of this catalyst was developed. The voltammogram of the catalyst showed three quasi-reversible redox events as the potential window was swept. Two of the redox events were shown to be the consecutive one electron reductions of the molybdenum catalyst while the third was shown to be ligand based redox. Voltammogram response to varying proton donor

strengths were tested and a Michaelis-Menten kinetic regime was observed for most donors tested. The strongest acid tested, TsOH, exhibited rapid saturation at four equivalents and no further change to the voltammogram was observed. The weakest acid, 4-methoxyphenol, showed that substitution of the  $\text{OPPh}_3$  as ancillary ligand was preferred over protonation of the oxo group. KL analysis extracted  $k_h$  and showed that the electron rate transfer was limited by the presence of proton donor. This leads to the conclusion that this molybdenum system undergoes a PTET mechanism.

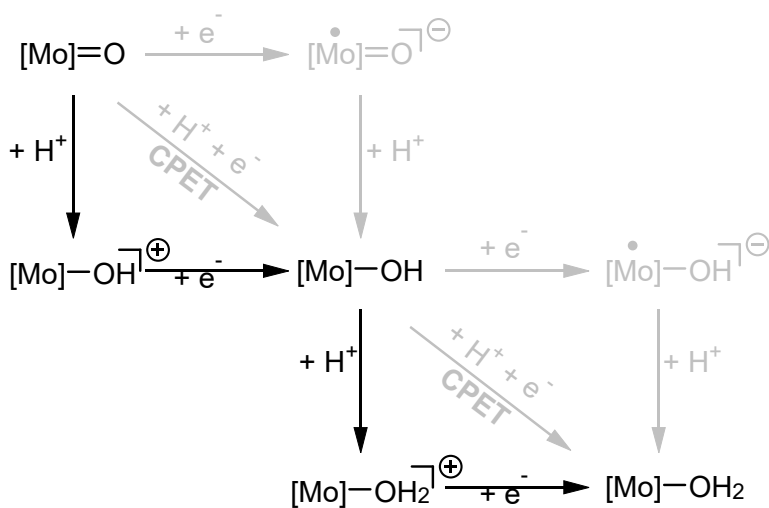


**Figure 7.** This molybdenum system undergoes PCET by proton transfer followed by electron transfer, generating the cationic intermediate.

## Experimental Procedure

All manipulations were performed in an inert atmosphere glovebox. Anhydrous tetrahydrofuran was dried over 3Å molecular sieves overnight and stored under inert atmosphere. Benzoic acid, 2,4-dichlorobenzoic acid, 3,4-dichlorobenzoic acid, 2,6-dihydroxybenzoic acid, 2-iodobenzoic acid, and 4-methoxyphenol were purchased from Sigma and used as received. The electrolyte, tetrabutylammonium hexafluorophosphate (TBAPF<sub>6</sub>), was stored under inert atmosphere and used as received. Synthesis of the molybdenum catalyst was previously reported and covered in Chapter 3. Electrochemical techniques were performed in THF using a 3-electrode setup using a CH instruments 760E potentiostat. Glassy carbon working electrodes (d = 3mm) were polished in 1.0-, 0.3-, and 0.05-micron alumina slurry, sonicated between each slurry to remove all trace alumina, washed with HPLC water, and dried prior to use. For chronoamperometry and linear sweep voltammetry, a carbon rotating disc electrode (d = 5mm) was used and polished in the same fashion as the stationary electrode. Rotation rates were varied from 1000-2000 rpm on a Metrohm Autolab. Conversion from rpm to rad/s was done by multiplying rpm by  $2\pi/60$ . A reference electrode was constructed using a silver wire in saturated AgNO<sub>3</sub> solution separated from the cell by a Vycor frit. Counter electrode was a platinum wire. All CVs were taken referenced to the Ag<sup>0/+</sup> couple and then true ferrocene was added at the end of each experiment and then absolutely referenced to the Fc<sup>0/+</sup> couple. All currents were normalized by the electrode's geometric surface area. Electrolyte backgrounds (TBAPF<sub>6</sub>, 4 mmol, 100mM) in THF (40 mL) were taken prior to addition of catalyst. The catalyst (0.04 mmol, 1 mM) was added. Increasing equivalents of acid were titrated into solution. Default scan rates for voltammograms were 0.1 V/s unless otherwise noted. The solution was stirred prior to each CV taken. CV's initial scan polarity was cathodic. Michaelis-Menten fitting was done using the generalized Hill equation where number of cooperative sites  $n = 1$ . Current densities were adjusted by a factor of -1 to fit the data. Lineweaver-Burk plots were

used to check for consistency. Bulk electrolysis with coulometry was performed in the presence of excess amounts of TsOH. A graphite post electrode or carbon foam was used for electrolysis experiments. Overpotentials were calculated at a 25% peak height; this puts the potential during the mixed control regime and after the activation region.

## References

- (1) Savéant, J.-M. Molecular Catalysis of Electrochemical Reactions. Mechanistic Aspects. *Chem. Rev.* **2008**, *108* (7), 2348–2378. <https://doi.org/10.1021/cr068079z>.
- (2) James M. Mayer. Proton-coupled electron transfer: A Reaction Chemist's View. *Annu. Rev. Phys. Chem.* 2004. 55:363–90
- (3) David R. Weinberg, Christopher J. Gagliardi, Jonathan F. Hull, Christine Fecenko Murphy, Caleb A. Kent, Brittany C. Westlake, Amit Paul, Daniel H. Ess, Dewey Granville McCafferty and Thomas J. Meyer. Proton-Coupled Electron Transfer. *Chem. Rev.* 2012, *112*, 4016–4093
- (4) Hinshaw, C. J.; Spence, J. T. Electron Paramagnetic Resonance Evidence for Electrochemical Formation of MoVO<sub>2</sub>, Cis-MoVO(OH), MoVO(S) and Cis-MoVO(SH) Centers. *Inorganica Chimica Acta* **1986**, *125* (2), L17–L21. [https://doi.org/10.1016/S0020-1693\(00\)82086-1](https://doi.org/10.1016/S0020-1693(00)82086-1).
- (5) Farchione, Frank.; Hanson, G. R.; Rodrigues, C. G.; Bailey, T. D.; Bagchi, R. N.; Bond, A. M.; Pilbrow, J. R.; Wedd, A. G. Generation of a Cis-[MoVO(OH)] Center: Proton- and Oxygen-17 Superhyperfine Parameters Relevant to Molybdoenzymes. *J. Am. Chem. Soc.* **1986**, *108* (4), 831–832. <https://doi.org/10.1021/ja00264a042>.
- (6) Ng, V. W. L.; Taylor, M. K.; White, J. M.; Young, C. G. Cis-Dioxo- and Cis-(Hydroxo)Oxo-Mo(V) Complexes Stabilized by Intramolecular Hydrogen-Bonding. *Inorg. Chem.* **2010**, *49* (20), 9460–9469. <https://doi.org/10.1021/ic1011428>.
- (7) Weinberg, D. R.; Gagliardi, C. J.; Hull, J. F.; Murphy, C. F.; Kent, C. A.; Westlake, B. C.; Paul, A.; Ess, D. H.; McCafferty, D. G.; Meyer, T. J. Proton-Coupled Electron Transfer. *Chem. Rev.* **2012**, *112* (7), 4016–4093. <https://doi.org/10.1021/cr200177j>.
- (8) Hammes-Schiffer, S. Proton-Coupled Electron Transfer: Classification Scheme and Guide to Theoretical Methods. *Energy Environ. Sci.* **2012**, *5* (7), 7696. <https://doi.org/10.1039/c2ee03361e>.
- (9) Morris, W. D.; Mayer, J. M. Separating Proton and Electron Transfer Effects in Three-Component Concerted Proton-Coupled Electron Transfer Reactions. *J. Am. Chem. Soc.* **2017**, *139* (30), 10312–10319. <https://doi.org/10.1021/jacs.7b03562>.
- (10) Hammes-Schiffer, S. Theory of Proton-Coupled Electron Transfer in Energy Conversion Processes. *Acc. Chem. Res.* **2009**, *42* (12), 1881–1889. <https://doi.org/10.1021/ar9001284>.
- (11) Karunadasa, H., Chang, C. & Long, J. A molecular molybdenum-oxo catalyst for generating hydrogen from water. *Nature* **464**, 1329–1333 (2010).
- (12) Fabrice Thomas et al. Electronic Structure and Reactivity of One-Electron-Oxidized Copper(II) Bis(phenolate)–Dipyrrin Complexes. *Inorg. Chem.* 2018, *57*, 16, 9708–9719
- (13) Shuhei Manabe, Curt M. Wong, and Christo S. Sevov\*. Direct and Scalable Electroreduction of Triphenylphosphine Oxide to Triphenylphosphine. *J. Am. Chem. Soc.* 2020, *142*, 6, 3024–3031

- (14) D. Barrón, J. Barbosa. Acid–base behaviour of substituted phenolic substances and resolution of acid strength in tetrahydrofuran. *Analytica Chimica Acta* 403 (2000) 339–347
- (15) J. Barbosa, D. Barron, E. Bosch, and M. Roses. Resolution of acid strength in tetrahydrofuran of substituted benzoic acids. *Analytica Chimica Acta*, 265 (1992) 157-165.

### Supporting Information

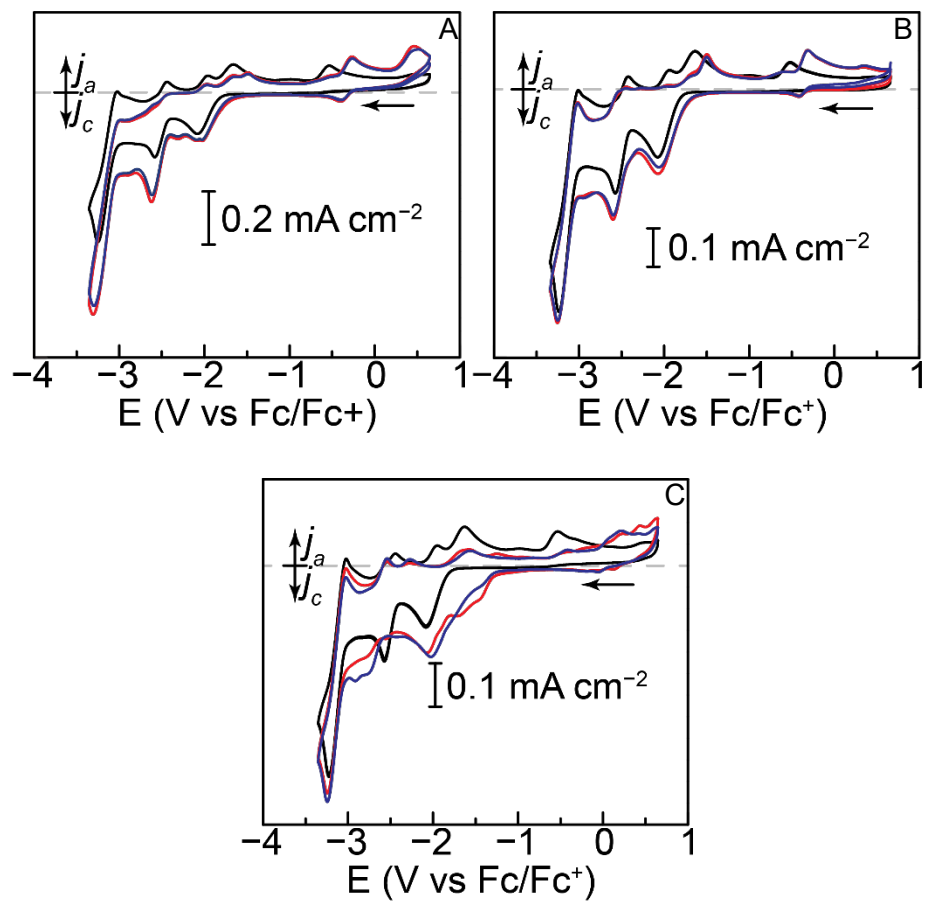
<b>Table T1. Fitted data of j vs [H<sup>+</sup>]</b>			
<b>Proton Donor</b>	<b>Exp</b>		<b>MM fitting</b>
Benzoic acid	166A (1x-10x)	Km	0.95785
pK <sub>a</sub> <sub>THF</sub> = 25.11		Vmax	-3.8106 x10 <sup>-4</sup>
		R <sup>2</sup>	0.96036
	177A (10x-60x)	Km	3.25933
		Vmax	-4.007 x10 <sup>-4</sup>
		R <sup>2</sup>	0.95608
2,4-Cl <sub>2</sub> benzoic acid	167A (1x-10x)	Km	1.29215
pK <sub>a</sub> <sub>THF</sub> = ~22		Vmax	-4.5007 x10 <sup>-4</sup>
		R <sup>2</sup>	0.99242
3,4-Cl <sub>2</sub> benzoic acid	144A (1x-10x)	Km	2.23754
pK <sub>a</sub> <sub>THF</sub> = ~22		Vmax	-6.3926 x10 <sup>-4</sup>

Table T1. Fitted data of j vs [H+] (cont.)			
Proton Donor	Exp		MM fitting
		R <sup>2</sup>	0.96801
	164A (1x-10x)	Km	0.91929
		Vmax	-3.94571 x10 <sup>4</sup>
		R <sup>2</sup>	0.97652
	168A (1x-10x)	Km	1.01262
		Vmax	-3.931 x10 <sup>-4</sup>
		R <sup>2</sup>	0.97133
2,6-dihydroxybenzoic acid	160A (1x-10x)	Linear	y = -1.04269 x10 <sup>-4</sup> - 1.4991 x10 <sup>-4</sup>
pK <sub>a</sub> <sub>THF</sub> < 20.24		R <sup>2</sup>	0.97973
4-MeOphenol	183A (1x-20x)	Km	0.12305
pK <sub>a</sub> <sub>THF</sub> > 29.23		Vmax	-1.8447 x10 <sup>-4</sup>
		R <sup>2</sup>	0.97761

Table T1. Fitted data of j vs [H+] (cont.)			
Proton Donor	Exp		MM fitting
		Linear	$y = (1.50336 \times 10^{-6})x - 1.92775 \times 10^{-4}$
		R <sup>2</sup>	0.97761
	184A (2x-40x)	Km	0.16285
		Vmax	$-1.8237 \times 10^{-4}$
		R <sup>2</sup>	0.98461
		Linear	$y = (8.89974 \times 10^{-7}) - 1.89258 \times 10^{-4}$
		R <sup>2</sup>	0.98461
2-iodobenzoic acid	180A (1x-20x)	Km	0.54016
pK <sub>a</sub> <sub>THF</sub> >23.44		Vmax	$-3.65386 \times 10^{-4}$
		R <sup>2</sup>	0.95898

<b>Table T2. Koutecky Levich data @-2.5V</b>				
<b>Conditions</b>	<b>B<sub>L</sub> Levich value</b>	<b>i<sub>k</sub> (A)</b>	<b>k<sub>h</sub></b>	<b>Rxn</b>
No proton	-1.1636 x 10 <sup>-5</sup>	-9.1602 x 10 <sup>-4</sup>	-4.7393 x 10 <sup>-2</sup>	193A
	-1.3310 x 10 <sup>-5</sup>	-7.1772 x 10 <sup>-4</sup>	-3.5384 x 10 <sup>-2</sup>	194A
	-1.0502 x 10 <sup>-5</sup>	-2.2945 x 10 <sup>-3</sup>	-1.2037 x 10 <sup>-1</sup>	195A
10x TsOH	-1.1876 x 10 <sup>-4</sup>	-9.7668 x 10 <sup>-4</sup>	-2.8939 x 10 <sup>-2</sup>	199A
10x benzH	-4.5405 x 10 <sup>-5</sup>	-5.9006 x 10 <sup>-4</sup>	-2.3950 x 10 <sup>-2</sup>	200A

<b>Table T3. Koutecky Levich data @-3.17V</b>				
<b>Conditions</b>	<b>B<sub>L</sub> Levich value</b>	<b>i<sub>k</sub> (A)</b>	<b>k<sub>h</sub> cm/s</b>	<b>Rxn</b>
No proton	-2.3385 x 10 <sup>-5</sup>	-2.3220 x 10 <sup>-3</sup>	-6.0088 x 10 <sup>-2</sup>	193A
	-2.5279 x 10 <sup>-5</sup>	-2.5938 x 10 <sup>-3</sup>	-6.3939 x 10 <sup>-2</sup>	194A
	-2.1107 x 10 <sup>-5</sup>	-1.5645 x 10 <sup>-2</sup>	-4.1037 x 10 <sup>-1</sup>	195A



**Figure S1:** Temporal stability of catalyst to certain acids, (A) 2,4-dichlorobenzoic acid (B) benzoic acid (C) TsOH

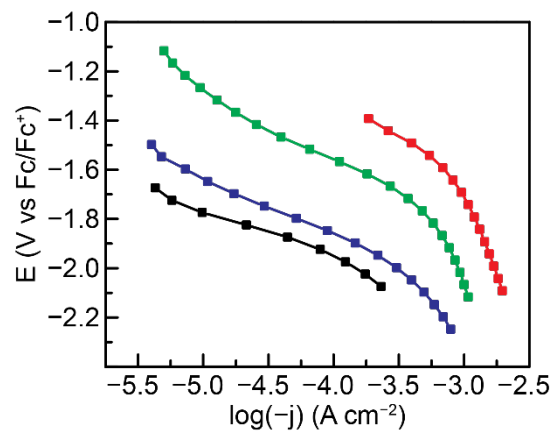


**Figure S2.** Combined Tafel plots of various conditions. No acid (black), 10x benzoic acid (blue). 10x TsOH (green), 100x TsOH (red).

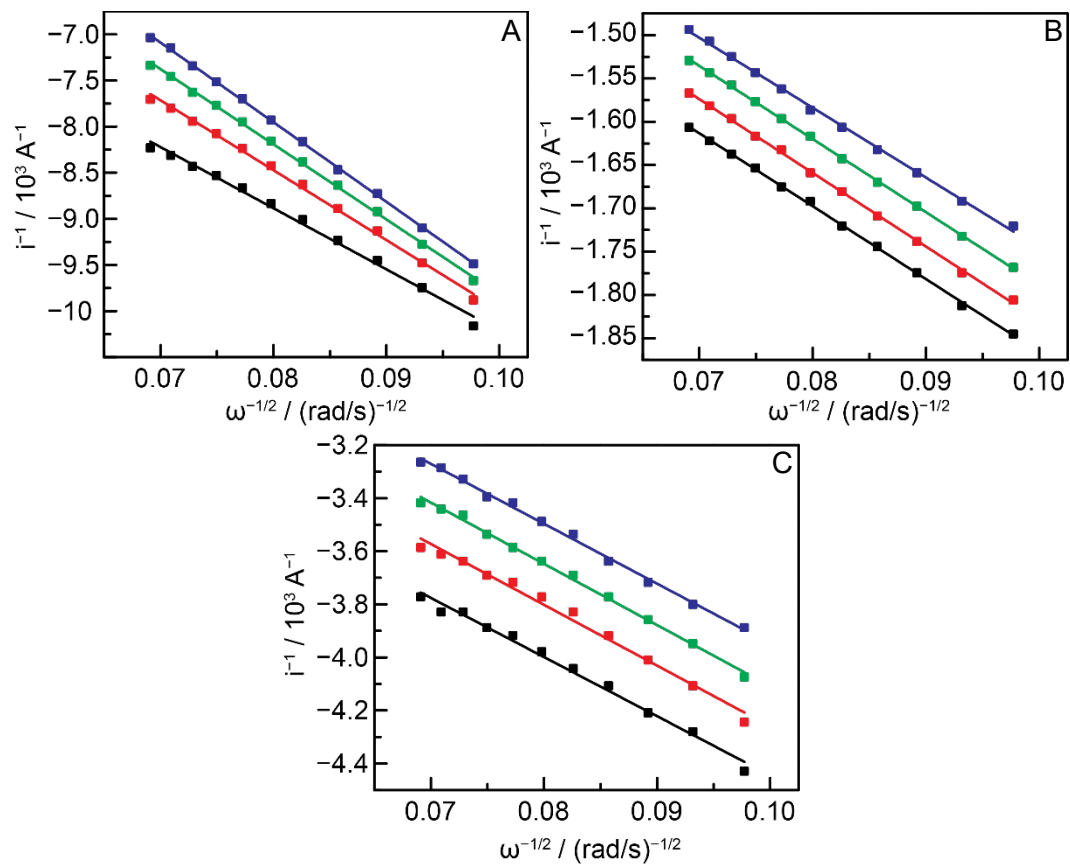


**Figure S3.** KL analysis plots in various conditions. (A) catalyst only. (B) 10x TsOH. (C) 10x benzoic acid. Each KL is 50mV apart.

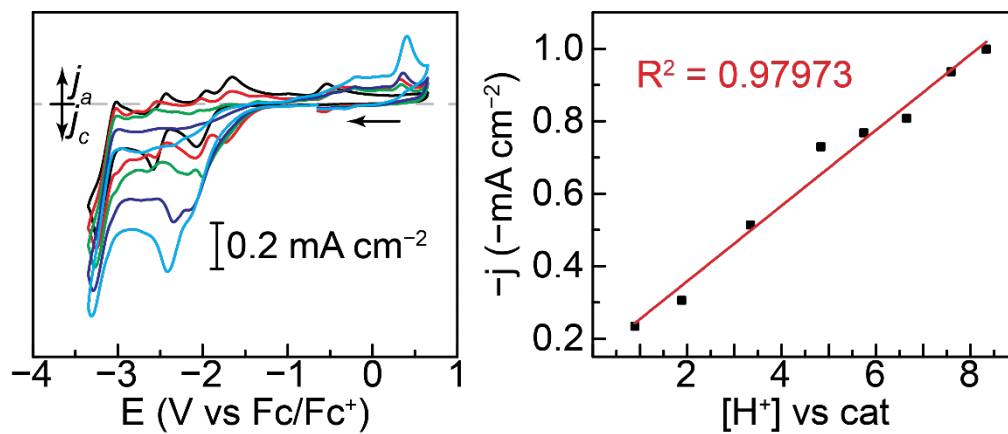


**Figure S4.** Current response to 2,6-dihydroxybenzoic acid.

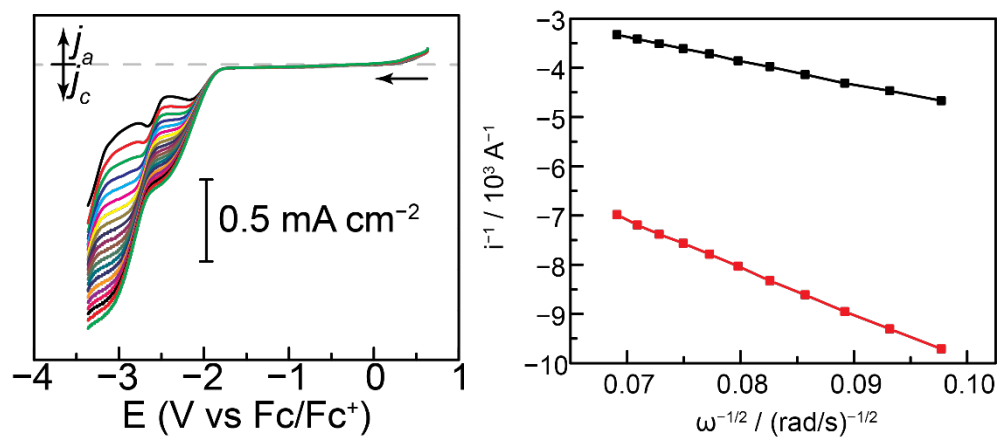


**Figure S5.** Left: LSV data from 100-2000rpm Right:  $\text{A}^{-1}$  response to  $\omega^{-0.5}$  at -2.5V (red) and -3.17V (black).

## Chapter 5

### Conclusions and Future Directions

Fossil fuels currently contribute 80% of the total fuel mix of the global energy economy.<sup>1,2</sup> There is estimation that current conventional oil reserves total near 2.3 billion barrels with potential for more as technologies advance to increase recoverable oil, meaning that the global energy needs can be met by fossil fuels at least through the mid-21<sup>st</sup> century. However, the short- and long-term effects of global warming must be addressed. Global warming is the direct result of rising CO<sub>2</sub> emissions from burning fossil fuels. Global warming has caused a 1°C increase above pre-industrial levels (a likely range of 0.8°C – 1.2°C) and current high confidence projections say that the increase will likely reach 1.5°C between 2030 and 2052 at this rate.<sup>3</sup> According to the Intergovernmental Panel on Climate Change (IPCC), the effects associated with a 1.5°C include but are not limited to: 1) higher mean temperatures globally 2) higher risks of drought and heavy precipitation 3) rising sea levels. The effects of these changes may lead to species extinction and disruption of ecosystems and severe impacts on human life. The global energy economy can lessen its reliance on fossil fuels by increasing the energy contribution from alternative sources. One such source is the potential of modern biomass derived from corn, sugar cane, and sorghum.<sup>4,5</sup> These sources currently account for 12% of energy demands.<sup>6,7</sup> The carbohydrate rich biomass serves as a platform for the generation of liquid biofuels and commodity chemicals. Industrial methods for deoxygenating biomass involve steam reforming and cracking,<sup>8</sup> relying on precious metal catalysts and harsh conditions.<sup>9,10</sup> The deoxygenation is desirable from an energy density view; solid biomass per energy unit occupies more volume than liquid biofuels per energy unit. Greater energy density allows for more efficient utilization of the energy.<sup>11</sup>

Deoxydehydration (DODH) is an alternative method that acts as a springboard to the generation of liquid biofuels and commodity chemicals. First reported in 1996,<sup>12</sup> it has sparked a

body of literature focused on the refinement and optimization of reaction conditions using various transition metals, substrates, and reductants. Initial systems used rhenium<sup>13-18</sup> but has since expanded into vanadium<sup>19-22</sup> and molybdenum<sup>23-29</sup> as earth abundant alternatives.

#### Evaluation of Results and Completion of Aims

This dissertation has established the development and study of dioxomolybdenum(VI) catalysts active for DODH. Chapter 2 chronicled the initial Mo catalyst, supported by dipicolinic acid, and its activity for DODH across a variety of substrates and reductants. It showed moderate yields (~30%) across several diols using PPh<sub>3</sub> as the reductant. Alternative reductants were also shown to be as competent yet slower than PPh<sub>3</sub>. 1-phenyl-1,2-ethanediol was the best performing substrate, yielding up to 49% alkene after 1 hour of heating. However, the styrene product was polymerized in-situ and caused an observed drop in product yield over time. Polymerization inhibition was successful and using a known polymerization inhibitor, *p*-hydroquinone, and the alkene yield was increased up to 69%. The mechanism of Mo-catalyzed DODH was studied using in-situ FTIR and was observed to be substrate directed. 1-phenyl-1,2-ethanediol with PPh<sub>3</sub> as reductant was shown to occur first by initial reduction of the molybdenum-dioxo followed by condensation of the diol to form the metal-diolate species. Alternatively, (R,R)-(+)-hydrobenzoin was shown to exclusively proceed through the deformylation path where 2 moles of substrate generate 1 mole of product and 2 moles of side product.

Chapter 3 outlined the changes in catalytic activity observed when the supporting ligand environment is modified to be more sterically demanding, a relatively bulky dianionic ONO pincer ligand. The expected outcome of these changes were: 1) increased energy of the metal-diolate species leading to increase rate of the RDS, olefin extrusion 2) the relative increase in steric bulk in turn disfavors the Mo(VI) – Mo(IV) dimerization leading to the Mo(V) – Mo(V) d1 dimer that was the suspected source of the polymerization of styrene observed in the previous

chapter. Crystals of the  $\text{MoO}_2(\text{ONO})(\text{L})$  ( $\text{L} = \text{OPPh}_3, \text{HMPA}, \text{none}$ ) were successfully isolated. They showed the 5- and 6-coordinate geometries around the molybdenum cis-dioxo center. The overall yields observed were much different than expected. The reaction times were much longer (48h) than in the previous catalyst and the yields of styrene were not larger as well, showing a maximum yields of 37% alkene. Other diols showed lessened or the same low yields as the previous. The positive changes observed were that the yield of 1-octene from 1,2-octanediol was shown to nearly double from 31% to 59% albeit requiring longer reaction time. The other positive change observed was the reductants were somewhat competitive with the deformylation of the (R,R)-(+)-hydrobenzoin substrate evidenced by the >50% yield of alkene product.

Chapter 4 is an electrochemical experiment studying the elementary proton and electron addition reactions across the metal oxo bond. It looked at the PCET behavior of the catalyst synthesized in chapter 3. Tafel plots using kinetic currents,  $i_k$ , derived from KL analysis showed an increasing apparent tafel slope as a function of increasing acid strength and concentration. Kinetic currents refer to the current observed if there were no mass-transport limitations. Therefore, the increasing tafel slopes within those plots confirm that the PCET is chemically limited by the rate of proton addition. The catalyst's current response to increasing proton concentration was shown to follow a Michaelis-Menten kinetic regime. The conclusion of this chapter: PTET. There is an initial equilibrium with the proton addition that is also the limiting step of the PCET followed by a relatively facile electron transfer.

#### Future Directions

The natural progression of this body of work is the further expansion of molybdenum catalysts active for DODH. Additional ligand fields could be rationally designed. Chapter 2 chronicles the effects of an electronically demanding ligand, 2,6-dipicolinic acid, on catalytic activity. It was shown that the yields for certain diols such as 1-phenyl-1,2-ethanediol were great

but competing side reactions caused the overall yield to be lower than ideal. Chapter 3 outlines the changes observed when the supporting ligand is altered to be more sterically demanding. The rationale was to increase the energy of the diolate intermediate to increase the rate of the olefin extrusion, the rate determining step. A rational step forward would then be to increase the denticity of the supporting ligand. Both chapters presented dioxomolybdenum(VI) catalysts supported by a meridional tridentate dianionic ONO ligand. This left an additional coordination site available that was left vacant (Chapter 3, catalyst 2) or occupied by an ancillary ligand (HMPA,  $\text{OPPh}_3$ , DMSO, etc.). The presence of these ancillary ligands fill empty coordination sites and to help deter the known  $\mu_2$ -oxo bridged molybdenum dimers that lead to catalyst deactivation. Increasing the denticity from tridentate to tetradentate would allow for cleaner synthesis, finer control of catalyst steric parameters, and lessen the chances of ligand dissociation.

Chapter 4 details the electrochemical proton-coupled electron transfer (PCET) behavior characterization of  $\text{MoO}_2(\text{bisphenolate})(\text{OPPh}_3)$ . The ultimate aim of that study was to electrochemically reduce the dioxomolybdenum(VI) into the oxomolybdenum(IV). This would sidestep the requirement for chemical reductant and the stoichiometrically generated chemical waste leading to a greener method for the transformation of agricultural feedstocks into platform chemicals and liquid biofuels. A limitation is the diffusion aspect. One could hold the electrochemical cell at the reducing potential of the catalyst, but it would be limited by how rapidly the target species diffuses from bulk solution to the electrode. Stirring the solution or rotation of the electrode can overcome the diffusion limiting effects but the aspect of hoping the target species coming close to the reaction site still exists. Using this work as a springboard, the next step is the immobilization of the catalysts via a tethering agent on the ligand onto the surface of an electrode. There are some advantages to tethering the catalyst such as lower catalyst loading due to size limitations on the electrode and dependence on diffusion of catalyst

to electrode is overcome. Immobilization of the catalyst allows for greater control of the oxidation state over time. Any changes can be driven directly by the electrode without worrying about its diffusion away from the surface.

## References

- (1) United Nations Development Program (2015) WORLD ENERGY ASSESSMENT: ENERGY AND THE CHALLENGE OF SUSTAINABILITY (United Nations, New York).
- (2) Jackson, R. B.; Le Quéré, C.; Andrew, R. M.; Canadell, J. G.; Korsbakken, J. I.; Liu, Z.; Peters, G. P.; Zheng, B. Global Energy Growth Is Outpacing Decarbonization. *Environ. Res. Lett.* **2018**, *13* (12), 120401. <https://doi.org/10.1088/1748-9326/aaf303>.
- (3) IPCC. Global Warming of 1.5°C.
- (4) Zhang, H.; Li, X.; Su, X.; Ang, E. L.; Zhang, Y.; Zhao, H. Production of Adipic Acid from Sugar Beet Residue by Combined Biological and Chemical Catalysis. *ChemCatChem* **2016**, *8* (8), 1500–1506. <https://doi.org/10.1002/cctc.201600069>.
- (5) Ragauskas, A. J. The Path Forward for Biofuels and Biomaterials. *Science* **2006**, *311* (5760), 484–489. <https://doi.org/10.1126/science.1114736>.
- (6) Popp, J.; Lakner, Z.; Harangi-Rákos, M.; Fári, M. The Effect of Bioenergy Expansion: Food, Energy, and Environment. *Renewable and Sustainable Energy Reviews* **2014**, *32*, 559–578. <https://doi.org/10.1016/j.rser.2014.01.056>.
- (7) Gallezot, P. Conversion of Biomass to Selected Chemical Products. *Chem. Soc. Rev.* **2012**, *41* (4), 1538–1558. <https://doi.org/10.1039/C1CS15147A>.
- (8) DeNike KA, Kilyanek SM. 2019. Deoxydehydration of vicinal diols by homogeneous catalysts: a mechanistic overview. *R. Soc. open sci.* *6*: 191165. <http://dx.doi.org/10.1098/rsos.191165>
- (9) Akah, A.; Williams, J.; Ghrami, M. An Overview of Light Olefins Production via Steam Enhanced Catalytic Cracking. *Catal Surv Asia* **2019**. <https://doi.org/10.1007/s10563-019-09280-6>
- (10) Dutta, S. Deoxygenation of Biomass-Derived Feedstocks: Hurdles and Opportunities. *ChemSusChem* **2012**, *5* (11), 2125–2127. <https://doi.org/10.1002/cssc.201200596>.
- (11) Kunkes, E. L.; Simonetti, D. A.; West, R. M.; Serrano-Ruiz, J. C.; Gartner, C. A.; Dumesic, J. A. Catalytic Conversion of Biomass to Monofunctional Hydrocarbons and Targeted Liquid-Fuel Classes. *Science* **2008**, *322* (5900), 417–421. <https://doi.org/10.1126/science.1159210>.
- (12) Cook, Gerald K.; Andrews, Mark A. Towards Nonoxidative Routes to Oxygenated Organics: Stereospecific Deoxydehydration of diols and Polyols to Alkenes and Allylic Alcohols Catalyzed by the Metal Oxo Complex (C<sub>5</sub>Me<sub>5</sub>)ReO<sub>3</sub>. *J. Am. Chem. Soc.* **1996**, *118*, 9448–9449
- (13) Shiramizu, M.; Toste, F. D. Deoxygenation of Biomass-Derived Feedstocks: Oxorhenium-Catalyzed Deoxydehydration of Sugars and Sugar Alcohols. *Angew. Chem. Int. Ed.* **2012**, *51* (32), 8082–8086. <https://doi.org/10.1002/anie.201203877>.

- (14) Shiramizu, M.; Toste, F. D. Expanding the Scope of Biomass-Derived Chemicals through Tandem Reactions Based on Oxorhenium-Catalyzed Deoxydehydration. *Angewandte Chemie* **2013**, *125* (49), 13143–13147. <https://doi.org/10.1002/ange.201307564>.
- (15) Vkuturi, S.; Chapman, G.; Ahmad, I.; Nicholas, K. M. Rhenium-Catalyzed Deoxydehydration of Glycols by Sulfite. *Inorg. Chem.* **2010**, *49* (11), 4744–4746. <https://doi.org/10.1021/ic100467p>.
- (16) Liu, S.; Senocak, A.; Smeltz, J. L.; Yang, L.; Wegenhart, B.; Yi, J.; Kenttämaa, H. I.; Ison, E. A.; Abu-Omar, M. M. Mechanism of MTO-Catalyzed Deoxydehydration of Diols to Alkenes Using Sacrificial Alcohols. *Organometallics* **2013**, *32* (11), 3210–3219. <https://doi.org/10.1021/om400127z>.
- (17) Boucher-Jacobs, C.; Nicholas, K. M. Oxo-Rhenium-Catalyzed Deoxydehydration of Polyols with Hydroaromatic Reductants. *Organometallics* **2015**, *34* (10), 1985–1990. <https://doi.org/10.1021/acs.organomet.5b00226>.
- (18) Dethlefsen, J. R.; Fristrup, P. In Situ Spectroscopic Investigation of the Rhenium-Catalyzed Deoxydehydration of Vicinal Diols. *ChemCatChem* **2015**, *7* (7), 1184–1196. <https://doi.org/10.1002/cctc.201403012>.
- (19) Gopaladasu, T. V.; Nicholas, K. M. Carbon Monoxide (CO)- and Hydrogen-Driven, Vanadium-Catalyzed Deoxydehydration of Glycols. *ACS Catal.* **2016**, *6* (3), 1901–1904. <https://doi.org/10.1021/acscatal.5b02667>.
- (20) Jiang, Y.-Y.; Jiang, J.-L.; Fu, Y. Mechanism of Vanadium-Catalyzed Deoxydehydration of Vicinal Diols: Spin-Crossover-Involved Processes. *Organometallics* **2016**, *35* (19), 3388–3396. <https://doi.org/10.1021/acs.organomet.6b00602>.
- (21) Petersen, A. R.; Nielsen, L. B.; Dethlefsen, J. R.; Fristrup, P. Vanadium-Catalyzed Deoxydehydration of Glycerol Without an External Reductant. *ChemCatChem* **2018**, *10* (4), 769–778. <https://doi.org/10.1002/cctc.201701049>.
- (22) Chapman, G.; Nicholas, K. M. Vanadium-Catalyzed Deoxydehydration of Glycols. *Chemical Communications* **2013**, *49* (74), 8199. <https://doi.org/10.1039/c3cc44656e>.
- (23) Dethlefsen, J. R.; Lupp, D.; Oh, B.-C.; Fristrup, P. Molybdenum-Catalyzed Deoxydehydration of Vicinal Diols. *ChemSusChem* **2014**, *7* (2), 425–428. <https://doi.org/10.1002/cssc.201300945>.
- (24) Dethlefsen, J. R.; Lupp, D.; Teshome, A.; Nielsen, L. B.; Fristrup, P. Molybdenum-Catalyzed Conversion of Diols and Biomass-Derived Polyols to Alkenes Using Isopropyl Alcohol as Reductant and Solvent. *ACS Catalysis* **2015**, *5* (6), 3638–3647. <https://doi.org/10.1021/acscatal.5b00427>.

- (25) Hills, L.; Moyano, R.; Montilla, F.; Pastor, A.; Galindo, A.; Álvarez, E.; Marchetti, F.; Pettinari, C. Dioxomolybdenum(VI) Complexes with Acylpyrazolonate Ligands: Synthesis, Structures, and Catalytic Properties. *European Journal of Inorganic Chemistry* **2013**, *2013* (19), 3352–3361. <https://doi.org/10.1002/ejic.201300098>.
- (26) Lupp, D.; Christensen, N. J.; Dethlefsen, J. R.; Fristrup, P. DFT Study of the Molybdenum-Catalyzed Deoxydehydration of Vicinal Diols. *Chem. Eur. J.* **2015**, *21* (8), 3435–3442. <https://doi.org/10.1002/chem.201405473>.
- (27) Navarro, C. A.; John, A. Deoxydehydration Using a Commercial Catalyst and Readily Available Reductant. *Inorganic Chemistry Communications* **2019**, *99*, 145–148. <https://doi.org/10.1016/j.inoche.2018.11.015>.
- (28) Tran, R.; Kilyanek, S. M. Deoxydehydration of Polyols Catalyzed by a Molybdenum Dioxo-Complex Supported by a Dianionic ONO Pincer Ligand. *Dalton Trans.* **2019**, *48* (43), 16304–16311. <https://doi.org/10.1039/C9DT03759D>.
- (29) Beckerle, K.; Sauer, A.; Spaniol, T. P.; Okuda, J. Bis(Phenolato)Molybdenum Complexes as Catalyst Precursors for the Deoxydehydration of Biomass-Derived Polyols. *Polyhedron* **2016**, *116*, 105–110. <https://doi.org/10.1016/j.poly.2016.03.053>.